DASA-1892-5

Weapons Radiation Shielding Handbook

Chapter 2 / Basic Concepts of Radiation Shielding Analysis

by Paul N. Stevens and H. Clyde Claiborne

Handbook Editors

Lorraine S. Abbott, H. Clyde Claiborne, and Charles E. Clifford

DEFENSE ATOMIC SUPPORT AGENCY

Washington, D. C. 20305

DISCLAIMER

Printed in the United States of America. Available from Clearinghouse for Federal
Scientific and Technical Information, National Bureau of Standards,
U.S. Department of Commerce, Springfield, Virginia 22151
Price: Printed Copy $3.00; Microfiche $0.65

DASA-1892-5

WEAPONS RADIATION SHIELDING HANDBOOK

Chapter 2. Basic Concepts of Radiation Shielding Analysis

by

Paul N. Stevens and H. Clyde Claiborne

Handbook Editors

Lorraine S. Abbott, H. Clyde Claiborne, and Charles E. Clifford

DEFENSE ATOMIC SUPPORT AGENCY

Washington, D.C. 20305

JUNE 1970

Preparing Agency
OAK RIDGE NATIONAL LABORATORY
Oak Ridge, Tennessee
Operated by UNION CARBIDE CORPORATION
for the U.S. ATOMIC ENERGY COMMISSION
DASA Order No. EO-806-65,
NWER Subtask PEO33

Preface

At the request of the Defense Atomic Support Agency, Oak Ridge National Laboratory has undertaken the preparation of a handbook to aid engineers charged with the responsibility of designing shields to protect military equipment and personnel in the vicinity of a nuclear weapons burst. This document constitutes the fifth chapter of the Handbook issued thus far, the earlier chapters being Chapter 3, "Methods for Calculating Neutron and Gamma-Ray Attenuation," Chapter 4, "Neutron and Gamma-Ray Albedos," Chapter 5, "Methods for Calculating Effects of Ducts, Access Ways, and Holes in Shields," and Chapter 6, "Methods for Predicting Radiation Fields Produced by Nuclear Weapons."

At the time Chapters 3, 4, and 5 were published it was planned that the Handbook would eventually be bound in two volumes, with Volume I serving as a textbook and ready reference and Volume II serving as an engineering guide. Volume I would include an introductory chapter, a chapter describing the radiation fields produced by nuclear detonations, and Chapters 3 through 5. Volume II would present two or more chapters describing engineering methods based on the more sophisticated techniques described in Volume I. During the preparation of Chapter 6, however, the plan to combine the individual chapters into volumes was abandoned – at least for the present – the primary reason being that it would complicate the later publication of updated chapters. We also changed the order of the chapters, with the result that the chapter originally planned as Chapter 2 was published as Chapter 6. One reason for shifting the chapter numbers was to improve the continuity of the Handbook by putting Chapter 6, which describes the various sources of radiation produced by a nuclear weapons burst and presents techniques for calculating the transport of the radiations from the point of burst to the surface of the shield, immediately preceding the engineering chapters. Another reason was that an additional chapter on basic shielding concepts, the present one, had been prepared and it would logically follow the introductory first chapter. With this reordering the basic information generally applicable to all neutron and gamma-ray shielding problems is presented in Chapters 2 through 5, and the information specifically applicable to nuclear weapons radiation shielding problems is presented in the chapters beginning with Chapter 6. The engineering methods dealing with the design of shields for protection against initial weapons radiation will be divided into two chapters: Chapter 7, entitled "Engineering Method for Designing Initial Radiation Shields for Blast-Hardened Underground Structures," which will be published very shortly, and Chapter 8, "Engineering Method for Designing Initial Radiation Shields for Above-Ground Structures." (Like Chapter 6, both Chapters 7 and 8 will be classified.) It now appears that methods for calculating dose rates in structures may be included as an additional chapter in the Handbook. Whether or not the Handbook will include a chapter dealing with shields to protect against fallout radiation is at present uncertain. If a fallout chapter is published, it will rely heavily on a method already available and will be integrated in the Handbook only so that all aspects of the radiation shielding problems will have been covered.

In order to prepare this Handbook, it has been necessary for Oak Ridge National Laboratory to obtain the assistance of several consultants and subcontractors. For this chapter, for example, Paul N. Stevens, a consultant from the University of Tennessee, together with H. Clyde Claiborne of the Laboratory, prepared the first draft with which the editors worked. Other chapters similarly represent a cooperative effort of ORNL staff members and those of other organizations.

As is always the case for handbooks, the authors and editors must rely heavily on the reviews of others as an aid in the development of the various chapters. The list of individuals who have contributed in this manner has already grown very large, and it would be almost impossible to acknowledge each person here. However, there are always reviewers who we feel have made such significant contributions as to warrant individual acknowledgement. With respect to this chapter, we particularly wish to acknowledge the help given by D. K. Trubey of the Laboratory, who spent considerable time reviewing and commenting on the entire chapter.

Appreciation is also expressed to Maj. F. A. Verser and to Lt. Cols. Charles D. Daniel and William A. Alfonte, who as past DASA Shielding Project Officers handled the early administration of the contract and assisted in establishing the scope of the Handbook. The work they began is currently being ably performed by Maj. R. W. Enz.

Finally, we wish to thank Mrs. Virginia M. Hamrick, who assisted in the editing of the chapter, and Mrs. Virginia Glidewell, who typed and helped proofread the many drafts which are always necessary precursors to such a publication.

Contents

2.0. Introduction

Weapons radiation shielding analysis usually involves three major steps: describing the field of radiation against which protection is required; determining the extent to which shielding materials will attenuate particles from that field; and converting the number of particles that penetrate the shield into a dose that can be related to a physical effect or to a biological response. This chapter describes the basic concepts underlying these steps. For those who plan to perform detailed shielding calculations by the methods described in Chapters 3 through 6, a thorough knowledge of these concepts is essential. Such knowledge is of less importance to those who plan to design shields merely by applying the engineering data provided in Chapter 7 and subsequent chapters, but it would be extremely helpful in all cases.

The first step in the analysis – describing the radiation field – begins, of course, with an examination of the data available on the design and burst conditions of the weapon to be considered.* The resulting description can vary from a simple statement of the total number of particles of a particular type at the "point" of detonation to a detailed specification of the energies of the particles and their locations and directions at all times over some specified volume. It is obvious that in a practical situation the consideration of volume introduces some type of shielding material (for example, the elements in the weapon or the atmosphere), and the effect that these materials have on the radiation field must be determined. As a result, the first two steps of the analysis become inseparable, the two together comprising a radiation transport problem. The custom is to divide the transport problem into two parts, one in which the attenuation by the atmosphere is calculated and another in which the attenuation by some barrier (a building or a specially designed shield) is determined.

The various methods that have been developed for attacking the transport problem are described in Chapter 3 of this Handbook, and the application of some of the methods is demonstrated in subsequent chapters. The present chapter is devoted primarily to describing the quantities required as input to these methods and to discussing the types and behavior of the particular radiations to which the methods are applied in weapons radiation shielding. The chapter also discusses how the results of the transport calculations can be related to a physical or a biological effect, that is, how the third step of the analysis can be accomplished.

Discussions of the quantities used to describe radiation fields are presented in Sections 2.1 and 2.2. The most detailed descriptions are given in seven-dimensional phase space and are required in very sophisticated transport calculations. However, many transport methods cannot handle such detail and because of this, plus the fact that the detailed descriptions are so difficult to obtain, descriptions based on fewer parameters have come into common use. Also, some special descriptions of radiation fields that are basic to many of the mathematical models have emerged and these forms will often suffice.

The extent to which shielding materials will attenuate particles from a radiation field depends both on the type and energy of the radiation and on the kind of materials comprising the shield. Some particles will pass through the shield unimpeded, and others will collide with the nuclei of the medium. Particle-nucleus collisions can result in a change in the direction and energy of the incident particle or in its absorption, the attenuation within the shield being determined by the probabilities for the various types of interactions. The quantities representing the probabilities, called *cross sections,* are discussed in Section 2.3.

The formal definitions and explanations given in Sections 2.1-2.3 are presented in terms of idealized particles and can represent any type of neutral radiation. Insofar as shielding against nuclear weapons is concerned, the only radiations that need be considered are neutrons and gamma rays. While both these radiations can be regarded as neutral particles, there are certain obvious differences in their behavior. For example, the speed of a gamma-ray "particle" is constant and does not depend on its energy, whereas

*The interrelation of these parameters is discussed in detail in Chapter 6.

the speed of a neutron is determined by its energy. Thus some caution must be exercised when specializing particle concepts to gamma rays.

Neutrons and gamma rays can undergo many different interactions with materials, and calculations of their transport through a shield can be quite difficult. The situation is complicated by the fact that the interaction of a neutron can produce a gamma ray. The converse is also possible, but is much less likely. The types of interactions that neutrons and gamma rays can undergo are discussed in Sections 2.5 and 2.7 respectively, and the interactions that give birth to these radiations are discussed in Sections 2.6 and 2.8 respectively.

Not all quantities that can be determined by transport calculations (for example, differential flux) are easily measured or easily related to a physical or biological effect. However, a quantity that has come to be known as *dose* and that is determined from the energy deposited by the radiation in the receiver (for example, in an instrument or in a human body) is measurable, and calculated results can be related to the same quantity. As a result, whenever a physical or a biological effect is being considered, dose is the quantity that is used to specify the design limit on the intensity of the radiation field.

Unfortunately, several concepts of dose exist, and considerable confusion has arisen with respect to their definitions. Because the problem has not yet been fully resolved, all viewpoints are presented in Section 2.9 of this chapter and the definitions that are employed in this Handbook are specified. Section 2.10 discusses allowable dose limits and the probable effects of such acute doses as might be encountered in a nuclear accident or in warfare.

Finally, it is pointed out that although this chapter was prepared primarily to describe basic concepts and particle interactions of especial interest to the designer of weapons radiation shields, its contents will be equally useful to those engaged in reactor shield design since the radiations involved are the same. The information will also be useful to those who design radiation shields for accelerators or spacecraft, but for these purposes it is incomplete since many more different types of radiations must be considered.

2.1. Quantities Used to Describe Radiation Fields

A complete description of a radiation field would specify the number of particles of a given type and energy which at a given time exist at a given position and travel in a given direction, with all particle types, energies, positions, and directions being considered at all times. However, such complete descriptions are seldom required – except in the most sophisticated particle transport calculations – and a radiation field cannot be measured in such detail. Therefore particle populations are usually described in terms of a fewer number of parameters. The quantities used most frequently in shielding analysis are listed in Table 2.1 and discussed in the following paragraphs. The names given to the differential quantities have not been standardized, and occasionally one finds that a term specifically identified as being differential is actually less differential than a companion term not so designated. While in the first column of Table 2.1 an attempt is made to specify the degree of differentiation in each case, the names used in the text are those in keeping with general usage.

2.1.1. PARTICLE DENSITIES

A knowledge of the particle density over all phase space is equivalent to a complete solution of a particle transport problem and comprises more information than is available from most calculational schemes now in use. When given in seven-dimensional phase space, which consists of three spatial coordinates, the particle's energy, two direction-defining angles, and time, this particle density is defined by

$n(\bar{r},E,\bar{\Omega},t)\,dE\,d\bar{\Omega} \equiv$ the number of particles per unit volume at space point $\bar{r}$ and time t having energies in dE about energy E and directions in $d\bar{\Omega}$ about the unit direction vector $\bar{\Omega}$.

The particle density so defined is doubly differential – in energy and in direction – and less detailed forms will often suffice. For example, one may use the steady-state* particle density differential in energy only, commonly referred to as *differential particle density* and defined by

$n(\bar{r},E)\,dE \equiv$ the number of particles per unit volume at space point $\bar{r}$ having energies in dE about E

$$= \int_{4\pi} n(\bar{r},E,\bar{\Omega})\,d\bar{\Omega}\,dE\,. \qquad (2.1)$$

Or one may use the steady-state *total particle density*, defined as the number of particles per unit volume at space point $\bar{r}$ and given by

$$n(\bar{r}) = \int_{4\pi}\int_0^\infty n(\bar{r},E,\bar{\Omega})\,dE\,d\bar{\Omega} = \int_0^\infty n(\bar{r},E)\,dE\,. \qquad (2.2)$$

2.1.2. FLUX DENSITIES

Even though the concept of particle density is basically simple and has a unique interpretation, experience has shown that the *flux density*[1] or, as it is more commonly referred to, the *flux*,† serves better as the dependent variable in solutions of the transport equation (refer to Chapter 3, Section 3.1). The flux is related to the particle density through the particle's speed, and when described in terms of seven-dimensional phase space the flux is given by

$$\Phi(\bar{r},E,\bar{\Omega},t) = v\,n(\bar{r},E,\bar{\Omega},t)\,, \qquad (2.3)$$

where v is the particle's speed and corresponds to the energy E. (The speed is the scalar magnitude of the particle's velocity vector $\bar{v}$.)

---

*The steady-state, or time-independent, condition will be denoted in phase space notation by dropping the time symbol t; for example, seven-dimensional phase space becomes six dimensional and in phase space notation is given by $(\bar{r},E,\bar{\Omega})$.

†Although this quantity is truly a density and the International Commission on Radiation Units and Measurements recommends the use of the term *flux density*, the simpler term *flux* is ingrained in shielding terminology and will be used in this and other chapters of this Handbook.

Table 2.1. Quantities Used to Describe Particle Populations

Quantity	Name Commonly Used	Symbol	Usual Units	Comments
Particle density differential in energy and angle	Particle density	$n(\bar{r},E,\bar{\Omega},t)$	$\frac{\text{particles}}{\text{cm}^3\cdot\text{MeV}\cdot\text{steradian}}$	$n(\bar{r},E,\bar{\Omega},t)\,dE\,d\bar{\Omega} \equiv$ number of particles per unit volume at the space point $\bar{r}$ and time t which have energies in dE about energy E and directions in $d\bar{\Omega}$ about the unit vector $\bar{\Omega}$.
Particle density differential in energy	Differential particle density	$n(\bar{r},E)$	$\frac{\text{particles}}{\text{cm}^3\cdot\text{MeV}}$	$n(\bar{r},E)\,dE = \int_{4\pi} n(\bar{r},E,\bar{\Omega})\,d\bar{\Omega}\,dE.$ $n(\bar{r},E)\,dE$ = number of particles per unit volume at the space point $\bar{r}$ that have energies in dE about E.
Total particle density	Particle density	$n(\bar{r})$	particles/cm^3	$n(\bar{r}) = \int_0^\infty n(\bar{r},E)\,dE.$ $n(\bar{r})$ = number of particles per unit volume at the space point $\bar{r}$.
Particle flux density differential in energy and angle	Angular flux	$\Phi(\bar{r},E,\bar{\Omega},t)$	$\frac{\text{particles}}{\text{cm}^2\cdot\text{sec}\cdot\text{MeV}\cdot\text{steradian}}$	$\Phi(\bar{r},E,\bar{\Omega},t) = v\,n(\bar{r},E,\bar{\Omega},t)$ = particle speed (v) times the particle density; that is, the units of the angular flux derive from (cm/sec) (particles/cm^3·MeV·steradian). $\Phi(\bar{r},E,\bar{\Omega},t)\,dE\,d\bar{\Omega}$ = flow per unit area and time at space point $\bar{r}$ and time t of particles having energies in dE about E and directions in $d\bar{\Omega}$ about $\bar{\Omega}$ or $\Phi(\bar{r},E,\bar{\Omega},t)\,dE\,d\bar{\Omega}$ = total tracklength traced by particles per unit volume and time at the space point $\bar{r}$ and time t which have energies in dE about E and directions in $d\bar{\Omega}$ about $\bar{\Omega}$; that is, the angular flux is viewed as (particles·cm/sec)/cm^3·MeV·steradian.
Particle flux density differential in energy	Differential flux	$\Phi(\bar{r},E)$	$\frac{\text{particles}}{\text{cm}^2\cdot\text{sec}\cdot\text{MeV}}$	$\Phi(\bar{r},E)\,dE = \int_{4\pi} \Phi(\bar{r},E,\bar{\Omega})\,dE\,d\bar{\Omega}.$ $\Phi(\bar{r},E)\,dE$ = number of particles having energies in dE about E which enter a sphere of unit cross section per unit time at the space point $\bar{r}$ or $\Phi(\bar{r},E)\,dE$ = total tracklength traced by particles per unit volume and time at the space point $\bar{r}$ which have energies in dE about E.
Total particle flux density	Flux	$\Phi(\bar{r})$	$\frac{\text{particles}}{\text{cm}^2\cdot\text{sec}}$	$\Phi(\bar{r}) = \int_0^\infty \Phi(\bar{r},E)\,dE.$ $\Phi(\bar{r})$ = number of particles which enter a sphere of unit cross section per unit time at the space point $\bar{r}$ or $\Phi(\bar{r})$ = total tracklength traced by particles per unit volume and time at the space point $\bar{r}$.

Table 2.1. (continued)

Quantity	Name Commonly Used	Symbol	Usual Units	Comments
Group flux density differential in angle	Group angular flux	$\Phi_G(\bar{r},\bar{\Omega})$,	$\frac{\text{particles}}{\text{cm}^2\cdot\text{sec}\cdot\text{steradian}}$	$\Phi_G(\bar{r},\bar{\Omega}) \equiv \int_{E_{g+1}}^{E_g} \Phi(\bar{r},E,\bar{\Omega})\, dE.$
		$\Phi_G(\bar{r},\mu)$	$\frac{\text{particles}}{\text{cm}^2\cdot\text{sec}\cdot\text{unit cosine}}$	$\Phi_G(\bar{r},\bar{\Omega})$ = angular flux within the energy group ΔE_G. $\Phi_G(\bar{r},\mu)\, d\mu \equiv \Phi_G(\bar{r},\bar{\Omega})\, d\bar{\Omega}$ = total tracklength per unit volume and time at the space point $\bar{r}$ of particles having energies within the energy group ΔE_g and directions defined by direction cosines in $d\mu$ about μ, where $\mu = \bar{\Omega}\cdot\bar{r}/\lvert\bar{r}\rvert$.
Group flux density	Group flux	$\Phi_G(\bar{r})$	$\frac{\text{particles}}{\text{cm}^2\cdot\text{sec}}$	$\Phi_G(\bar{r}) \equiv \int_{E_{g+1}}^{E_g} \Phi(\bar{r},E)\, dE.$ $\Phi_G(\bar{r})$ = total flux within the energy group ΔE_G.
Discrete ordinates flux density	Discrete ordinates flux	$\Phi_{i,G,D}$	$\frac{\text{particles}}{\text{cm}^2\cdot\text{sec}\cdot\text{unit cosine}}$	$\Phi_{i,G,D} \equiv \frac{1}{\Delta\mu_D} \int_{\mu_{d+1}}^{\mu_d} \Phi_G(\bar{r},\mu)\, d\mu.$ $\Phi_{i,G,D} \equiv$ group angular flux averaged over specified segments of μ-space, $\Delta\mu_D$, and corresponding to discrete spatial mesh points $\bar{r}_i$.
Energy flux differential in energy and angle	Angular energy flux	$I(\bar{r},E,\bar{\Omega},t)$	$\frac{\text{MeV}}{\text{cm}^2\cdot\text{sec}\cdot\text{MeV}\cdot\text{steradian}}$	$I(\bar{r},E,\bar{\Omega},t)dE\, d\bar{\Omega} = E\,\Phi(\bar{r},E,\bar{\Omega},t)\, dE\, d\bar{\Omega}$ = energy flow per unit area and time at the space point $\bar{r}$ and time t due to particles which have energies in dE about E and directions in $d\bar{\Omega}$ about $\bar{\Omega}$; here the units of $E\,\Phi(\bar{r},E,\bar{\Omega},t)$, which is equivalent to $I(\bar{r},E,\bar{\Omega},t)$, are (MeV/particle) (particles/cm^2·sec·MeV·steradian).
Energy flux differential in energy	Differential energy flux	$I(\bar{r},E)$	$\frac{\text{MeV}}{\text{cm}^2\cdot\text{sec}\cdot\text{MeV}}$	$I(\bar{r},E)\, dE = E\,\Phi(\bar{r},E)\, dE$ = energy flow per unit time into a sphere of unit cross section at the space point $\bar{r}$ due to particles which have energies in dE about E.
Total energy flux	Total energy flux	$I(\bar{r})$	$\frac{\text{MeV}}{\text{cm}^2\cdot\text{sec}}$	$I(\bar{r}) = \int_0^\infty I(\bar{r},E)\, dE.$ $I(\bar{r})$ = total energy flow per unit time into a sphere of unit cross section at the space point $\bar{r}$.
Fluence	Fluence	ψ	Appropriate units for flux integrated over a specified time interval Δt	$\psi = \int_{t_1}^{t_1+\Delta t} \Phi(t)\, dt.$ ψ = time-integrated flux, where $\Phi(t)$ is any of the fluxes listed above.

Table 2.1. (continued)

Quantity	Name Commonly Used	Symbol	Usual Units	Comments
Current differential in energy and angle	Angular current	$\bar{J}(\bar{r},v,\bar{\Omega},t)$,	$\frac{\text{particles}}{\text{cm}^2\cdot\text{sec}\cdot(\text{cm/sec})\cdot\text{steradian}}$	$\bar{J}(\bar{r},v,\bar{\Omega},t)\,dv\,d\bar{\Omega} = \bar{\Omega}\,v\,n(\bar{r},v,\bar{\Omega},t)\,dv\,d\bar{\Omega}$ = directed flow per unit area (normal to the $\bar{\Omega}$ direction) and time at the space point $\bar{r}$ and time t of particles having speeds in dv about v and directions $d\bar{\Omega}$ about $\bar{\Omega}$.
		$\bar{J}(\bar{r},E,\bar{\Omega},t)$	$\frac{\text{particles}}{\text{cm}^2\cdot\text{sec}\cdot\text{MeV}\cdot\text{steradian}}$	$\bar{J}(\bar{r},E,\bar{\Omega},t)\,dE\,d\bar{\Omega} = \bar{\Omega}\,v\,n(\bar{r},E,\bar{\Omega},t)\,dE\,d\bar{\Omega} = \bar{\Omega}\Phi(\bar{r},E,\bar{\Omega},t)\,dE\,d\bar{\Omega}$ = direction vector $\bar{\Omega}$ times the angular flux.
Current differential in angle	Total angular current	$\bar{J}(\bar{r},\bar{\Omega})$	$\frac{\text{particles}}{\text{cm}^2\cdot\text{sec}\cdot\text{steradian}}$	$\bar{J}(\bar{r},\bar{\Omega}) = \int_0^\infty \bar{J}(\bar{r},E,\bar{\Omega})\,dE = \bar{\Omega}\Phi(\bar{r},\bar{\Omega})$. $\bar{J}(\bar{r},\bar{\Omega})d\bar{\Omega}$ = directed flow per unit area (normal to the $\bar{\Omega}$ direction) and time at the space point $\bar{r}$ and time t of particles having directions in $d\bar{\Omega}$ about $\bar{\Omega}$.
Net current differential in energy	Differential net current	$\bar{J}(\bar{r},E,t)$	$\frac{\text{particles}}{\text{cm}^2\cdot\text{sec}\cdot\text{MeV}}$	$\bar{J}(\bar{r},E,t)\,dE = \int_{4\pi} \bar{J}(\bar{r},E,\bar{\Omega},t)\,d\bar{\Omega} = \int_{4\pi} \bar{\Omega}\Phi(\bar{r},E,\bar{\Omega},t)\,d\bar{\Omega}$. $\bar{J}(\bar{r},E,t)\,dE$ = net flow per unit area and time at the space point $\bar{r}$ and time t of particles having energies in dE about E where the unit area is normal to the direction of the resultant vector $\bar{J}(\bar{r},E,t)$ (which is simply the angular flux-weighted vector summation of the unit vectors $\bar{\Omega}$ over 4π solid angle).
Total net current	Net current	$\bar{J}(\bar{r})$	$\frac{\text{particles}}{\text{cm}^2\cdot\text{sec}}$	$\bar{J}(\bar{r}) = \int_{4\pi} \bar{J}(\bar{r},\bar{\Omega})\,d\bar{\Omega} = \int_{4\pi} \bar{\Omega}\Phi(\bar{r},\bar{\Omega})\,d\bar{\Omega}$. $\bar{J}(\bar{r})$ = net flow of particles per unit area and time at the space point $\bar{r}$ where the unit area is normal to the direction of the resultant vector.
Group current differential in angle	Group angular current	$\bar{J}_G(\bar{r},\bar{\Omega})$	$\frac{\text{particles}}{\text{cm}^2\cdot\text{sec}\cdot\text{steradian}}$	$\bar{J}_G(\bar{r},\bar{\Omega}) = \int_{E_{g+1}}^{E_g} \bar{J}(\bar{r},E,\bar{\Omega})\,dE = \bar{\Omega}\Phi_G(\bar{r},\bar{\Omega})$. $\bar{J}_G(\bar{r},\bar{\Omega})\,d\bar{\Omega}$ = the directed flow per unit area (normal to the $\bar{\Omega}$ direction) and time at the space point $\bar{r}$ and time t of particles having energies within the energy group ΔE_G and having directions in $d\bar{\Omega}$ about $\bar{\Omega}$.
Group net current density	Group net current	$\bar{J}_G(\bar{r})$	$\frac{\text{particles}}{\text{cm}^2\cdot\text{sec}}$	$\bar{J}_G(\bar{r}) = \int_{4\pi} \bar{J}_G(\bar{r},\bar{\Omega})\,d\bar{\Omega} = \int_{4\pi} \bar{\Omega}\Phi_G(\bar{r},\bar{\Omega})\,d\bar{\Omega}$. $\bar{J}_G(\bar{r})$ = net flow of particles per unit area and time at the space point $\bar{r}$ having energies within the energy group ΔE_G, where the unit area is normal to the direction of the resultant vector.

The flux defined in the preceding paragraph is doubly differential and is usually referred to as the *angular flux*. Greater insight into the use of the angular flux as the dependent variable in mathematical descriptions of particle transport is provided by its interpretation either as the tracklengths traversed per unit volume and time or as the flow of particles per unit area and time.

The tracklength interpretation of angular flux follows from the observation that the speed of an individual particle can be considered as its scalar tracklength per unit time. The product of particle density and speed is then the sum of the tracklengths traced by all the particles within a unit volume per unit time,* in which case the definition of the angular flux would be

$\Phi(\bar{r},E,\bar{\Omega},t)\,dE\,d\bar{\Omega} \equiv$ the total tracklengths traversed per unit volume and time at space point $\bar{r}$ and time t by particles having energies in dE about energy E and directions in $d\bar{\Omega}$ about $\bar{\Omega}$.

The interpretation of the angular flux as a flow of particles per unit area and time is closely related to the concept of angular current (see discussion of angular current in Section 2.1.4). It will be shown in the discussion on current that the angular flux is identical with the magnitude of the current vector $\bar{J}$ and thus can be interpreted as

$\Phi(\bar{r},E,\bar{\Omega},t)\,dE\,d\bar{\Omega} \equiv$ the flow per unit area and time at space point $\bar{r}$ and time t of particles having energies in dE about E and directions in $d\bar{\Omega}$ about $\bar{\Omega}$.

When the transport and deposition of the particle's kinetic energy are of concern, the energy flux differential in energy and angle is often used. This quantity, referred to as the *angular energy flux*, is defined by

$I(\bar{r},E,\bar{\Omega},t)\,dE\,d\bar{\Omega} \equiv$ the energy flow per unit area and time at space point $\bar{r}$ and time t due to particles having energies in dE about E and directions in $d\bar{\Omega}$ about $\bar{\Omega}$,

and is related to the angular flux by

$$I(\bar{r},E,\bar{\Omega},t) = E\,\Phi(\bar{r},E,\bar{\Omega},t)\,. \tag{2.4}$$

Many calculational models employ less detailed descriptions of the flux; for example, they may use a description in which steady state is assumed and the angular dependencies are removed by the appropriate solid-angle integration. This reduces the description to four-dimensional phase space and results in a dependent variable representing the particle flux differential in energy. Commonly known as the *differential flux*, this quantity is given by

$$\Phi(\bar{r},E) = \int_{4\pi} \Phi(\bar{r},E,\bar{\Omega})\,d\bar{\Omega}\,. \tag{2.5}$$

Like the angular flux, the differential flux can be interpreted in terms of tracklength per unit volume and time or in terms of the number of particles that enter a unit sphere per unit time. In the latter case, the solid-angle integration can be regarded as a summing of particles that enter a sphere of unit cross section, regardless of their directions of motion. The sphere is in effect generated by the rotation of a circular unit area during the integration over 4π solid angle (see Fig. 2.1). In this context the definition for the differential flux can be restated as

$\Phi(\bar{r},E)\,dE \equiv$ number of particles having energies in dE about E which enter a sphere of unit cross section per unit time at space point $\bar{r}$.

While this definition of the differential flux is descriptive, it is not exact. The mathematically rigorous definition is

$$\Phi(\bar{r},E)\,dE \equiv \lim_{\Delta A \to 0} \frac{N(E)\,dE}{\Delta A}\,, \tag{2.6}$$

which implies the limit process $\Delta A \to 0$, with $N(E)\,dE$ denoting the number of particles having energies in dE about E which enter an "incremental" sphere of cross section ΔA per unit time.

The concept of the incremental sphere is the best way to visualize the energy flux differential in energy. Referred to as the *differential energy flux*, this quantity may be defined by

$I(\bar{r},E)\,dE \equiv$ the energy flow per unit time into a sphere of unit cross section at space point $\bar{r}$ due to particles having energies in dE about E.

*Note that the per-unit-time units of the flux are associated with the particle's speed, which is a function only of the energy. However, the time dependence of the flux is a consequence of the time behavior of the particle density, which does not have time units even though the time symbol t is included in the phase space notation to denote a dependence on time; that is, $n(\bar{r},E,\bar{\Omega},t)$.

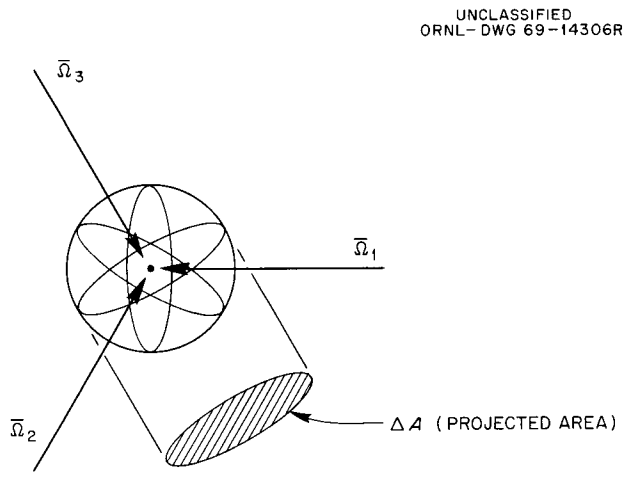

Fig. 2.1. Incremental Sphere Concept of Flux.

The differential energy flux is given by

$$I(\bar{r},E)\,dE = \int_{4\pi} I(\bar{r},E,\bar{\Omega})\,d\bar{\Omega}\,dE = E\,\Phi(\bar{r},E)\,dE\,. \qquad (2.7)$$

Other quantities used are the *total flux*, the *total energy flux*, the *group flux*, the *group angular flux*, and the *discrete ordinates flux*. The total flux, defined alternatively as the total particle tracklength per unit volume and time at space point $\bar{r}$ or as the number of particles that enter a sphere of unit cross section per unit time at space point $\bar{r}$, is obtained by integrating the differential flux over all energies:

$$\Phi(\bar{r}) = \int_0^\infty \Phi(\bar{r},E)\,dE\,. \qquad (2.8)$$

Similarly, the total energy flux, defined as the total energy flow per unit time into a sphere of unit cross section at space point $\bar{r}$, is obtained by an integration of the differential energy flux over all energies:

$$I(\bar{r}) = \int_0^\infty I(\bar{r},E)\,dE\,. \qquad (2.9)$$

The total flux has only limited application to practical shielding problems because of the strongly energy-dependent nature of the particle's behavior. A more useful approach is to divide the total energy range into *NOG* energy intervals, called energy groups,

$$\Delta E_G \equiv E_g - E_{g+1},^*\ G = 1,2\ldots NOG,$$

*The subscripts g and $g+1$ refer to the upper and lower limits respectively of the Gth energy group, and $G=1$ corresponds to the highest energy group. An alternate convention would associate $G=1$ with the lowest energy group and the subscripts $g+1$ and g would then correspond to the upper and lower energy limits.

and to define the *group flux* as the integral of the differential flux over the corresponding energy group:

$$\Phi_G(\bar{r}) \equiv \int_{E_{g+1}}^{E_g} \Phi(\bar{r},E)\,dE\,, \qquad (2.10)$$

with the obvious constraint that

$$\Phi(\bar{r}) = \sum_{NOG} \Phi_G(\bar{r})\,. \qquad (2.11)$$

The group angular flux (group flux differential in angle) has a similar definition and is obtained by integrating the angular flux over a specific energy group:

$$\Phi_G(\bar{r},\bar{\Omega}) \equiv \int_{E_{g+1}}^{E_g} \Phi(\bar{r},E,\bar{\Omega})\,dE\,. \qquad (2.12)$$

For problems that involve directional symmetry, the group angular flux can be rewritten in terms of a new angular variable $\mu = \bar{\Omega}\cdot\bar{r}/|\bar{r}|$, the direction cosine:

$$\Phi_G(\bar{r},\mu)\,d\mu = \Phi_G(\bar{r},\bar{\Omega})\,d\bar{\Omega}\,. \qquad (2.13)$$

The group angular flux can then be defined as the total particle tracklength per unit volume and time at space point $\bar{r}$ of particles with energies within energy group ΔE_G and directions defined by direction cosines which lie in $d\mu$ about μ.

A mathematical treatment which evaluates the angular flux at discrete angles, called discrete ordinates forms the bases for many detailed numerical solutions of the transport equation. A form of discrete ordinates could be simply group-angular-flux values that correspond to given spatial positions and particle directions. However, a more useful form is obtained by integrating the group angular flux over specified segments of μ space, $\Delta\mu_D = \mu_d - \mu_{d+1}$, $D = 1,2\ldots NOA$,

$$\Phi_{G,D}(\bar{r}) \equiv \frac{1}{\Delta\mu_D}\int_{\mu_{d+1}}^{\mu_d} \Phi_G(\bar{r},\mu)\,d\mu\,. \qquad (2.14)$$

The "mean value" approximation to Eq. 2.14 is given by

$$\Phi_{G,D}(\bar{r}) \equiv \Phi_G(\bar{r},\mu_D), \qquad (2.15)$$

where μ_D is a mean value* for the direction cosine over the increment $\Delta\mu_D$. The *discrete ordinate fluxes* $\Phi_{i,G,D}$† are those values of $\Phi_{G,D}(\bar{r})$ which correspond to the spatial meshpoints $\bar{r}_i$:

$$\Phi_{i,G,D} \equiv \Phi_{G,D}(\bar{r}_i) . \tag{2.16}$$

2.1.3. FLUENCES

A useful measure of total exposure to a flux for applications involving energy deposition or dose is the integral quantity called *fluence.* Fluence is defined by the International Commission on Radiation Units and Measurements as the quotient of ΔN divided by ΔA, where ΔN is the number of particles that enter a sphere of cross-sectional area ΔA and the Δ's imply a limiting process.[1] This definition is equivalent to regarding fluence as a time-integrated flux over some specified time interval. As such, the fluence can be written as

$$\psi = \int_{t_1}^{t_2 = t_1 + \Delta t} \Phi(t)\, dt , \tag{2.17}$$

where Δt corresponds to some specified time interval and $\Phi(t)$ can be any one of the several kinds of flux described in Section 2.1.2. For example, the *energy fluence* is

$$F(\bar{r}) = \int_{t_1}^{t_2 = t_1 + \Delta t} I(\bar{r},t)\, dt . \tag{2.18}$$

(NOTE: The symbolism for particle fluences and fluxes has been confusing in the past, with the symbols nvt and Φ being used for both. In order to avoid confusion in this chapter, Φ is reserved for particle fluxes and when particle fluences are intended, the symbol ψ is used.)

*μ_D may be adjusted to give the equality; for well-behaved functions the closer μ_D is to the true mean, the better the approximation.

†The following subscript notation is used throughout this section and in Chapter 3: subscripts *I, G,* and *D* denote functions whose values are associated with the *I*th space interval, the *G*th energy group, and the *D*th angular interval, respectively; *i* and *i*+1 refer to a function evaluated at the lower and upper limits of the *I*th space interval; *g*+1 and *g* refer to a function evaluated at the lower and upper limits of the *G*th energy group; *d*+1 and *d* refer to a function evaluated at the lower and upper limits of the *D*th angular interval.

2.1.4. CURRENT DENSITIES

The characteristic property of the current variable is its close relation to the convective (leakage) effects in the theoretical description of particle transport. The most general form of the current variable is differential both in energy (or speed) and in angle. Called the *angular current density* or, more frequently the *angular current*, this quantity is symbolized by $\bar{J}(\bar{r},v,\bar{\Omega},t)$ and is defined as the directed flow per unit area (normal to the $\bar{\Omega}$ direction) and time at the space point $\bar{r}$ and time t of particles having speeds in dv about v and directions in $d\bar{\Omega}$ about $\bar{\Omega}$.

The relation between current and particle density can be established by considering that (1) the product of $\bar{v}$ and the particle density can be regarded as a vector sum of the individual co-directional velocity vectors ($\bar{v}$), yielding the resultant vector $\bar{J} = n\,\bar{v}$, or (2) the ($v \times dt \times dA \times n$) particles contained within the volume element shown in Fig. 2.2 will all exit through the differential area dA within differential time dt if $\bar{v} = v\bar{\Omega}$. These models can be expressed mathematically in terms of the angular current as

$$\bar{J}(\bar{r},v,\bar{\Omega},t)\, dv\, d\bar{\Omega} = \bar{\Omega}\, v\, n(\bar{r},v,\bar{\Omega},t)\, dv\, d\bar{\Omega} , \tag{2.19}$$

and since the particle's kinetic energy is a function of its speed, Eq. 2.19 can be rewritten as

$$\bar{J}(\bar{r},E,\bar{\Omega},t)\, dE\, d\bar{\Omega} = \bar{\Omega}\, v\, n(\bar{r},E,\bar{\Omega},t)\, dE\, d\bar{\Omega} , \tag{2.20}$$

where $\bar{J}(\bar{r},E,\bar{\Omega},t)\, dE = \bar{J}(\bar{r},v,\bar{\Omega},t)\, dv$ and $n(\bar{r},E,\bar{\Omega},t)\, dE = n(\bar{r},v,\bar{\Omega},t)\, dv$. Then when $v\, n(\bar{r},E,\bar{\Omega},t)$ is identified as the angular flux, the relation between the angular flux

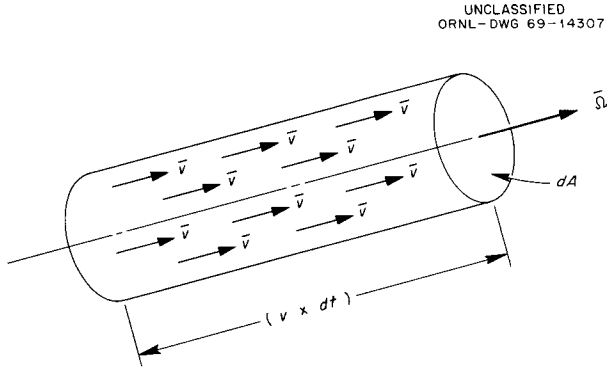

Fig. 2.2. Particle Flow Concept of Current. The particles contained within the volume element will all exit through the differential area dA within dt if $\bar{v} = v\bar{\Omega}$.

and the angular current pointed out in Section 2.1.2 is obtained:

$$\bar{J}(\bar{r},E,\bar{\Omega},t)\,dE\,d\bar{\Omega} = \bar{\Omega}\,\Phi(\bar{r},E,\bar{\Omega},t)\,dE\,d\bar{\Omega}\,. \qquad (2.21)$$

Other less detailed forms of the angular current are the *group angular current* $\bar{J}_G(\bar{r},\bar{\Omega})$ and the total angular current $\bar{J}(\bar{r},\bar{\Omega})$, which are obtained by integrations over an energy group and all energies, respectively:

$$\bar{J}_G(\bar{r},\bar{\Omega}) \equiv \int_{E_{g+1}}^{E_g} \bar{J}(\bar{r},E,\bar{\Omega})\,dE = \bar{\Omega}\,\Phi_G(\bar{r},\bar{\Omega})\,; \qquad (2.22)$$

$$\bar{J}(\bar{r},\bar{\Omega}) \equiv \int_0^{\infty} \bar{J}(\bar{r},E,\bar{\Omega})\,dE = \bar{\Omega}\,\Phi(\bar{r},\bar{\Omega})\,. \qquad (2.23)$$

It is apparent that the angular current variables all have essentially the same simple relation with the corresponding angular flux variables, because the energy integrations are performed directly on the flux variables. For example, in the case of the group angular current,

$$\bar{J}_G(\bar{r},\bar{\Omega}) = \int_{E_{g+1}}^{E_g} \bar{\Omega}\,\Phi(\bar{r},E,\bar{\Omega})\,dE$$

$$= \bar{\Omega}\int_{E_{g+1}}^{E_g} \Phi(\bar{r},E,\bar{\Omega})\,dE = \bar{\Omega}\,\Phi_G(\bar{r},\bar{\Omega})\,. \qquad (2.24)$$

The integral of the angular current over all directions (4π solid angle) constitutes a vector summation, and the resultant vector is regarded as the *net current*, often called simply *current.*

The net current differential in energy only, referred to as the *differential net current,* is defined by

$\bar{J}(\bar{r},E,t)\,dE \equiv$ the net flow per unit area and time at space point $\bar{r}$ and time t of particles having energies in dE about E, where the unit area is normal to the direction of the resultant vector $\bar{J}(\bar{r},E,t)$

$$= \int_{4\pi} \bar{J}(\bar{r},E,\bar{\Omega},t)\,d\bar{\Omega}\,dE$$

$$= \int_{4\pi} \bar{\Omega}\,\Phi(\bar{r},E,\bar{\Omega},t)\,d\bar{\Omega}\,dE\,, \qquad (2.25)$$

which is the angular flux-weighted vector summation of the unit vectors $\bar{\Omega}$ over 4π solid angle. The *group net current* $J_G(\bar{r})$ and *total net current* $\bar{J}(\bar{r})$ are 4π solid-angle integrations of the group angular current and total angular current, respectively:

$$\bar{J}_G(\bar{r}) = \int_{4\pi} \bar{J}_G(\bar{r},\bar{\Omega})\,d\bar{\Omega} = \int_{4\pi} \bar{\Omega}\,\Phi_G(\bar{r},\bar{\Omega})\,d\bar{\Omega}\,; \qquad (2.26)$$

$$\bar{J}(\bar{r}) = \int_{4\pi} \bar{J}(\bar{r},\bar{\Omega})\,d\bar{\Omega} = \int_{4\pi} \bar{\Omega}\,\Phi(\bar{r},\bar{\Omega})\,d\bar{\Omega}\,. \qquad (2.27)$$

The flow of $\bar{\Omega}$-directed particles across an arbitrarily oriented differential area is a necessary concept in the description of the directed flow of particles in terms of a specific coordinate system and can be related to the angular current $\bar{J}(\bar{\Omega})$* by consideration of Fig. 2.3, where the direction vector $\bar{n}$ is normal to the differential area. The number of $\bar{\Omega}$-directed particles crossing the differential area dA per unit time is equal to $\bar{J}(\bar{\Omega})\cdot(\bar{n}\,dA)$. A scalar current $J_n(\bar{\Omega})$ that describes the flow of the $\bar{\Omega}$-directed particles per unit area normal to the direction $\bar{n}$ is defined as

$$J_n(\bar{\Omega})\,dA \equiv \bar{J}(\bar{\Omega})\cdot(\bar{n}\,dA)\,; \qquad (2.28)$$

it follows that

$$J_n(\bar{\Omega}) = \bar{n}\cdot\bar{J}(\bar{\Omega}) = \bar{\Omega}\cdot\bar{n}\,\Phi(\bar{\Omega}) = \cos\theta\,\Phi(\bar{\Omega})\,, \qquad (2.29)$$

where

$\bar{n}$ = the unit vector corresponding to an arbitrary direction,

n = a coordinate-identifying subscript, for example, $n \equiv x$ when $\bar{n} \equiv \bar{i}$,

$J_n(\bar{\Omega})$ = the flow of $\bar{\Omega}$-directed particles per unit area (normal to the direction $\bar{n}$) and time,

$\Phi(\bar{\Omega})$ = the angular flux variable corresponding to the angular current $\bar{J}(\bar{\Omega})$.

Note that $J_n(\bar{\Omega})$ is a scalar quantity but is uniquely related to the coordinate system through the direction unit vector $\bar{n}$. The corresponding vector current is given by

$$\bar{J}_n(\bar{\Omega}) = \bar{n}\,J_n(\bar{\Omega}) = \bar{n}\,\bar{J}(\bar{\Omega})\cdot\bar{n}\,, \qquad (2.30)$$

where the vector $\bar{J}_n(\bar{\Omega})$ is the component of the vector $\bar{J}(\bar{\Omega})$ with respect to the $\bar{n}$ direction and $J_n(\bar{\Omega})$ is the

*In this further discussion of current, the notation $\bar{J}(\bar{\Omega})$ will be used to denote any of the angular currents and $\bar{J}$ the corresponding net current: for example, $\bar{J}(\bar{\Omega})$ may represent $\bar{J}(\bar{r},E,\bar{\Omega},t)$, $\bar{J}_G(\bar{r},\bar{\Omega},t)$, or $\bar{J}(\bar{r},\bar{\Omega})$ and $\bar{J}$ may represent $\bar{J}(\bar{r},E,t)$, $\bar{J}_G(\bar{r})$, or $\bar{J}(\bar{r})$.

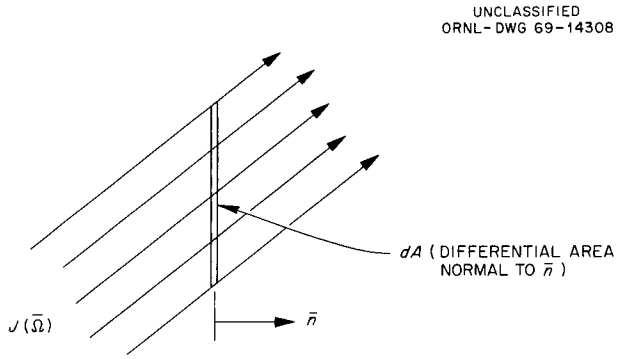

Fig. 2.3. Schematic of Particle Flow Across an Arbitrarily Oriented Surface.

projection of the vector $\bar{J}(\bar{\Omega})$ on the $\bar{n}$ axis and also the magnitude of the component $\bar{J}_n(\bar{\Omega})$.

The three components of $\bar{J}(\bar{\Omega})$ in cartesian coordinates are given by

$$\bar{J}_x(\Omega) = \bar{i}\, J_x(\bar{\Omega}) = \bar{i}\, \Phi(\bar{\Omega})\, (\bar{i}\cdot\bar{\Omega}) ,$$

$$\bar{J}_y(\Omega) = \bar{j}\, J_y(\bar{\Omega}) = \bar{j}\, \Phi(\bar{\Omega})\, (\bar{j}\cdot\bar{\Omega}) , \qquad (2.31)$$

$$\bar{J}_z(\Omega) = \bar{k}\, J_z(\bar{\Omega}) = \bar{k}\, \Phi(\bar{\Omega})\, (\bar{k}\cdot\bar{\Omega}) ,$$

and $\bar{J}(\bar{\Omega})$ is equal to the vector sum of the three components:

$$\begin{aligned}\bar{J}(\bar{\Omega}) &= \bar{J}_x(\bar{\Omega}) + \bar{J}_y(\bar{\Omega}) + \bar{J}_z(\bar{\Omega}) \\ &= \bar{i}\, J_x(\bar{\Omega}) + \bar{j}\, J_y(\bar{\Omega}) + \bar{k}\, J_z(\bar{\Omega}) . \end{aligned} \qquad (2.32)$$

The net flow of particles across a unit area normal to the $\bar{n}$ direction is obtained by integrating $J_n(\bar{\Omega})$ over all directions:

$$J_n = \int_{4\pi} J_n(\bar{\Omega})\, d\bar{\Omega} = \int_{4\pi} \bar{n}\cdot\bar{J}(\bar{\Omega})\, d\bar{\Omega} = \bar{n}\cdot\bar{J} . \qquad (2.33)$$

Further, J_n can be represented in terms of the partial currents* J_n^+ and J_n^- such that

$$J_n = J_n^+ - J_n^- , \qquad (2.34)$$

where

$J_n^+ \equiv$ the flow per unit area (normal to the $\bar{n}$ direction) and time of particles having *positive* direction cosines relative to the $\bar{n}$ direction $= \int_{\bar{\Omega}\cdot\bar{n} > 0} J_n(\bar{\Omega})\, d\bar{\Omega}$,

$J_n^- \equiv$ the flow per unit area (normal to the $\bar{n}$ direction) and time of particles having *negative* direction cosines relative to the $\bar{n}$ direction $= \int_{\bar{\Omega}\cdot\bar{n} < 0} J_n(\bar{\Omega})\, d\bar{\Omega}$.

The partial currents do not occur explicitly in most theoretical formulations of particle transport; however, the boundary conditions of many problems of interest are best expressed in terms of the partial current variable.

2.1.5. ADJOINT FLUX

The *adjoint flux* does not correspond in the usual sense to a real physical quantity. Instead it is the flux associated with the adjoint equation when that equation is interpreted to describe the transport of hypothetical radiation particles, sometimes called "adjunctons." The rationale of the concept of adjunctons follows at least in part from the similarity of the adjoint equation to the Boltzmann transport equation.† Integral forms of these two equations are given by Eqs. 2.35 and 2.36 respectively, and a coupling between the two is provided by Eq. 2.37:

$$\Phi^*(P) = \int K(P \to P')\, \Phi^*(P')\, dP' + f(P) , \qquad (2.35)$$

$$\chi(P) = \int \chi(P')\, K(P' \to P)\, dP' + S(P) , \qquad (2.36)$$

$$\lambda = \int S(P)\, \Phi^*(P)\, dP = \int \chi(P)\, f(P)\, dP , \qquad (2.37)$$

where

$\Phi^*(P) =$ the adjoint flux, defined as the expected value of the present and future contributions to the effect of interest by a radiation particle leaving a collision at a point whose coordinates in phase space are denoted by P,

*The partial currents are usually defined to be positive numbers, with their difference $(J_n^+ - J_n^-)$ determining the sign of J_n.

†Derivations, relations, and other useful and interesting properties of the various forms of the Boltzmann equation are given in Chapter 3 of this Handbook.

$K(P' \rightarrow P)\, dP$ = the probability that a particle experiencing an event at a point P' in phase space will experience another event at a point whose phase space coordinates lie within dP about P,

$f(P)$ = the payoff function, which is the probable, or expected, direct contribution to the effect of interest by a particle leaving a collision at point P in phase space,

$\chi(P)\, dP$ = the expected number of particles leaving collisions at points whose phase space coordinates lie within dP about P, $\chi(P)$ being called the "emergent particle density,"

$S(P)\, dP$ = the expected number of initial (source) events which occur within the phase space coordinates dP about P,

λ = the effect of interest which can be calculated if either (the adjoint flux and source function) or (the emergent particle density and payoff function) are known.

The adjoint equation, which mathematically defines the characteristics of the adjunctons, has often been referred to as the "backward" equation because the movement of adjunctons is backward to that of real particles. That is, they originate at a point in phase space associated with the detector and move in the direction of phase space that corresponds to the real source. This behavior requires that in a collision the adjuncton gain energy, which contradicts the usual energy conservation principles unless *prior to the collision* the target nucleus has the kinetic energy it would have acquired in a real collision process and the particle has the final energy of the adjuncton. This precludes the assignment of physical properties to the adjunctons that would resemble those of real particles.

The lack of physical properties is not a serious shortcoming, however, since adjunctons are not useful as radiation particles per se. Rather, the adjoint flux which may be mathematically evaluated for some point in phase space has the precise interpretation of "value function." The value function has been defined to be a measure of the present and future contributions of a real particle at some point in phase space to an effect of interest and as such has been used to bias the Monte Carlo analysis of the behavior of real particles (neutrons and gamma rays). This is accomplished by modifying the basic stochastic processes so that event densities that contribute most strongly to the effect of interest are sampled most frequently. The transmission probability used in the Monte Carlo analysis is modified by using the value function as an importance function, with the particle's "weight" being adjusted to preserve parity with the true analog calculation.

Calculation of the answer of interest through Monte Carlo solution of the adjoint problem avoids the difficulties associated with estimation to a point detector, provided, of course, that the source has a more agreeable configuration. Also, the adjoint concept provides a fundamental basis for perturbation analyses.

Since the adjoint equation is very similar to the usual Boltzmann transport equation, it is not surprising that methods developed to solve the latter will also apply to the former. For example, adjoint fluxes have been calculated using the techniques of diffusion theory, Monte Carlo, and transport theory. Consequently, there should be no serious practical or fundamental difficulties in calculating the adjoint flux.

2.2. Special Radiation Fields

Certain radiation fields are basic to many of the mathematical models that describe particle transport, and they possess functional simplicities that sometimes permit analytical solutions. In this section four such fields are presented in terms of the various flux and current variables. They are a monodirectional beam, an isotropic flux field, a point source, and an isotropic plane source.

2.2.1. MONODIRECTIONAL BEAM

The monodirectional beam, shown schematically in Fig. 2.4, consists of a one-dimensional system of particles that are all moving in the same direction $\bar{\Omega}_0$. It is described in most detail in terms of the angular current:

$$\bar{J}(\bar{r},E,\bar{\Omega})\,dE\,d\bar{\Omega} = \bar{\Omega}\,J_0\,F(E)\,\delta(\bar{\Omega},\bar{\Omega}_0)\,dE\,d\bar{\Omega}\,, \quad (2.38)$$

where J_0 is the magnitude of the current (particles cm^{-2} sec^{-1}) for a unit area normal to the $\bar{\Omega}_0$ direction, $F(E)$ is the normalized energy spectrum with the property

$$\int_0^\infty F(E)\,dE = 1\,, \quad (2.39)$$

and $\delta(\bar{\Omega},\bar{\Omega}_0)$ is an angular delta function* with the property

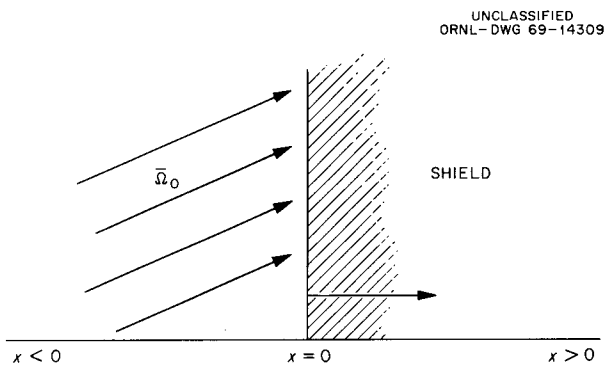

Fig. 2.4. Monodirectional Beam Incident on the Shield.

$$\int_{4\pi} g(\bar{\Omega})\,\delta(\bar{\Omega},\bar{\Omega}_0)\,d\bar{\Omega} = g(\bar{\Omega}_0)\,, \quad (2.40)$$

a mathematical operation that aligns all direction vectors with $\bar{\Omega}_0$.

When the monodirectional beam is specified to be monoenergetic, which it frequently is for calculational convenience, the Dirac delta function with the property

$$\int_0^\infty f(E)\,\delta(E - E_0)\,dE = f(E_0) \quad (2.41)$$

may be used to describe the energy "spectrum" of the beam. That is,

$$\bar{J}(\bar{r},E,\bar{\Omega})\,dE\,d\bar{\Omega} = \bar{\Omega}\,J_0\,\delta(E - E_0)\,\delta(\bar{\Omega},\bar{\Omega}_0)\,dE\,d\bar{\Omega}\,. \quad (2.42)$$

Integration of Eq. 2.42 over all directions (4π solid angle) yields the differential net current

$$\bar{J}(\bar{r},E) = \int_{4\pi} \bar{J}(\bar{r},E,\bar{\Omega})\,d\bar{\Omega} = J_0 F(E) \int_{4\pi} \bar{\Omega}\delta(\bar{\Omega},\bar{\Omega}_0)\,d\bar{\Omega} = \bar{\Omega}_0\,J_0\,F(E)\,, \quad (2.43)$$

and a subsequent integration over all energies gives the total net current

$$\bar{J}(\bar{r}) = \int_0^\infty \bar{J}(\bar{r},E)\,dE = \bar{\Omega}_0\,J_0 \int_0^\infty F(E)\,dE = \bar{\Omega}_0\,J_0\,. \quad (2.44)$$

*A delta function is simply a mathematical notation to indicate that the function is non-zero at only one particular value of the argument.

The angular flux* for the beam is equal to the scalar magnitude of the angular current and is given by

$$\Phi(\bar{r},E,\bar{\Omega}) = J_0\ \delta(E - E_0)\ \delta(\bar{\Omega},\bar{\Omega}_0)\ . \qquad (2.45)$$

The differential flux is obtained by integrating the angular flux over 4π steradians,

$$\Phi(\bar{r},E) = \int_{4\pi} \Phi(\bar{r},E,\bar{\Omega})\, d\bar{\Omega}$$

$$= J_0\ \delta(E - E_0)\ , \qquad (2.46)$$

and the total flux is obtained by integrating the differential flux over all energies,

$$\Phi(\bar{r}) = \int_0^\infty \Phi(\bar{r},E)\, dE = J_0\ . \qquad (2.47)$$

The beam concept is primarily used to specify a source configuration at a surface boundary and as such is usually regarded as a boundary condition. The partial current with respect to the positive x direction is

$$J_x^+ = (\bar{\Omega}_0 \cdot \bar{i})\ J_0\ . \qquad (2.48)$$

The partial current in the negative direction, J_x^-, cannot be used as a boundary condition in this situation because the reflected particles would also contribute to the partial current in the negative direction, which is unknown prior to the solution of a problem with an incident beam source configuration.

2.2.2. ISOTROPIC FLUX FIELD

The radiation field for many physical situations can be regarded as being isotropic with respect to the angular distribution of the particle velocity vectors; that is, motion in any direction is equally probable. The angular flux for this condition is simply the differential flux $\Phi_0(\bar{r},E)$ divided by 4π steradians,

$$\Phi(\bar{r},E,\bar{\Omega}) = \frac{\Phi_0(\bar{r},E)}{4\pi}\ , \qquad (2.49)$$

and the total flux is the differential flux integrated over all energies,

$$\Phi_0(\bar{r}) = \int_0^\infty \Phi_0(\bar{r},E)\, dE\ . \qquad (2.50)$$

The angular current is

$$\bar{J}(\bar{r},E,\bar{\Omega}) = \bar{\Omega}\ \Phi(\bar{r},E,\bar{\Omega}) = \frac{\bar{\Omega}\Phi_0(\bar{r},E)}{4\pi}\ , \qquad (2.51)$$

and the differential net current is obtained by integrating the angular current over all directions. For an isotropic flux field the differential net current is characteristically zero:

$$\bar{J}(\bar{r},E) = \int \bar{J}(\bar{r},E,\bar{\Omega})\, d\bar{\Omega}$$

$$= \frac{\Phi_0(\bar{r},E)}{4\pi} \int_{4\pi} \bar{\Omega}\, d\bar{\Omega} = 0\ . \qquad (2.52)$$

Under the concept of an isotropic flux field the positive partial current is sometimes used to specify an equivalent surface source configuration. Consider, for example, a unit area normal to the direction vector $\bar{n}$ as shown in Fig. 2.5. The scalar angular current that

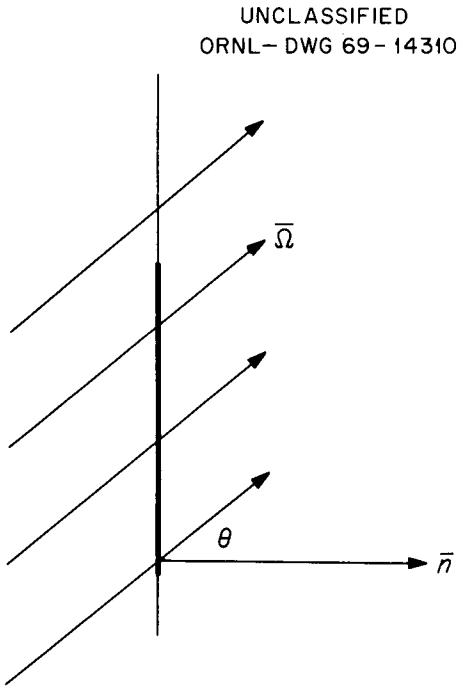

Fig. 2.5. Orientation of $\bar{\Omega}$-Directed Particles with Respect to a Unit Area Normal to the Direction Vector $\bar{n}$.

*The flux, usually referred to as the "incident flux," would not be the flux existing in a real situation since backscattering would contribute to the flux at a surface.

describes the flow of $\bar{\Omega}$-directed particles in terms of a unit area normal to the $\bar{n}$ direction is given by

$$J_n(\bar{r},E,\bar{\Omega}) = \bar{n}\cdot\bar{J}(\bar{r},E,\bar{\Omega}) = \bar{n}\cdot\bar{\Omega}\,\Phi(\bar{r},E,\bar{\Omega}) , \qquad (2.53)$$

and the positive partial current that corresponds to the $\bar{n}$ direction is obtained by appropriate integrations:

$$\begin{aligned} J_n^+(\bar{r}) &= \int_{\bar{n}\cdot\bar{\Omega}>0} \int_0^\infty J_n(\bar{r},E,\bar{\Omega})\, dE\, d\bar{\Omega} \\ &= \int_{\bar{n}\cdot\bar{\Omega}>0} \int_0^\infty \bar{n}\cdot\bar{\Omega}\,\frac{\Phi_0(\bar{r},E)}{4\pi}\, dE\, d\bar{\Omega} \\ &= \frac{\Phi_0(\bar{r})}{4\pi} \int_0^{\pi/2} \cos\theta(2\pi\sin\theta\, d\theta) \\ &= \frac{\Phi_0(\bar{r})}{4} . \end{aligned} \qquad (2.54)$$

It can be seen that the total flux $\Phi_0(\bar{r})$, which corresponds to a 4π solid-angle integration of the angular flux, is exactly four times as large as the corresponding positive partial current.

In many real situations the angular flux, although anisotropic, can be regarded as being isotropic in the forward half-space (or in 2π angular directions). For this case the positive partial current would have essentially the same magnitude as a positive partial current in an isotropic flux field would have. As a result it has become standard practice in shielding calculations to define a new total flux, referred to as the 2π total flux* and given by

$$\Phi_0^{2\pi}(\bar{r}) = \int_{2\pi} \Phi(\bar{r},\bar{\Omega})\, d\bar{\Omega} . \qquad (2.55)$$

where the 2π solid-angle integration is accomplished in the forward half-space. Since for the isotropic flux field the 4π total flux is exactly two times the 2π total flux, the positive partial current can be expressed as

$$J^+(\bar{r}) = \Phi_0^{2\pi}(\bar{r})/2 . \qquad (2.56)$$

From the above it is obvious that care must be exercised in applying this formula, which was derived on the basis of a $J_n^+(\bar{r})$ source condition, since either the 2π total flux $\Phi_0^{2\pi}(\bar{r})$ or the 4π total flux $\Phi_0(\bar{r})$ may be specified for a typical problem. The corresponding partial current would be either $\Phi_0^{2\pi}(\bar{r})/2$ or $\Phi_0(\bar{r})/4$, and a factor-of-2 error could result unless it is clear which total flux is specified.

*The 2π total flux is also called the *incident flux*.

2.2.3. POINT SOURCE

The general volumetric source term in seven-dimensional phase space is defined as

$S(\bar{r},E,\bar{\Omega},t)\, d\bar{r}\, dE\, d\bar{\Omega}$ = the number of particles having energies in dE about E and directions in $d\bar{\Omega}$ about $\bar{\Omega}$ that are emitted per unit time at the time t from the differential volume $d\bar{r}$ at the space point $\bar{r}$.

A useful specialization of the general source term is the *angular point source,* which is given by

$S_0(\bar{r}_0,E,\bar{\Omega},t)\, dE\, d\bar{\Omega}$ = the number of particles having energies in dE about E and directions in $d\bar{\Omega}$ about $\bar{\Omega}$ that are emitted per unit time at time t from a point source located at the space point $\bar{r}_0$.

The angular point source is related to the general source term by the identity

$$S_0(\bar{r}_0,E,\bar{\Omega},t) \equiv \int_{4\pi}\int_{\text{all space}} S(\bar{r},E,\bar{\Omega}',t)\,\delta(\bar{\Omega},\bar{\Omega}')\, d\bar{r}\, d\bar{\Omega}' , \qquad (2.57)$$

where the general source term is specialized for the point-source configuration by inclusion of the Dirac delta function

$$S(\bar{r},E,\bar{\Omega}',t) = \delta(\bar{r}-\bar{r}_0)\, S_0(E,\bar{\Omega}',t) , \qquad (2.58)$$

and $S_0(E,\bar{\Omega}',t)$ is an energy-, angle-, and time-dependent source intensity factor. For the usual problem the assumption of energy-angle separability is permissible, and the source intensity factor can be expressed as

$$S_0(E,\bar{\Omega},t) = S_0(t)\, F(E)\, g(\bar{\Omega}) , \qquad (2.59)$$

where $S_0(t)$, the source intensity factor, is

$$S_0(t) = \int_{4\pi}\int_0^\infty S_0(E,\bar{\Omega},t)\, dE\, d\bar{\Omega} , \qquad (2.60)$$

and the other terms are defined as

$\delta(\bar{r}-\bar{r}_0)$ = the Dirac delta function which locates the point source at $\bar{r}_0$,

$F(E)$ = normalized energy spectrum,

$g(\bar{\Omega})$ = normalized directional probability density function having the property $\int_{4\pi} g(\bar{\Omega})\, d\bar{\Omega} = 1$,

$g(\bar{\Omega})\, d\bar{\Omega}$ = fraction of particles having directions in $d\bar{\Omega}$ about $\bar{\Omega}$,

$\delta(\bar{\Omega},\bar{\Omega}')$ = angular delta function which aligns the directions of the emitted particles with the direction $\bar{\Omega}$,

$\bar{\Omega}$ = direction vector which lies along the vector $\bar{r} - \bar{r}_0$ as shown in Fig. 2.6.

Evaluation of the integrals in Eq. 2.57 shows that

$$S_0(\bar{r}_0,E,\bar{\Omega},t) = S_0(t)\, F(E)\, g(\bar{\Omega})\,. \qquad (2.61)$$

For isotropic emission $g(\bar{\Omega})\, d\bar{\Omega} = d\bar{\Omega}/4\pi$, in which case

$$S_0(\bar{r}_0,E,\bar{\Omega},t) = \frac{S_0(t)}{4\pi} F(E)\,. \qquad (2.62)$$

The differential point source is obtained by integrating Eq. 2.61 over all directions. Thus

$$S_0(\bar{r}_0,E,t) = S_0(t)\, F(E)\,. \qquad (2.63)$$

Similarly, the total number of particles emitted per unit time at time t, $S_0(t)$, is obtained by integrating the differential point source over all energies. Finally, if total emission of particles is desired, the time-dependent source intensity factor $S_0(t)$ is integrated over some specific interval of time. It should be noted that the various mathematical descriptions of the point source presented here apply to both steady-state and time-dependent source conditions. For the steady-state problem the phase space notation becomes $(\bar{r},E,\bar{\Omega})$, and an emission rate constant in time is presumed.

Many source configurations can be represented by a point source or a simple arrangement of point sources; for example, isotropic line and plane sources consist of appropriate distributions of isotropic point sources. Also, the kernel technique, known as the method of Green's functions, has for its basis the point kernel, the point kernel being the solution to a problem with a unit point source. In summary, the point source is a most elementary and versatile source configuration and has considerable application to complex source configurations such as the detonation of a nuclear weapon.

2.2.4. ISOTROPIC PLANE SOURCE

An isotropic plane source, depicted in Fig. 2.7, can be regarded as an arbitrary distribution of unit isotropic point sources, and in six-dimensional phase space is defined as

$S(x_0,y,z,E,\bar{\Omega})\, dE\, d\bar{\Omega} \equiv$ the number of particles having energies in dE about E and directions in $d\bar{\Omega}$ about $\bar{\Omega}$ that are emitted per unit time from a unit area located at x_0,y,z and normal to the direction vector $\bar{n}$

$$= S(y,z)\frac{F(E)}{4\pi} dE\, d\bar{\Omega}\,, \qquad (2.64)$$

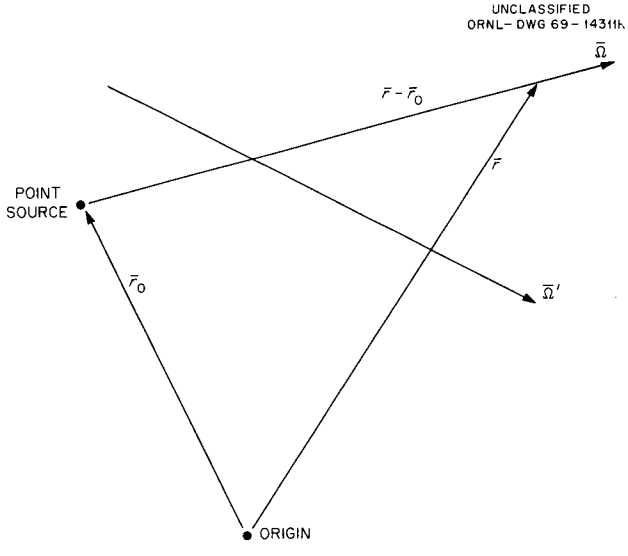

Fig. 2.6. Point Source Specified in General $\bar{r}$ Space.

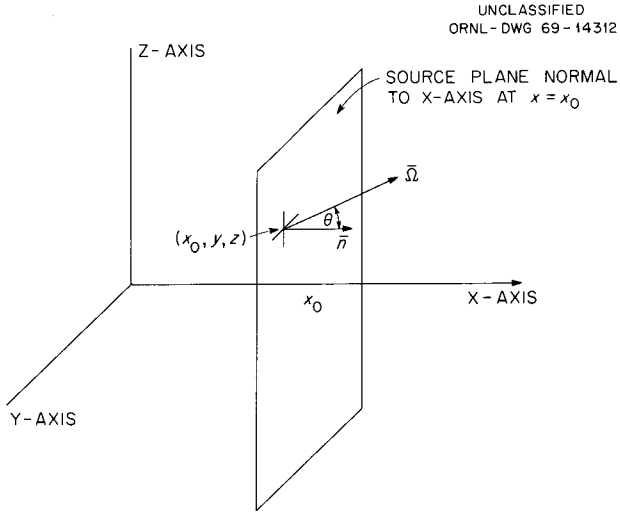

Fig. 2.7. Orientation of Isotropic Plane Source with Respect to the Rectangular Coordinate System.

where

x_0 = location of the source plane along the x axis,

$S(y,z)$ = planar distribution of unit isotropic point sources,

$\frac{F(E)}{4\pi}$ = unit angular point source energy distribution for isotropic emission.

For an isotropic plane source having a uniform distribution of point sources, $S(y,z) = S$ (particles cm^{-2} sec^{-1}), and the expression for the source becomes

$$S(x_0,E,\bar{\Omega})\,dE\,d\bar{\Omega} = S\frac{F(E)}{4\pi}\,dE\,d\bar{\Omega}\,. \qquad (2.65)$$

This source is of considerable importance in shielding work; for example, it is used to represent radiation fields such as those due to radioactive fallout.

Note that $S(x_0,E,\bar{\Omega})$ is based on a unit area that is normal to the x axis. The angular flux that corresponds to the isotropic plane source has for its basis a unit area normal to the $\bar{\Omega}$ direction and therefore differs from $S(x_0,E,\bar{\Omega})$ by a factor of $(\bar{\Omega}\cdot\bar{n})^{-1}$ or $\cos\theta$ with azimuthal symmetry; that is,

$$\Phi(x_0,E,\bar{\Omega}) = (\bar{\Omega}\cdot\bar{n})^{-1}\,S(x_0,E,\bar{\Omega}) = S\frac{F(E)}{4\pi}\frac{1}{(\bar{\Omega}\cdot\bar{n})}\,. \qquad (2.66)$$

The utility of $\Phi(x_0,E,\bar{\Omega})$ is sometimes limited by the singularity experienced as $(\bar{\Omega}\cdot\bar{n})$ approaches zero. The term $S(x_0,E,\bar{\Omega})$ has proved to be the more useful form, and integrations over direction $\bar{\Omega}$ and energy E lead to physically meaningful quantities.

The differential form for the plane source is obtained by integrating Eq. 2.64 over all directions,

$$S(x_0,E) = \int_{4\pi} S(x_0,E,\bar{\Omega})\,d\bar{\Omega} = S\,F(E)\,, \qquad (2.67)$$

and the total emission (particles cm^{-2} sec^{-1}) is obtained by the subsequent integration over all energies,

$$S(x_0) = \int_0^\infty S(x_0,E)\,dE = S_0\,. \qquad (2.68)$$

2.3. Quantities Used to Describe Radiation Interactions

In describing the transport of radiation through matter, the interactions that the various particles may have with the nuclei of the medium must be considered. The probability of the occurrence of a given interaction, which will vary with the type of particle, its energy, and the material it traverses, is usually given in terms of microscopic or macroscopic cross sections. These cross sections are described in the following paragraphs, along with their relation to reaction probabilities and reaction rates.

2.3.1. MICROSCOPIC CROSS SECTIONS

The microscopic cross section, designated by the symbol σ, can be considered to be the *effective* area that a nucleus presents to an oncoming particle, regardless of the particle direction. That is, a particle will interact with a nucleus with a probability of unity when the particle is incident on the area and with a probability of zero when it misses the area. The units usually associated with σ are cm^2/atom or barns/atom, where 1 barn* = 10^{-24} cm^2. Because of the wave-like behavior of the particles and the complex nature of the nucleus, the magnitude of σ in general bears no direct relation with the physical size of the nucleus, but is strictly a function of the properties of the atom and the energy and type of the interacting particle.

2.3.2. REACTION PROBABILITIES

If a nucleus having a cross section σ is contained within some characteristic volume of material, V_c, which has a projected area A_c, then the probability that a particle incident on the volume will interact with that particular nucleus is the ratio of the effective area σ to the projected area A_c (see Fig. 2.8*a*). It follows then that σ/A_c is the reaction probability per nucleus associated with the area A_c and that it can be interpreted as the average number of reactions occurring in V_c per incident particle.

If the nuclide density N (nuclides/cm^3) is uniform throughout V_c, the total number of nuclei contained within V_c is given by NV_c and the reaction probability associated with the total number of nuclides is equal to the linear sum of the reaction probabilities associated with the individual nuclei *provided that* the characteristic volume V_c is optically thin (no self shielding). The reaction probability now associated with the characteristic volume V_c is $NV_c(\sigma/A_c)$.

This summation of probabilities is shown schematically in Fig. 2.8*b*. The optically thin condition is assured if the characteristic volume V_c is differential in size. (The characteristic area A_c would also be differential in size.) Otherwise, the condition shown in Fig. 2.8*c* might result, in which case the effective cross section per nucleus would be decreased because of the self-shielding effect. This follows since the reaction probability would no longer be a simple linear summation of the individual probabilities. This can easily be seen for the example of an opaque volume; increasing the thickness has no further effect.

2.3.3. MACROSCOPIC CROSS SECTIONS

The reaction probability associated with the optically thin characteristic volume V_c can be rearranged and written as $(\sigma N)(V_c/A_c)$. If V_c/A_c is recognized as the characteristic differential distance dS_c traveled by particles within V_c and if σN is identified as the macroscopic cross section Σ,† then ΣdS_c is the reaction probability associated with the differential tracklength dS_c. It follows that a formal definition for the macroscopic cross section Σ is the reaction probability per differential tracklength, or, presuming that differential tracklength is implicit in Σ and interpreting reaction probability as reactions per incident particle, the definition for Σ becomes the number of reactions per particle tracklength. However, the units for Σ are usually given as reciprocal centimeters (cm^{-1}).

*The term barn is attributed to have resulted from a humorous remark to the effect that 10^{-24} cm^2 looked as big as a barn to a neutron.

†The symbol μ is used for gamma rays.

There is another approach in defining the macroscopic cross section. In particle transport problems large numbers of particles are involved, and so it is sometimes convenient to describe the process in terms of averages or expected values. It can be assumed that the particle has a certain probability of undergoing an interaction with a nuclide within a distance dx. This average or expected value, called the macroscopic cross section Σ in units of inverse length, depends on the particle energy and the density and nuclear properties of the medium. Thus in penetrating a distance dx in a medium, a particle will suffer Σdx average number of interactions per unit time.

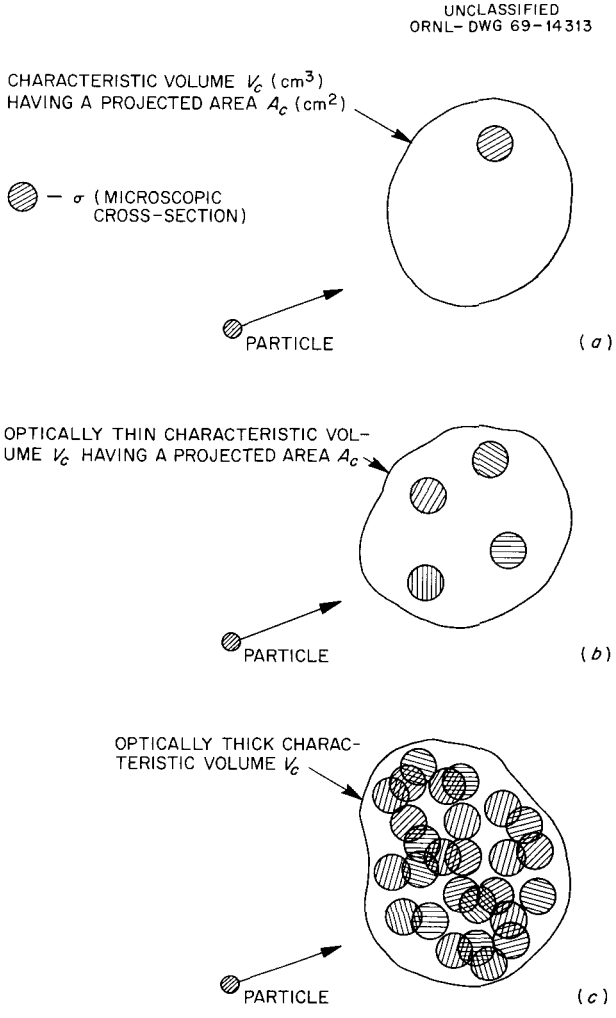

Fig. 2.8. Relationship Between Microscopic Cross Sections and Reaction Probabilities.

(*a*) A nucleus having a microscopic cross section σ is contained within a characteristic volume of material V_c which has a projected area A_c. A particle is entering V_c and the probability that it will interact with the nucleus is given by the ratio σ/A_c. This ratio can be interpreted as the number of reactions per incident particle per nucleus.

(*b*) Several nuclei, each having a microscopic cross section σ are contained within the volume V_c, which is sufficiently thin that the σ's will not overlap. The probability that the incident particle will interact with a nucleus in V_c is given by $(\sigma/A_c)NV_c$, where N is the number of nuclides per cm^3 in V_c.

(*c*) The characteristic volume V_c is sufficiently thick for the σ's to overlap. In this case the self-shielding effect would prevent the reaction probability from being a simple linear summation of the individual probabilities.

In order to examine the concept more closely, consider the simple model of a beam of particles normally incident on an infinite slab of some material. Let $\Phi(x)$ be the uncollided flux at thickness x. The number being removed in dx is

$$-d\Phi(x) = \Phi(x)\Sigma dx\,, \tag{2.69}$$

which integrates to

$$\Phi(x) = \Phi_0 e^{-\Sigma x}\,, \tag{2.70}$$

where Φ_0 is the incident flux. The probability that a particle will suffer an interaction in a distance less than L is

$$P(x \leqslant L) = \int_0^L \frac{\Sigma\Phi(x)dx}{\Phi_0} = \int_0^L \Sigma e^{-\Sigma x}dx = 1 - e^{-\Sigma L}\,, \tag{2.71}$$

where $\Sigma e^{-\Sigma x}$ is the probability density function for an interaction. The mean distance a particle will travel (the *mean-free path* λ) before it suffers an interaction is

$$\lambda = \int_0^\infty x\Sigma e^{-\Sigma x}dx = \frac{1}{\Sigma}\,. \tag{2.72}$$

If the foregoing discussion is accepted as establishing the definition of a macroscopic cross section, which is a function of both the properties of the nuclide (nucleus only for the neutron) and the particle energy and type, the microscopic cross section σ can be defined as simply Σ/N, where N is the nuclear density and σ represents the cross-sectional area per nucleus seen by the incident particles.

It should be clear on the basis of the foregoing discussion that Σ should not be used as a probability density function to determine reaction probabilities except in special cases. Even though the reaction probability for a particle normally incident on a differential volume dx within the slab is given by Σdx, the probability that a reaction will occur within the

optically thick slab is not simply $\int_0^L \Sigma dx = \Sigma L$. As was shown above, the reaction probability for the slab is given by $(1 - e^{-\Sigma L})$, which approaches ΣL only for the special case of an optically thin slab since $(1 - e^{-\Sigma L}) \rightarrow \Sigma L$ for $\Sigma L \ll 1$.*

2.3.4. REACTION RATES

The concept of a macroscopic cross section as described in the preceding section suggests that particles which move through matter will undergo interactions at a rate proportional to the total particle tracklength, a quantity that is closely related to the particle flux $\Phi(\bar{r})$ (see Table 2.1). The macroscopic cross section Σ is in fact the required proportionality constant between the reaction rate and the particle flux; the reaction rate per unit volume at the space point $\bar{r}$ is given by

$$R(\bar{r}) = \Sigma\Phi(\bar{r}) , \tag{2.73}$$

the dimensional correctness of which is verified by noting that

$$\frac{\text{reactions}}{\text{cm}^3\cdot\text{sec}} = \frac{\text{reactions}}{\text{particle}\cdot\text{cm}} \cdot \frac{\text{particle}\cdot\text{cm}}{\text{cm}^3\cdot\text{sec}} .$$

The differential reaction rate is related to the differential particle flux and is given by

$$R(\bar{r},E) = \Sigma(E)\ \Phi(\bar{r},E) , \tag{2.74}$$

where

$R(\bar{r},E)\,dE$ = number of reactions at space point $\bar{r}$ per unit volume and time which involve particles having energies in dE about the energy E,

$\Sigma(E)$ = macroscopic cross section for the reaction, which depends on the particle's energy as well as the nuclear characteristics of the medium,

$\Phi(\bar{r},E)$ = differential particle flux density.

The reaction rate for an energy interval, or group $(\Delta E_G = E_g - E_{g+1})$, is simply related to the differential reaction rate by

$$R_G(\bar{r}) = \int_{E_{g+1}}^{E_g} R(\bar{r},E)\,dE$$

$$= \int_{E_{g+1}}^{E_g} \Sigma(E)\ \Phi(\bar{r},E)\,dE . \tag{2.75}$$

This leads to a definition of the reaction rate in terms of an energy-averaged macroscopic cross section Σ_G (group cross section) and the group flux:

$$R_G(\bar{r}) = \Sigma_G\Phi_G(\bar{r}) , \tag{2.76}$$

where

$$\Sigma_G = \frac{\int_{E_{g+1}}^{E_g} \Sigma(E)\ \Phi(\bar{r},E)\,dE}{\int_{E_{g+1}}^{E_g} \Phi(\bar{r},E)\,dE} \tag{2.77}$$

and

$$\Phi_G(\bar{r}) = \int_{E_{g+1}}^{E_g} \Phi(\bar{r},E)\,dE . \tag{2.78}$$

The concept of the reaction rate in its many forms is fundamental to the formulation of the various equations that analytically describe particle transport (for example, the Boltzmann transport equation) and to the determination of useful information, such as energy deposition and biological dose from known or calculated values of the particle flux density.

*Another and more definitive description of the optically thin condition.

2.4. Radiations Produced in Nuclear Weapons

As pointed out in the introduction to this chapter, several types of radiations are produced by nuclear detonations, but generally the only radiations that the shield designer must be concerned with are neutrons and gamma rays. It is the nature and classification of these radiations that are discussed in the following paragraphs. The processes whereby neutrons and gamma rays interact with materials are discussed in Sections 2.5 and 2.7 respectively, and the processes whereby they are produced are described in Sections 2.6 and 2.8 respectively.

2.4.1. NEUTRONS

The presence of a highly penetrating electrically neutral radiation had already been experimentally demonstrated* by several groups of investigators when Chadwick[2] in 1932 established the existence of a neutral particle having a mass nearly equal to that of a proton. Since then, this neutral particle, which has become known as the *neutron,* has proved to be not only a key to nuclear weaponry but also a bane to those persons charged with providing protection against nuclear radiation fields.

Neutrons, like protons, are constituents of the nucleus, and both are referred to as nucleons. The ability of a neutron to transform into a proton – and the converse – suggests that protons and neutrons may be simply different states of a single particle, and a full understanding of the relation between the two is one of the current problems in nuclear physics. Neutrons can be regarded as fundamental particles since they are readily identifiable by the following physical properties:

Charge	0
Rest mass	1.00898 atomic mass units
Spin	½
Magnetic dipole moment	−1.913 nuclear magnetons
Statistics	Fermi
Intrinsic parity	Even

*This radiation was produced when beryllium was bombarded by alpha particles.

Outside a nucleus the neutron is *not* a stable particle and decays with a half life of 12.8 min. However, this effect is always neglected in neutron transport problems because of the extremely short transport lifetimes (in general much less than 1 sec).

The theory of wave mechanics suggests that all moving particles, including neutrons, have wave properties. The deBroglie wavelength h/p can be assigned to a neutron, and if its kinetic energy is less than the energy equivalent of its rest mass,† that is, if $E < 939.5$ MeV, the nonrelativistic wavelength is given by

$$\lambda = \frac{h}{p} \cong \frac{2.8600 \times 10^{-12}}{E^{1/2}}, \tag{2.79}$$

where

λ = deBroglie wavelength (cm),

E = neutron energy (MeV),

h = Planck's constant (6.624×10^{-27} erg·sec, or 4.132×10^{-15} eV·sec),

p = momentum of the neutron.

The neutron's wavelength is inversely proportional to its velocity and provides valuable insight into the general nature of neutron interactions with matter. Thermal neutrons have wavelengths of the same order as the atomic spacings in crystals. Therefore, when thermal neutrons interact with a crystal, diffraction patterns in accordance with Bragg's law are produced. (The main difference between the diffraction of neutrons and of gamma rays is that neutrons interact with the nuclei whereas gamma rays interact primarily with the orbital electrons.) Neutrons with energies from 1 to 100 MeV have wavelengths of the order of nuclear dimensions, and neutrons with relativistic energies greater than 10 GeV have wavelengths comparable with

†The conversion factor that relates a particle's rest mass in atomic mass units (amu) to the energy equivalent of its rest mass is 931 MeV/amu. The mass of a neutron is 1.00898 amu, which when multiplied by 931 MeV/amu yields 939.5 MeV for its energy equivalent.

the spacing of nucleons within the nucleus, which provides another tool for exploring the structure of the nucleus.*

Neutrons are classified according to energy, with the divisions occurring somewhat naturally because of behavior peculiar to particular energy ranges. In some cases the divisions are somewhat arbitrary, and they can be ambiguous since the energy structures overlap and differences in opinion exist as to the proper terminology. However, classification is helpful in discussing neutron behavior. Some of the classifications used are given below.

Slow Neutrons. Neutrons with energies from zero to about 1 or 2 keV are sometimes referred to as slow neutrons. This is a broad classification, however, and is not in general use since it does not serve as a very precise description of the energy state of low-energy neutrons. In reactor physics and technology jargon, the term "slow neutrons" refers to thermal neutrons.

Thermal Neutrons. Thermal neutrons are in thermal equilibrium with the atoms (or molecules) of the medium in which they are present. A particular thermal neutron may gain or lose energy in any one collision with the nuclei of the medium, but there is no net energy change for a large number of neutrons diffusing in a nonabsorbing medium. For this condition the kinetic energy of the neutrons is distributed statistically according to the Maxwell-Boltzmann equation as derived from the kinetic theory of gases. The equation for the spectral distribution is

$$n(E) = \frac{dn}{dE} = \frac{2\pi n}{(\pi kT)^{3/2}} e^{-E/kT} E^{1/2} , \qquad (2.80)$$

where

$dn = n(E)\,dE$ = number of neutrons having energies in the energy interval dE about E,

n = total number of neutrons in the system,

E = neutron energy (eV),

k = Boltzmann constant (8.61×10^{-5} eV per °K),

T = absolute temperature (°K).

It can be shown that, when the Maxwell-Boltzmann distribution applies, the energy corresponding to the most probable neutron velocity (2200 m/sec at 20°C) is given by kT (0.0252 eV), the average kinetic energy of thermal neutrons is $\frac{3}{2}kT$, and the most probable neutron energy is $\frac{1}{2}kT$.

For absorbing media the true energy distribution of the neutrons deviates from the Maxwell-Boltzmann distribution because neutron absorptions tend to increase with decreasing energy, which causes an increase in the average energy.[4] This tendency is illustrated in Fig. 2.9. The spectral distribution shown in Fig. 2.9*a* exhibits very little distortion, which is characteristic of poorly absorbing media, while the distribution shown in Fig. 2.9*b* clearly demonstrates the effects of the preferential absorptions at the lower neutron energies. This phenomenon is called hardening and can in part be compensated for by the use of an "effective neutron temperature" T_n, which is defined as a number that, when used in the Maxwell-Boltzmann distribution, gives the best least-squares fit to the true distribution as determined by a Monte Carlo calculation. The effective neutron temperature T_n has been found to be approximately related to the environmental temperature T_m in the following way:[4]

$$T_n = T_m \left[1 + \frac{1.84\,\Sigma_a(kT)}{\xi\Sigma_s}\right] = T_m\,[1 + 0.46\Delta] , \qquad (2.81)$$

where

$\Sigma_a(kT)$ = macroscopic absorption cross section evaluated at the energy kT,

Σ_s = macroscopic scattering cross section for thermal neutrons,

ξ = average logarithmic energy decrement per collision,

$$\Delta \equiv \frac{4\Sigma_a(kT)}{\xi\Sigma_s} .$$

Cold Neutrons. – Neutrons with an average energy less than that of thermal neutrons are sometimes referred to as cold neutrons. They are of no concern in shielding calculations.

Epithermal Neutrons. – Epithermal neutrons are the neutrons in a system whose energies exceed those of a Maxwell-Boltzmann distribution for the effective temperature of the neutron-supporting medium.

Resonance Neutrons. – Neutrons having energies in the range between 1 and 100 eV are frequently called resonance neutrons. Many nuclei exhibit strong absorption of neutrons at well-defined energies in this energy range, and these absorptions are commonly referred to as resonance absorptions.

*Additional details on the properties of neutrons are available in most texts on nuclear theory (see, for example, a book by Evans[3]).

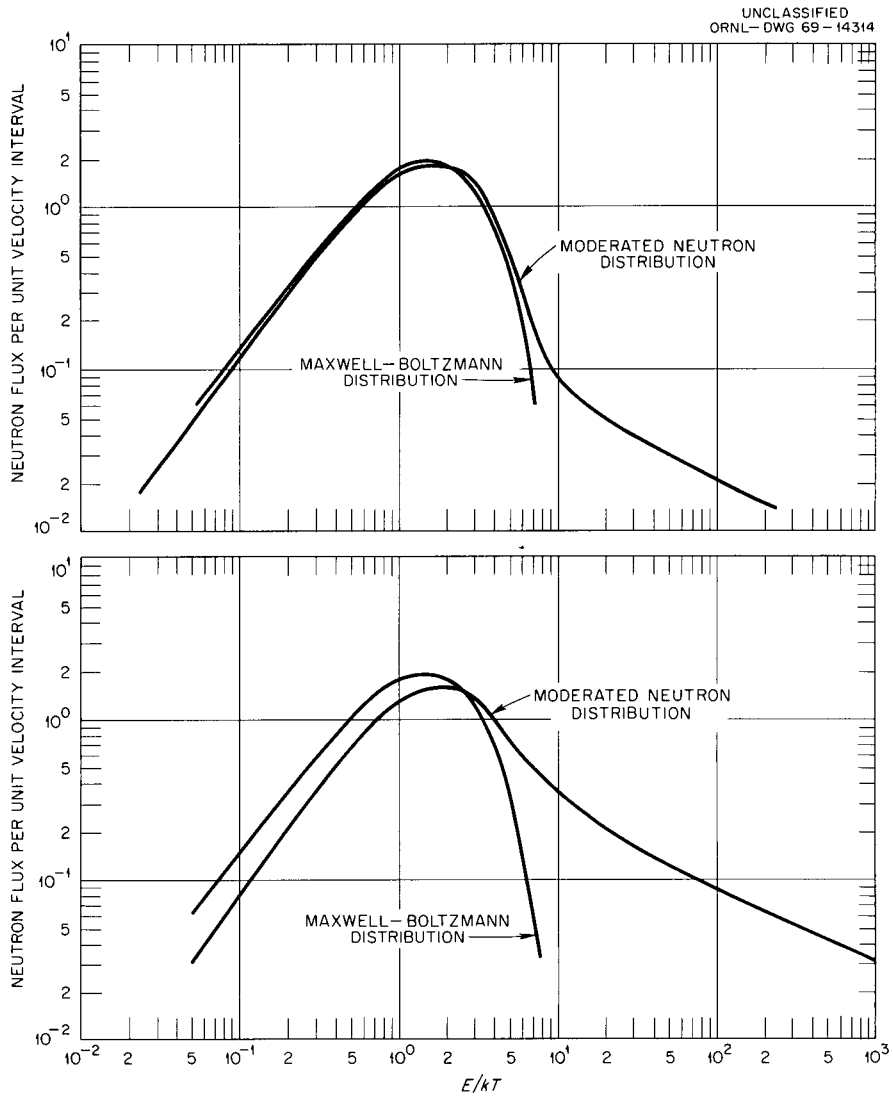

Fig. 2.9. Comparison of the Neutron Energy Disbributions with Maxwell-Boltzmann Distribution in (*a*) Poorly Absorbing Medium and (*b*) Highly Absorbing Medium. (From Coveyou *et al.*, ref. 4.)

Intermediate Neutrons. – Neutrons in the energy range 1 keV to about 0.5 MeV are often referred to as intermediate neutrons. The slowing down and removal aspects of neutron transport primarily involve intermediate neutrons, and their behavior strongly affects the design of high-performance shields.

Fast Neutrons. – Neutrons having energies between 0.5 MeV and about 15 MeV are regarded as fast neutrons. Most neutrons produced by fission and fusion reactions are fast neutrons.

Very High Energy and Ultra High Energy Neutrons. – Neutrons referred to as having very high energy usually fall in the 15- to 50-MeV range and those referred to as having ultra high energy fall in the range > 50 MeV. These neutrons are either cosmic radiations or by-product particles produced during accelerator operations. They are not of interest in weapons radiation shielding, but are included here to complete the neutron classifications.

2.4.2 GAMMA RAYS

During early investigations of radioactive materials three types of radiation were observed that were arbitrarily identified as alpha, beta, and gamma rays.

Gamma rays, unlike the alpha and beta rays, which were found to carry positive and negative charges respectively and to be easily stopped, were found to be electrically neutral and highly penetrating. It was postulated that gamma rays were actually electromagnetic radiations similar to X rays, and this was confirmed experimentally in 1914 by E. Rutherford.

According to classical theory, electromagnetic radiation consists of transverse electric and magnetic fields that propagate as waves at the speed of light. They may exist in regions that are void of matter and contain no electric charges or currents. Within the framework of classical theory a continuous flow of energy is associated with the propagation of the electromagnetic wave, and there is no upper or lower limit to the amount of energy that can be transported by electromagnetic radiations.

While wave theory gives a good description of the diffraction, reflection, and interference of electromagnetic radiations, it is quite inadequate for describing phenomena such as nuclear emission, the photoelectric effect, Compton scattering, and bremsstrahlung.* However, the quantum theory, which was formulated by Max Planck in 1900, does provide a satisfactory explanation for such phenomena. This theory suggests that electromagnetic radiations are emitted as discrete bundles of energy of size $h\nu$, where Planck's constant h is equal to 6.624×10^{-27} ergs/sec and ν is the frequency. These pseudo-particles are commonly referred to as *photons*. They have energies of $E = h\nu$ and possess the properties of momentum ($p = h\nu/c$) and relativistic mass ($M = h\nu/c^2$).

Wave theory and quantum theory seemingly contradict each other in many ways, but in 1928 Max Born argued that electromagnetic radiation was indeed quantum in nature and that the classical wave theory could be interpreted as the probability of finding a photon at a particular point in space and time. It is within the context of quantum theory that electromagnetic radiations are treated in this chapter.

In the years since 1914 it has been established that electromagnetic radiations originate whenever transitions take place between two energy levels of nuclei or between two electronic levels of an atom. The frequencies and wavelengths of the radiations are determined by

$$\Gamma = h\nu = hc/\lambda , \tag{2.82}$$

where the level width Γ is the difference in the excitation energy of the two levels. Since the level widths are greater for nuclear transitions than for electronic transitions, the radiations accompanying nuclear transitions are characteristically of higher energy than those accompanying electronic transitions. For historical reasons the radiations produced by nuclear transitions are usually referred to as *gamma rays* and those produced by atomic transitions are called *characteristic X rays.* Typical of the latter are the soft X rays (fluorescence radiation) produced as a result of the photoelectric effect discussed in Section 2.7. Two other types of electromagnetic radiations are *bremsstrahlung* and *annihilation* radiation. Bremsstrahlung radiation arises as a result of the acceleration or deceleration of free charged particles, and annihilation radiation is produced when a positron and an electron combine, both particles being annihilated in the process. (Positrons are produced by the pair-production process described in Section 2.7.2).

From the foregoing it is seen that electromagnetic radiations are classified by origin; that is, (1) gamma rays accompany nuclear transitions, (2) X rays are emitted in atomic transitions, (3) bremsstrahlung radiation results from the acceleration or deceleration of free charged particles, and (4) annihilation radiation is emitted when a positron combines with an electron. As it turns out, and as is discussed in Section 2.7, bremsstrahlung and annihilation radiations, as well as soft X rays, are not usually highly penetrating and the transport of these radiations is usually ignored in shielding design.

*These phenomena are discussed in Section 2.7.

2.5. Interactions of Neutrons

Neutrons are attenuated by interactions with the nuclei of the elements comprising the medium that they are traversing. The neutron interactions most important to shielding are elastic scattering, inelastic scattering, radiative capture, and charged-particle reactions. The relative importance of these interactions is, at least in part, determined by their respective cross sections, the magnitude of which varies with the neutron energy and the element (see Section 2.3).

The relation of the various cross sections is shown in Fig. 2.10. From this figure it is apparent that the total cross section for a neutron interaction can be thought of as being the sum of the elastic-scattering cross section and the nonelastic cross section. The two classifications distinguish between those interactions in which the neutron and nucleus collide as two perfectly elastic spheres (sometimes referred to as billiard-ball collisions) and all other interactions. The total cross section can also be thought of as the sum of the total scattering cross section and the total absorption cross section. In the latter interpretation the scattering cross section includes both elastic and nonelastic scatterings, and the absorption cross section includes all processes that cause the product nucleus to differ either in atomic number or in atomic weight from the target nucleus. Because of the change in the target nucleus, absorption processes are usually referred to as nuclear *re*actions rather than *inter*actions, although the two terms are often used interchangeably.

The accuracy (or reliability) of a given calculation can be strongly influenced by the quality of the cross-section data used. Despite their obvious importance,

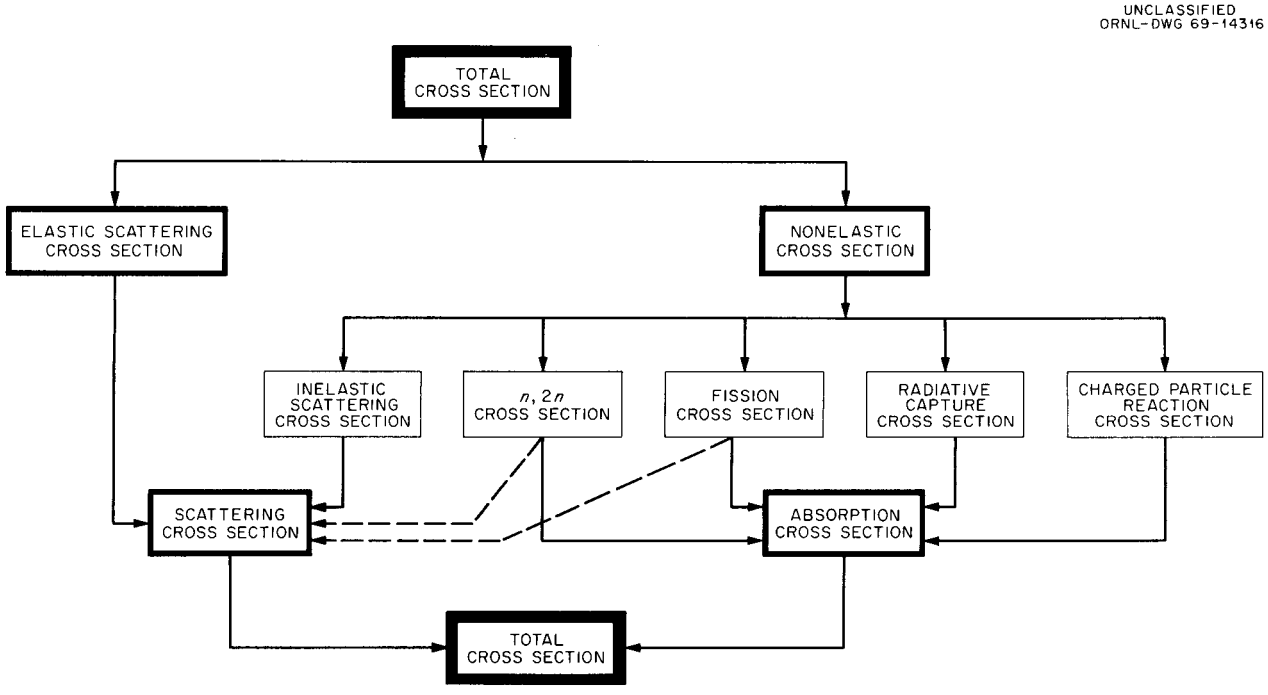

Fig. 2.10. Relation of Neutron Cross Sections. (Note: In some neutron transport calculations all neutron-nucleus interactions in which neutrons leave the target nucleus are considered to be scattering processes, in which case the $n,2n$ and fission processes would be scattering processes, as indicated by the dashed lines. In most shield attenuation calculations neither process is important, however.)

detailed neutron cross sections are not presented in this document because of the vastness and complexity of the information. Much cross-section data are readily available in a number of publications.[5–9] Also available is a comprehensive and periodically updated index[10] to the latest literature on microscopic neutron data.

2.5.1. ELASTIC SCATTERING

As mentioned above, the elastic scattering of neutrons with nuclei can be viewed as the collision of perfectly elastic spheres.* This process is characterized by the conservation of kinetic energy and momentum and is exactly described by the methods of classical mechanics. The various theoretical analyses are usually performed in the center-of-mass (c.m.) frame of reference, which assumes that the center of mass of the neutron-nucleus system remains at rest. An external observer (e.g., one performing a physical measurement) would view the collision process in the laboratory frame of reference. Theoretical results are more useful when expressed in terms of the laboratory system coordinates, but the theoretical relations are more easily derived in the c.m. system.

If it is assumed that the target nucleus in the laboratory system is stationary, the change in kinetic energy experienced by the neutron is uniquely related to its change in direction by the following equation:

$$E = \frac{E_0}{(A+1)^2}(A^2 + 2\eta A + 1)\,, \tag{2.83}$$

where

E_0 = initial neutron energy in the laboratory system,

E = final neutron energy in the laboratory system,

A = ratio of the atomic mass of the nuclide to the mass of the neutron,

$\eta = \cos\theta$, the cosine of the scattering angle in the c.m. system.

The minimum value of E/E_0, which corresponds to the maximum loss in energy experienced by a neutron in a single collision, occurs for a head-on collision, $\theta = \pi$ or $\eta = -1$. The minimum final neutron energy is given by

$$E_{\min} = \alpha E_0\,, \tag{2.84}$$

where

$$\alpha = [(A-1)/(A+1)]^2\,. \tag{2.85}$$

The cosine of the scattering angle in the laboratory system, symbolized by μ, is simply related to the cosine of the scattering angle in the c.m. system by

$$\mu = \frac{1 + \eta A}{(A^2 + 2\eta A + 1)^{1/2}}\,. \tag{2.86}$$

If it is further assumed that the scattering in the c.m. system is isotropic (an excellent assumption for hydrogen), then the following relations hold for the elastic-scattering process:

1. The probability that a neutron will undergo a change of direction into a differential solid angle $d\bar{\Omega}$ corresponding to a conical element defined by the scattering angles θ and $\theta + d\theta$ in the c.m. system is

$$p(\theta)\,d\theta = \frac{d\bar{\Omega}}{4\pi} = \frac{1}{2}\sin\theta\,d\theta\,. \tag{2.87}$$

2. The fraction of all elastic-scattering collisions that involve neutrons of energy E_0 scattered into the energy interval dE about the final energy E is given by

$$p(E;E_0)\,dE = \frac{dE}{E_0(1-\alpha)}\,. \tag{2.88}$$

3. The average final energy of all neutrons of initial energy E_0 is given by

$$\bar{E} = \int_{\alpha E_0}^{E_0} E\,p(E;E_0)\,dE = [(1+\alpha)/2]\,E_0\,. \tag{2.89}$$

4. The average value of the cosine of the scattering angle in the laboratory system, an important parameter in neutron transport calculations, is given by

$$\bar{\mu} = \frac{2}{3A}\,. \tag{2.90}$$

5. The average logarithmic energy decrement per collision is defined by

$$\xi \equiv \overline{\ln\frac{E_0}{E}} = \int_{\alpha E_0}^{E_0} \ln\frac{E_0}{E}\,p(E;E_0)\,dE = 1 + \frac{\alpha\ln\alpha}{1-\alpha}\,. \tag{2.91}$$

*This description applies only to "potential" elastic scattering, which is the type discussed in this section. Another kind of elastic scattering, called capture scattering, is very much like inelastic scattering in that it involves the formation of a compound nucleus and the subsequent emission of a neutron with nearly its original kinetic energy (see later discussion).

An interesting property of ξ is its independence of the initial energy of the neutron. The quantity ξ can also be interpreted as the average change in lethargy per collision, where the lethargy u is defined as

$$u \equiv \ln \frac{E_0}{E} , \tag{2.92}$$

and the average change in lethargy per collision is given by

$$\overline{u - u_0} = \overline{\ln \frac{E_0}{E} - \ln \frac{E_0}{E_0}} = \overline{\ln \frac{E_0}{E}} = \xi . \tag{2.93}$$

The lethargy is a useful alternate energy variable in the description of the slowing-down process for neutrons.

For most nuclides the isotropic assumption generally gives a good description of the elastic-scattering process for neutrons in the thermal-to-keV energy range; however, it is invalid for high-energy (MeV) neutrons or for interactions in which chemical binding energies are important. Thus in shielding calculations, which usually involve high-energy neutrons, the isotropic assumption cannot be made safely except for hydrogen, for which the scattering is virtually isotropic in the c.m. system for neutron energies up to 14 MeV.

In a more general treatment of the scattering process, which can apply to inelastic as well as to elastic scattering, the cross sections for scattering are represented by an expansion in a series of Legendre polynomials:

$$\sigma_e(E,\eta) = \frac{\sigma_e(E)}{2\pi} \sum_m \frac{2m+1}{2} A_m(E) P_m(\eta) , \tag{2.94}$$

where

$\sigma_e(E,\eta)$ = energy-dependent differential cross section for the elastic scattering of neutrons of energy E through an angle in the c.m. system whose cosine is η per unit solid angle,

$A_m(E)$ = energy-dependent Legendre coefficients (except that $A_0 = 1$ always),

$P_m(\eta)$ = Legendre polynomials.

The energy-dependent elastic-scattering cross section $\sigma_e(E)$ is obtained by integrating the differential elastic-scattering cross section $\sigma_e(E,\eta)$ over all possible values of η:

$$\sigma_e(E) = 2\pi \int_{-1}^{+1} \sigma_e(E,\eta)\, d\eta . \tag{2.95}$$

Representation of the cross section as an expanded series of orthogonal functions is necessary in the spherical harmonics and S_n solutions of the Boltzmann equation (see Chapter 3). Other orthogonal functions can be used – and have been – but the Legendre polynomials generally give best fits and are universally used.

Note that the first term (*zero*th order) of Eq. 2.94 gives the angular cross section for isotropic scattering $\sigma_e/4\pi$. The coefficients $A_m(E)$ obtained by fitting angular cross-section data are reported in both laboratory and c.m. systems. Usually the c.m. coefficients must be transformed to the laboratory system for transport calculations. As the atomic number increases, however, the difference becomes small.

The elastic-collision process is an important energy degradation mechanism and is most important for the light elements, particularly hydrogen. Efficient neutron shields always contain hydrogenous materials.

2.5.2. NONELASTIC REACTIONS

All reactions that are not elastic scatterings are called nonelastic reactions, and the sum of their cross sections is referred to as the nonelastic cross section. In experimental determinations of neutron cross sections in the energy range 3 to 15 MeV, the nonelastic cross section is the quantity that is actually measured. Or, in other words, the quantity measured is the total cross section minus the elastic-scattering cross section.

Many models are available for describing nonelastic neutron reactions with nuclei, but the one most frequently used is the Bohr model. In this model the interaction is envisioned as beginning when the neutron comes within the range of the nuclear forces of the nucleus and as terminating when the products of the interaction depart from this region. In the interim the combination of the neutron and target nucleus is called simply the compound nucleus. It is convenient to consider the interaction as occurring in two distinct stages:

1. A compound nucleus is formed when the incident neutron loses its identity and becomes assimilated into the unstable new system. This event brings to the newly formed compound nucleus an excitation energy that consists of the available portion* of the neutron's kinetic energy of motion and its binding energy† with

*Due to conservation of momentum, some of the kinetic energy of the incident neutron must appear as translational energy at the compound nucleus and is therefore unavailable as excitation energy.

†The binding energy per nucleon is the average energy required per nucleon to separate the nucleus into its constituent particles. Refer to subsequent discussions of binding energy under "Nuclear Reactions."

respect to the compound nucleus. The excitation energy is statistically shared by all the nucleons.

2. The unstable compound nucleus separates into its products when one or more of the nucleons acquire sufficient energy to escape, that is, when the nucleons acquire energy that is equal to or greater than their binding energy. In some cases the unstable compound nucleus may give off excitation energy in the form of gamma radiation. In either case the resulting product nucleus may itself be unstable and undergo radioactive transformation, but in all cases the end result is a system of stable products. A schematic representation of the two stages of neutron interaction with a nucleus is shown in Fig. 2.11. (The example given in the figure is specifically for the inelastic-scattering process described below.)

The compound nucleus concept is being replaced by more elaborate models; however, it will continue to be useful in providing an easily understood representation of nonelastic neutron interactions with nuclei.

The nonelastic neutron reactions are divided into scattering processes and absorption processes, the absorption processes often being referred to as nuclear reactions. They include radiative capture, charged-particle reactions, $(n,2n)$ reactions, and fission. Insofar as shielding attenuation is concerned, the $(n,2n)$ and fission reactions are usually unimportant unless materials such as beryllium and depleted uranium are used. The fission reaction is, of course, very important as a neutron source in weapons detonations and as the energy source in the production of electric power (see Section 2.6).

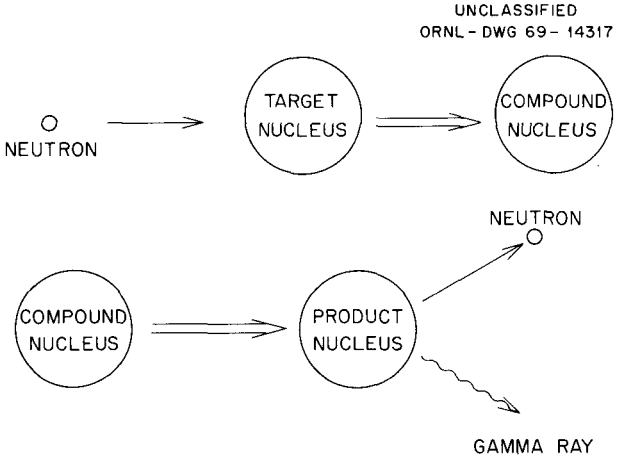

Fig. 2.11. Schematic Representation of a Nonelastic Interaction of a Neutron with a Nucleus (Inelastic Scattering).

Inelastic Scattering

In inelastic scattering the incident neutron and target nucleus form a compound nucleus from which a neutron is subsequently emitted. If the kinetic energy of the incident neutron is greater than the lowest energy level of the target nucleus,* the nucleus may be left in an excited state following the neutron emission. This results in the emitted neutron having substantially less energy than the incident neutron, thereby contributing strongly to the energy degradation process and therefore to the attenuation of neutrons in shields. The excited nucleus then returns to its ground state by the emission of gamma rays. An energy level diagram of this process is shown in Fig. 2.12.

Determining the detailed cross sections for inelastic scattering is a complicated and difficult task, whether accomplished by experiment or by theory. Consequently, the inelastic-scattering cross sections for many elements are unknown and a large fraction of those used in shielding calculations are little more than a best guess. However, there are some generalizations that can be made:

1. The cross section usually increases with increasing neutron energy.
2. The cross section usually increases with increasing atomic weight.
3. The threshold for the interaction in light elements is generally several MeV, and the gamma rays emitted are correspondingly harder than those produced in interactions with lower energy thresholds.
4. The threshold for the interaction in heavy elements is lower, sometimes much lower, than for that in light elements.

Nuclear Reactions

The term nuclear reaction is often reserved for those interactions in which the product nucleus differs either in atomic number or atomic weight from the target nucleus. The type of reaction that occurs depends on several factors, the most important being the nuclear structure of the target nucleus and the energy of the incident neutrons. Some reactions are possible for neutrons of any energy, while others have threshold energies. In some cases more than one de-excitation process is possible, with the relative probabilities of each being given by their respective reaction cross sections.

*If this condition is not satisfied, the capture scattering form of elastic scattering may occur.

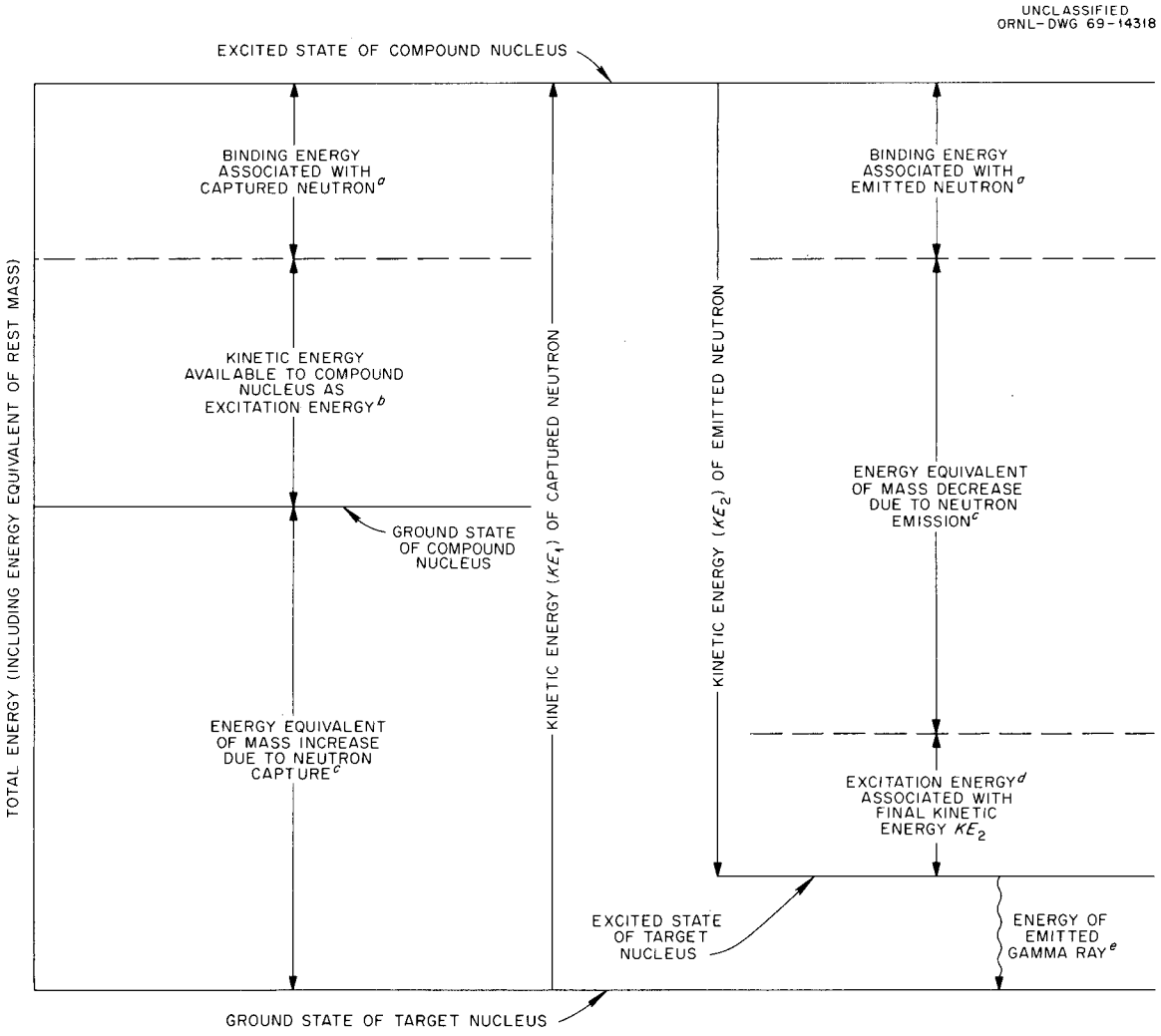

Fig. 2.12. Energy Diagram for the Inelastic Scattering of a Neutron with a Target Nucleus.

[a]Given by 931 MeV $[(M_X + M_n) - M_Y] \approx 7$ MeV, where M_X, M_n, and M_Y are the masses, in atomic mass units, of the target nucleus, the neutron, and the compound nucleus, respectively.

[b]Given by $KE_1\ [M_X/(M_X + M_n)]$. Due to the conservation of momentum, some of the kinetic energy of the incident neutron must appear as translational energy of the compound nucleus and is therefore unavailable as excitation energy.

[c]Given by 931 $(M_Y - M_X) \approx 931$ MeV.

[d]Given by $KE_2\ [(M_X + M_n)/M_X]$.

[e]Given by $KE_1\ [M_X/(M_X + M_n)] - KE_2\ [(M_X + M_n)/M_X]$.

The equation for a reaction between a target nucleus and a neutron with essentially zero kinetic energy is given by

$$ {}_{Z_1}X^A + {}_0n^1 \rightarrow [{}_{Z_1}X^{A+1}] \rightarrow {}_{(Z_1-Z_2)}Y^{A+1-b} + {}_{Z_2}Y^b + Q , \quad (2.96) $$

where

$ {}_{Z_1}X^A $ = target nucleus with atomic number Z_1 and mass number A,

$ {}_0n^1 $ = incident neutron with atomic number 0, mass number 1, and essentially zero kinetic energy,

$ [{}_{Z_1}X^{A+1}] $ = compound nucleus in its excited state,

$ {}_{(Z_1-Z_2)}Y^{A+1-b} $ = product nucleus,

$ {}_{Z_2}Y^b $ = emitted particle,

Q = nuclear reaction energy.

Equation 2.96 requires that a balance exist with respect to both the atomic number and the mass number and is useful in analyzing nuclear reactions.

The nuclear reaction energy Q is determined by the change in mass experienced by the individual components of the reaction. The original equation can be written as a total energy equation. (All masses are expressed in terms of their energy equivalent, with 1 amu being equal to 931 MeV.) The explicit expression for Q is given by

$$ Q = 931\ [M_X + M_n - (M_Y + M_y)] , \quad (2.97) $$

where

Q = nuclear reaction energy (MeV),

M_X = mass of the target nucleus (amu),

M_n = mass of the incident neutron (amu),

M_Y = mass of the product nucleus (amu),

M_y = mass of the emitted particle (amu).

It is noted that if Q is positive the reaction is exoergic and neutrons with essentially zero kinetic energy can produce the reaction. If, on the other hand, Q is negative, the reaction is endoergic and the neutron must possess sufficient kinetic energy to make up the deficit. It can be shown that the threshold energy required of the neutron is given by

$$ E_T = \frac{M_X + M_n}{M_X} Q . \quad (2.98) $$

This follows from the law of the conservation of momentum when applied to the formation of the compound nucleus, since it requires that some of the neutron's kinetic energy must appear as translational energy of the compound nucleus and is therefore unavailable as excitation energy.

As pointed out above, those processes that fall in the category of nuclear reactions all contribute to the absorption cross section (see Fig. 2.10) and include radiative capture, $(n,2n)$ reactions, charged-particle reactions, and fission. Of these processes, radiative capture is the most important experienced by low-energy neutrons in shields. Following radiative capture, the complete de-excitation of the compound nucleus is accomplished by the emission of gamma radiation. The binding energy of the neutron in the compound nucleus resulting from slow-neutron capture is given by

$$ E_b = 931\ [(M_X + M_n) - M_Y] . \quad (2.99) $$

In this case the total excitation energy is equivalent to the binding energy and is about 8 MeV.

The other nuclear reactions become increasingly more important as the energy of the neutron increases, because other forms of de-excitation become more probable. However, epithermal radiative captures do occur and the gamma rays thus produced may contribute significantly to or even dominate the overall shielding problem.

Because of limitations in basic nuclear theories and the scarcity of experimental data, the standard practice has been to assume that the energy spectra of the epithermal radiative capture gamma rays are the same as those due to thermal capture. Yost and Solomito[11] have shown that this assumption is inappropriate for many materials and that the exclusive use of thermal-capture spectra can introduce considerable error in the subsequent gamma-ray transport problem and may, in fact, be the most questionable of the nuclear data used in the calculation. Yost[12] developed a method for determining capture gamma-ray spectra as a function of neutron energy (capture states) and wrote a machine code to generate capture gamma-ray spectra with a desired group structure resulting from capture of neutrons of each energy group. The code is based upon an appropriate nuclear model involving the spin and parity of the nucleus.

The $(n,2n)$ reaction involves the emission of two neutrons and its occurrence is usually limited to neutrons with high incident kinetic energies – greater than 10 MeV. The product nucleus is an isotope of the target nucleus and is frequently radioactive. The thresh-

old energy for the $(n,2n)$ reaction is approximately equal to the binding energy per nucleon of the compound nucleus and is related to the threshold energy for the photoneutron (γ,n) reaction by the relation

$$E_{T(n,2n)} = \frac{M_X + M_n}{M_X} E_{T(\gamma,n)} . \qquad (2.100)$$

For certain very light or very heavy nuclides the thresholds for the $(n,2n)$ reaction are sometimes much less than 10 MeV. For example, ${}^{2}_{1}\mathrm{H}$, ${}^{6}_{3}\mathrm{Li}$, and ${}^{9}_{4}\mathrm{B}$ have thresholds of 3.34 MeV, 6.2 MeV, and 1.85 MeV respectively, and ${}^{209}_{83}\mathrm{Bi}$, ${}^{232}_{90}\mathrm{Th}$, and ${}^{238}_{92}\mathrm{U}$ have thresholds of 7.4 MeV, 6.44 MeV, and 6.0 MeV respectively. The $(n,2n)$ production of neutrons is usually ignored in shield design; however, it is possible that this effect could be important for shield systems containing significant amounts of certain materials (beryllium, for example).

In charged-particle reactions the de-excitation of a compound nucleus formed by neutron capture is accomplished by the emission of a charged particle, either a proton or an alpha particle.* This type of reaction is most probable in the MeV range; however, there are several important charged-particle reactions for slow neutrons. Consider the following two methods for producing tritium:

$${}^{3}_{2}\mathrm{He} + {}^{1}_{0}n \rightarrow [{}^{4}_{2}\mathrm{He}]^* \rightarrow {}^{3}_{1}\mathrm{H} + {}^{1}_{1}\mathrm{H} + 0.764 \text{ MeV K. E.}$$

$${}^{6}_{3}\mathrm{Li} + {}^{1}_{0}n \rightarrow [{}^{7}_{3}\mathrm{Li}]^* \rightarrow {}^{3}_{1}\mathrm{H} + {}^{4}_{2}\mathrm{He} + 4.785 \text{ MeV K.E.}$$

Another important charged-particle reaction involves the ${}^{10}\mathrm{B}$ isotope of boron:

$${}^{10}_{5}\mathrm{B} + {}^{1}_{0}n \rightarrow [{}^{11}_{5}\mathrm{B}]^* \rightarrow {}^{7}_{3}\mathrm{Li}^* + {}^{4}_{2}\mathrm{He} + 2.30 \text{ MeV K.E.}$$

$${}^{7}_{3}\mathrm{Li}^* \rightarrow {}^{7}_{3}\mathrm{Li} + 0.478 \text{ MeV } \gamma$$

The ${}^{10}\mathrm{B}(n,\alpha)$ reaction is useful for the detection of slow neutrons because of its large thermal cross section. Also, ${}^{10}\mathrm{B}$ serves as an important constituent for shields designed to suppress high-energy capture gamma-ray production.

In fission reactions the compound nucleus separates into fission fragments, concomitantly releasing neutrons and gamma rays. This process rarely occurs except in a few of the very heavy elements, which, with the exception of depleted uranium, are not used in shields. (See further discussion of fission reaction in Section 2.6.)

2.5.3. NEUTRON TRANSPORT CROSS SECTION

The neutron transport cross section is defined as

$$\sigma_{tr} \equiv \sigma_t - \int_{4\pi} \sigma_e(\theta) \cos\theta \, d\bar{\Omega} , \qquad (2.101)$$

where

σ_t = total microscopic cross section,

$\sigma_e(\theta)$ = differential microscopic cross section for elastic scattering through a given angle θ per unit solid angle,

θ = scattering angle in the laboratory frame of reference.

The reaction rate $\Sigma_{tr}\,\Phi$ may be regarded as an estimate of the rate at which neutrons lose their forward momentum. In this context the transport cross section has been used as an approximation to the energy-dependent removal cross section (see Chapter 3, Section 3.8.2). Quite often, σ_{tr} appears naturally in the results of a derivation[13] which has other formal bases.

*An alpha particle is He^{++}.

2.6. Neutron Production Processes

Except for the small contributions made by such reactions as the $(n,2n)$, $(n,3n)$, and (γ,n) reactions, the neutrons emitted in the detonation of a nuclear weapon are produced directly by the fission process or the fusion process. In the fission process the resulting neutrons cover a wide range of energies, whereas in the fusion process the emissions are essentially monoenergetic, with the energies being determined by the type of fusion reaction.

2.6.1. FISSION REACTION

The details of the fission process are very complex and only a brief description is presented here.* As in other nonelastic neutron interactions (see Section 2.5.2), fission begins with the formation of a compound nucleus in an excited state. If the excitation energy exceeds a critical energy, then fission may occur.† Calculated values of the fission threshold energy are shown in Table 2.2 for a wide range of atomic weights.[14] It is apparent that only the very heavy nuclides ($A > 230$) have reasonably low threshold energies.

Experimental values of the fission thresholds for the nuclear fuel nuclides of practical interest are given in Table 2.3 (ref. 14). The significance of a negative threshold energy (^{233}U, ^{235}U, and ^{239}Pu) is that neutrons with essentially zero kinetic energy can produce the fissioning of these nuclides (thermal fission). All the other nuclides (^{232}Th, ^{234}U, ^{236}U, ^{238}U, and ^{237}Np) can undergo fast fission only.

When fission occurs, the highly unstable compound nucleus almost always splits into two fission fragments. Splitting into three or more fragments is theoretically possible, but such an occurrence is rare and is generally ignored. The nucleons are more firmly bound within their respective fission fragments than they were in the original fissile nuclide, thereby liberating the very large energy of fission (about 200 MeV per fission for the very heavy nuclides). Fissioning usually results in the prompt emission of several neutrons, the average number released per fission being a function of the neutron energy and the fissile material. For example, fissioning of ^{235}U and ^{239}Pu by thermal neutrons produces about 2.5 and 2.9 neutrons/fission respec-

Table 2.2. Computed Neutron Fission Thresholds as a Function of Nuclear Mass*

Mass No., A	Fission Threshold (MeV)
16	18.5
60	48
100	47
140	62
200	40
236	~5

*From ref. 14, p. 107.

Table 2.3. Experimental Neutron Fission Thresholds of Nuclear Fuel Nuclides*

Target Nucleus	Compound Nucleus	Fission Threshold (MeV)
^{232}Th	^{233}Th	1.3
^{233}U	^{234}U	<0
^{234}U	^{235}U	0.4
^{235}U	^{236}U	<0
^{236}U	^{237}U	0.8
^{238}U	^{239}U	1.2
^{237}Np	^{238}Np	0.4
^{239}Pu	^{240}Pu	<0

*From ref. 14, p. 108.

*Although this discussion is limited to the fission of the heavy nuclei by neutrons, it is pointed out that any nucleus except hydrogen may undergo fission if its level of excitation is sufficiently high and if this excitation can be imparted to the target nucleus by its interaction with gamma radiation (photofission) or with a variety of high-energy particles.

†The alternative to the fission mode of de-excitation is the emission of gamma radiation, which returns the compound nucleus to its ground state, i.e., effectively radiative capture.

tively. In addition, some of the fission fragments contain nuclides with neutrons in excess of those required for nuclear stability. These unstable nuclides have half-lives up to about 1 min, and the neutrons emitted are called delayed neutrons.* (It is these neutrons that make control of a nuclear reactor relatively easy. If all neutrons were prompt, every reactivity excursion would be prompt critical, and a reactor would be difficult to operate safely.) Also, because the fission fragments are neutron-rich, they undergo radioactive decay, emitting primarily beta and gamma radiations.

The mass numbers of the fission fragments versus the corresponding fission yields are shown in Fig. 2.13 for the thermal fission of ^{235}U, ^{238}U, and ^{239}Pu (ref. 15). The fission yield is defined as the percentage of the total fissions yielding products of a given mass number. As the energy of the incident neutron increases, the probability of producing two fission fragments of nearly the same size increases and the characteristic dip of the thermal-fission-yield curves at a mass number of about 120 disappears.

The energy spectrum of fission neutrons has been experimentally determined for ^{235}U, the nuclide used most frequently as a nuclear fuel, and is most conveniently represented by formulas known as the fission spectra of Watt,[16] of Cranberg *et al.*,[17] and of Los Alamos.[18]

The formula for the fission spectrum as determined by Watt is

$$N(E) = 0.484 \sinh \sqrt{2E}\, e^{-E}\,, \qquad (2.102)$$

where $N(E)$ is the fraction of neutrons emitted per fission with an energy E, in MeV, per unit energy range. This formula is regarded as adequate for the energy range 0.075 to 17 MeV, which includes the energy range of importance to shielding (3 to 17 MeV). Table 2.4 presents values of $N(E)$, together with two other useful quantities, $F(E)$ and $1 - F(E)$; $F(E)$ is the fraction of neutrons with energies greater than the energy E and is given by

$$F(E) = \int_E^\infty N(E')\, dE'\,. \qquad (2.103)$$

The quantity $1 - F(E)$ is the fraction of neutrons with energies less than the energy E and is given by

$$1 - F(E) = \int_0^E N(E')\, dE'\,. \qquad (2.104)$$

The formula for the fission spectrum obtained by Cranberg *et al.*[17] is

$$N(E) = 0.453\, e^{-E/0.965} \sinh \sqrt{2.29E}\,. \qquad (2.105)$$

The measurements on which this formula is based involved an energy range of 0.18 to 12.0 MeV and represent no substantial deviation from Watt's earlier

Table 2.4. Watt Prompt-Neutron Spectrum Due to Fission of ^{235}U by Thermal Neutrons[a]

E (MeV)	$N(E)$ (MeV^{-1})	$1 - F(E)$	$F(E)$
0.1	0.2023	0.014	0.9860
0.2	0.2676	0.377	0.9623
0.3	0.3068	0.663	0.9337
0.4	0.3300	0.987	0.9013
0.5	0.3450	0.1321	0.8679
0.6	0.3528	0.1669	0.8331
0.7	0.3557	0.2027	0.7973
0.8	0.3542	0.2385	0.7615
0.9	0.3513	0.2729	0.7271
1.0	0.3446	0.3082	0.6918
1.1	0.3368	0.3425	0.6575
1.2	0.3271	0.3759	0.6241
1.3	0.3179	0.4074	0.5926
1.4	0.3073	0.4383	0.5617
1.6	0.2841	0.4983	0.5017
1.8	0.2604	0.5631	0.4369
2.0	0.2371	0.6028	0.3972
2.5	0.1839	0.7073	0.2927
3.0	0.1384	0.7876	0.2124
3.5	0.1026	0.8476	0.1524
4.0	0.07472	0.8914	0.1086
4.5	0.05381	0.9192	0.0808
5.0	0.03847	0.9463	0.0537
5.5	0.02729	0.9624	0.0376
6.0	0.01916	0.9739	0.0261
6.5	0.01336	0.9821	0.0179
7.0	9.316(−3)[b]	0.9876	0.0124
7.5	6.436(−3)	0.9916	0.0084
8.0	4.423(−3)	0.9943	0.0057
8.5	3.034(−3)	0.9960	0.0040
9.0	2.076(−3)	0.9973	0.0027
9.5	1.418(−3)	0.9982	0.0018
10.0	9.53(−4)	0.9988	1.211(−3)
11.0	4.384(−4)	0.9994	5.501(−4)
12.0	1.994(−4)	0.9998	2.473(−4)
13.0	8.953(−5)	0.9999	1.103(−4)
14.0	3.997(−5)	1.0	4.875(−5)
15.0	1.771(−5)	1.0	2.148(−5)

[a]From ref. 16.

[b]Read: 9.316×10^{-3}, etc.

*For thermal fissioning of ^{235}U and ^{239}Pu, the delayed neutron fraction is about 0.7% and 0.2% respectively.

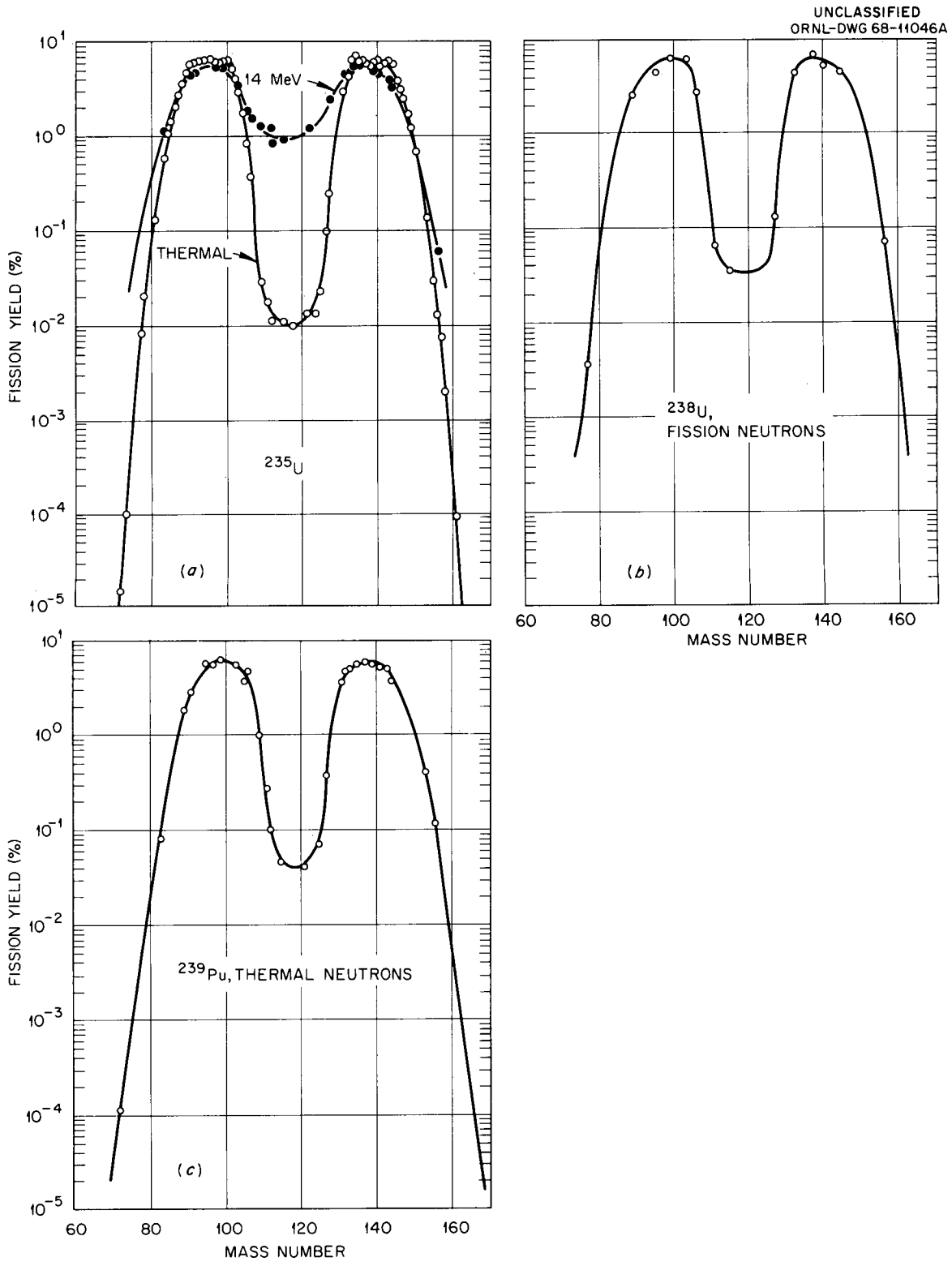

Fig. 2.13. Mass Distribution of Fission Products from the Fission of (*a*) ^{235}U, (*b*) ^{238}U, and (*c*) ^{239}Pu. (From *Reactor Handbook*, ref. 15.)

Table 2.5. Cranberg *et al.* Prompt-Neutron Spectrum Due to Fission of ^{235}U by Thermal Neutrons[a]

E (MeV)	$N(E)$ (MeV^{-1})	$F(E)$	$G(E)$ (MeV)
0.00	0.000	1.000	1.981
0.25	0.290	0.948	1.973
0.50	0.347	0.867	1.942
0.75	0.358	0.779	1.887
1.00	0.347	0.690	1.810
1.25	0.325	0.606	1.715
1.50	0.298	0.528	1.608
1.75	0.268	0.457	1.493
2.00	0.239	0.394	1.374
2.50	0.184	0.2884	1.138
3.00	0.138	0.2082	0.919
3.50	0.102	0.1486	0.726
4.00	0.0738	0.1050	0.563
4.50	0.0528	0.0736	0.430
5.00	0.0375	0.0512	0.324
5.50	0.0263	0.03544	0.241
6.00	0.0184	0.02439	0.178
6.50	0.0127	0.01669	0.130
7.00	8.77(−3)[b]	0.01138	9.41(−2)
7.50	6.01(−3)	7.72(−3)	6.76(−2)
8.00	4.10(−3)	5.22(−3)	4.83(−2)
8.50	2.79(−3)	3.52(−3)	3.43(−2)
9.00	1.88(−3)	2.364(−3)	2.42(−2)
9.50	1.27(−3)	1.583(−3)	1.70(−2)
10.00	8.56(−4)	1.058(−3)	1.187(−2)
10.50	5.74(−4)	7.05(−4)	8.25(−3)
11.00	3.84(−4)	4.686(−4)	5.72(−3)
11.50	2.56(−4)	3.108(−4)	3.947(−3)
12.00	1.70(−4)	2.058(−4)	2.714(−3)
13.00	7.48(−5)	8.97(−5)	1.271(−3)
14.00	3.26(−5)	3.88(−5)	5.88(−4)
15.00	1.41(−5)	1.67(−5)	2.69(−4)
16.00	6.07(−6)	7.10(−6)	1.22(−4)
17.00	2.59(−6)	3.00(−6)	5.48(−5)
18.00	1.10(−6)	1.26(−6)	2.44(−5)

[a]From ref. 18, p. 48.
[b]Read: 8.77×10^{-3}, etc.

results. Values of $N(E)$ and $F(E)$ as calculated from Cranberg's spectrum are presented in Table 2.5, along with values of $G(E)$, which is the energy per fission carried by neutrons having energies greater than E and is given by

$$G(E) = \int_E^\infty E' \, N(E') \, dE' . \tag{2.106}$$

The formula developed by Los Alamos[18] for the fission spectrum in the energy range below 9 MeV is

$$N(E) = 0.77E^{1/2} \, e^{-0.776E} . \tag{2.107}$$

This equation is a simpler approximation to the experimental data and is used primarily for reactor core calculations. The error associated with the formula is less than 12% for the specified energy range. For the energy range 4 to 14 MeV the Los Alamos formula has been reduced to the simple exponential

$$N(E) = 1.75 \, e^{-0.766E} . \tag{2.108}$$

The error associated with this formula is always less than 15% and is less than 7% for energies from 5 to 13 MeV.

2.6.2. FUSION REACTION

The fusion reaction involves the nuclear combination of two light nuclei having sufficient kinetic energy to overcome the repulsive force that exists between nuclei. Because the mean binding energy per nucleon for certain light nuclei is less than that for nuclei of intermediate mass (essentially the same change-in-mass phenomenon which characterizes the fission process), the fusing process of these nuclei is accompanied by considerable energy release and by the emission of nucleons.

The fusion processes of practical interest involve the light nuclei deuterium, tritium, and ^{3}He. Under proper conditions several combinations of these nuclei can undergo fusion, the reactions being represented in equation form as follows:

$$^2_1\mathrm{D} + {}^2_1\mathrm{D} \rightarrow {}^3_2\mathrm{He}(0.82\ \mathrm{MeV}) + {}^1_0n(2.45\ \mathrm{MeV})$$

$$^2_1\mathrm{D} + {}^2_1\mathrm{D} \rightarrow {}^3_1\mathrm{T}(1.01\ \mathrm{MeV}) + {}^1_1\mathrm{H}(3.02\ \mathrm{MeV})$$

$$^2_1\mathrm{D} + {}^3_1\mathrm{T} \rightarrow {}^4_2\mathrm{He}(3.5\ \mathrm{MeV}) + {}^1_0n(14.1\ \mathrm{MeV})$$

$$^2_1\mathrm{D} + {}^3_2\mathrm{He} \rightarrow {}^4_2\mathrm{He}(3.6\ \mathrm{MeV}) + {}^1_1\mathrm{H}(14.7\ \mathrm{MeV})$$

It is the 2.45- and 14.1-MeV neutrons produced in the D-D and D-T reactions utilized in nuclear detonations that are primarily of concern in shield design.

Unlike in the fission process, no prompt gamma rays are emitted in the fusion process and neither are the products radioactive. Bremsstrahlung radiation (see Section 2.4.2) is produced in conjunction with charged-particle deflections by the Coulomb field of other charged particles, but such radiation does not contribute significantly to the shielding problem.

2.7. Interactions of Gamma Rays

There are many possible processes by which gamma rays may interact with matter; however, the attenuation of gamma rays in a shield is completely dominated by three processes: the photoelectric effect, pair production, and Compton scattering. The three processes are described below, as are a number of processes that are usually neglected in shielding calculations.

2.7.1. PHOTOELECTRIC EFFECT

The photoelectric effect is characterized by the complete absorption of the gamma ray. The gamma ray interacts directly with an orbital electron, which is initially bound in an atom. The momentum is conserved by the recoil of the entire atom, thereby allowing a complete loss of energy by the gamma ray. Consequently, the more tightly bound electrons have the greatest probability of absorbing the gamma ray. It has been shown[19] that about 80% of the photoelectric absorptions involve the K-shell electrons. The orbital electron (photoelectron) is ejected from the atom having a kinetic energy $T = E_\gamma - B_e$, where B_e is the binding energy of the ejected electron. The remainder of the energy, which is equal to B_e, appears as very soft characteristic X rays, usually referred to as fluorescence radiation.

The photoelectric process does not lend itself to theoretical analysis and most cross-section data for this interaction are empirical, with theoretical methods being employed for interpolation and extrapolation of the data. The qualitative dependence of the probability for the photoelectric effect is given by the approximation

$$\sigma_{PE} \propto \frac{Z^4}{E_\gamma^3}, \tag{2.109}$$

where E_γ is the incident photon energy and Z is the atomic number. Equation 2.109 shows that the photoelectric effect is important for low-energy gamma rays and large-atomic-number materials, such as lead. Table 2.6 gives, for the elements of greatest importance to shielding, the energy at which the photoelectric effect provides one-half the total absorption coefficient, along with the ionization energy of the K shell.

Table 2.6. Gamma-Ray Energies at Which Photoelectric Effect Provides One-Half the Total Absorption Coefficient*

Atomic No., Z	Element	Gamma-Ray Energy (MeV)	K-Shell Ionization Energy (MeV)
1	Hydrogen	10^{-4}	1.4×10^{-5}
4	Beryllium	0.011	2.2×10^{-4}
6	Carbon	0.016	2.8×10^{-4}
8	Oxygen	0.025	5.2×10^{-4}
13	Aluminum	0.046	1.5×10^{-3}
20	Calcium	0.079	4.0×10^{-3}
26	Iron	0.11	6.9×10^{-3}
42	Molybdenum	0.195	2.0×10^{-2}
50	Tin	0.25	2.9×10^{-2}
74	Tungsten	0.42	6.06×10^{-2}
82	Lead	0.50	8.8×10^{-2}
92	Uranium	0.62	1.16×10^{-1}

*From ref. 18, p. 144.

The fluorescence radiation associated with the photoelectric effect is significant only when the interaction occurs in heavy elements. Even then the range of the emitted X rays is comparable to that of the photoelectrons, and their contribution to the penetrating dose is so small that they can be assumed to be absorbed at their point of origin.

2.7.2. PAIR PRODUCTION

The pair-production process has a threshold energy of 1.02 MeV and becomes increasingly more probable as the gamma-ray energy increases above 1.02 MeV. In this process the gamma ray is completely absorbed and an electron-positron pair appears in its place. Pair production must occur within the electrostatic field of a charged particle. The momentum is conserved in the process by the recoil of the charged particle, thereby making possible the complete absorption of the gamma ray. Either a nucleus or an atomic electron can provide

the necessary electrostatic field; however, due to the greater charge of a nucleus, the interactions are primarily nuclear.

The sum of the kinetic energies of the electron pair is equal to the initial gamma-ray energy less the energy equivalent of their rest masses and the kinetic energy of the recoil nucleus:

$$T_+ + T_- = E_\gamma - 2m_0c^2 - T_{\text{recoil}} . \qquad (2.110)$$

The kinetic energy acquired by the recoil nucleus can be neglected because of the relatively large mass of the nucleus. If, however, the process occurs in the field of an atomic electron, considerable energy is transferred to the recoil electron and a *triplet* is produced. The triplet consists of the newly created electron pair (one positron and one electron) and of the recoil electron. Because of momentum considerations, the threshold energy for triplet production is 2.04 MeV.

Every positron created in pair production loses its kinetic energy by ionization and then ultimately interacts with an ordinary electron, converting the electron and itself into electromagnetic radiation called *annihilation* radiation. Thus for each positron, two 0.51-MeV gamma rays are emitted in opposite directions. These secondary gamma rays are most important for high-energy gamma-ray sources (greater than 6 MeV) and medium-to-heavy elements. They are usually assumed to be absorbed at the point of formation; however, in the more refined Monte Carlo and S_n calculations, transport of the 0.51-MeV annihilation gamma rays can be included.

Aside from the effects of screening,* the nuclear pair-production cross sections σ_{PPN} are theoretically and experimentally proportional to Z^2. Analytical expressions are available only for two special cases:

(1) If screening is neglected and $m_0c^2 \ll E_\gamma \ll 137\, m_0c^2\, Z^{-1/3}$, then

$$\sigma_{\text{PP}} = \sigma_0 Z^2 \left[\frac{28}{9}\ln\left(\frac{2E_\gamma}{m_0c^2}\right) - \frac{218}{27}\right] . \qquad (2.111)$$

(2) If complete screening is considered and $E_\gamma \gg 137\, m_0c^2\, Z^{-1/3}$,

$$\sigma_{\text{PP}} = \sigma_0 Z^2 \left[\frac{28}{9}\ln\left(183\, Z^{-1/3}\right) - \frac{2}{27}\right] , \qquad (2.112)$$

where

$$\sigma_0 = \frac{1}{137}\left(\frac{e^2}{m_0c^2}\right)^2$$

$$= 5.80 \times 10^{-28} \text{ cm}^2/\text{nucleus} , \qquad (2.113)$$

m_0c^2 = energy equivalent of the rest mass of an electron

= 0.5110 MeV,

m_0 = electron rest mass

$= 0.5488 \times 10^{-3}$ amu $= 9.108 \times 10^{-28}$ g,

c = speed of light in a vacuum

$= 2.99793 \times 10^{10}$ cm/sec.

Table 2.7 gives the gamma-ray energies at which pair production provides one-half the total absorption coefficient for elements of greatest interest in shielding calculations.

Electronic pair production can occur when the gamma-ray energy exceeds 2.04 MeV. The analysis of this effect is difficult because of screening by other electrons and by the nucleus. However, the ratio of the total cross section for Z electrons of a given atom, $Z\sigma_{\text{PPE}}$, to the cross section for nuclear pair production, σ_{PPN}, can be written as

$$\frac{Z\sigma_{\text{PPE}}}{\sigma_{\text{PPN}}} = \frac{1}{CZ} , \qquad (2.114)$$

Table 2.7. Gamma-Ray Energies at Which Pair Production Provides One-Half the Total Absorption Coefficient*

Atomic No., Z	Element	Gamma-Ray Energy (MeV)
1	Hydrogen	78
4	Beryllium	35
6	Carbon	28
8	Oxygen	20
13	Aluminum	15
20	Calcium	12
26	Iron	9.5
42	Molybdenum	7.5
50	Tin	6.5
74	Tungsten	5.2
82	Lead	5.0
92	Uranium	4.8

*From ref. 18, p. 145.

*The positive charge of the nucleus can, in effect, be reduced by the cloud of negatively charged orbital electrons.

where the constant C depends upon E_γ and varies from about 2.6 at E_γ = 6.5 MeV to about 1.2 at E_γ = 100 MeV.

The effect of the electronic pair production can be included in a total pair-production cross section as

$$\sigma_{PP} = \sigma_{PPN} + Z\sigma_{PPE} = \sigma_{PPN}\left(1 + \frac{1}{CZ}\right), \quad (2.115)$$

where $1/CZ = 0$ if $E_\gamma < 2.04$ MeV.

2.7.3. COMPTON SCATTERING

The Compton scattering process, named for the experimentalist A. H. Compton, can be described as an elastic collision between the incident gamma ray and a free electron.* Under these conditions the kinetic energy, as well as the momentum, is conserved, which results in a precise relation between the loss of gamma-ray energy and its change in direction. The functional representation of this relation is given by

$$E = \frac{E_0}{1 + \frac{E_0}{m_0c^2}(1 - \cos\theta)}, \quad (2.116)$$

where

E_0 = initial gamma-ray energy,

E = final gamma-ray energy,

θ = angular change experienced by the gamma ray,

m_0c^2 = 0.5110 MeV,

m_0 = 0.5488 × 10^{-3} amu = 9.108 × 10^{-28} g,

c = 2.99793 × 10^{10} cm/sec.

A plot of Eq. 2.116, which is referred to as Compton's equation, is shown in Fig. 2.14.

Another useful form of Compton's equation is obtained if the gamma-ray energy E and wavelength λ are expressed in units of the electron rest-mass energy (mc^2 = 0.5110 MeV) and the Compton wavelength (h/mc = 0.02426 Å) respectively. In these units the wavelength and energy variables are simply reciprocals of each other and Compton's equation assumes the form

$$\lambda - \lambda_0 = 1 - \cos\theta, \quad (2.117)$$

where λ is the final wavelength.

*As the energy of the incident gamma ray increases, even the tightly bound orbital electron behave as free electrons.

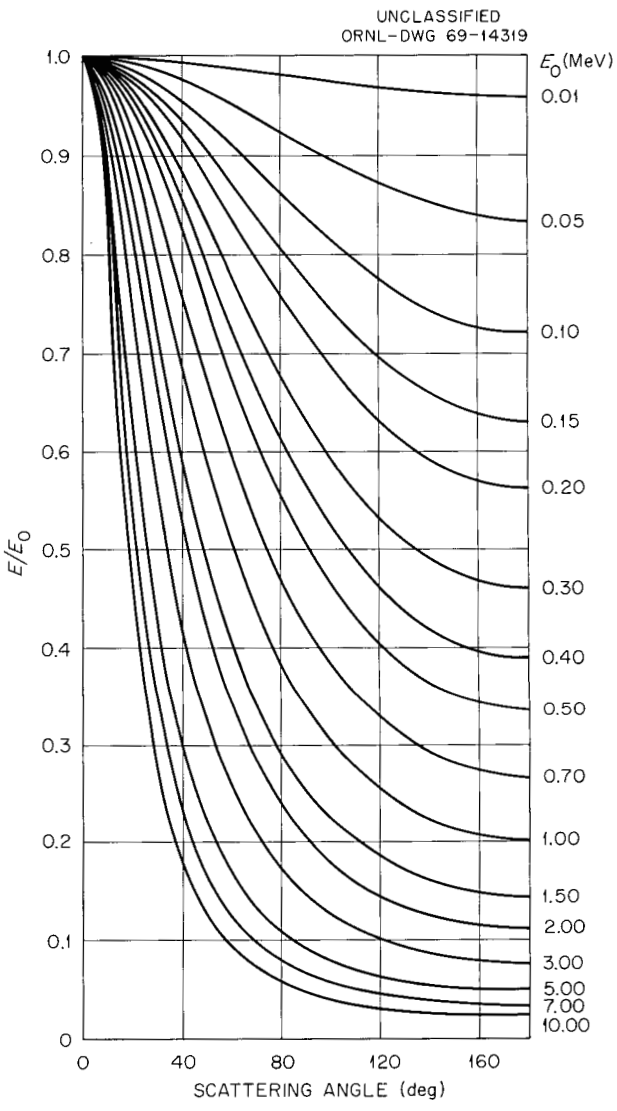

Fig. 2.14. Reduction in Gamma-Ray Energy by Compton Scattering. (E_0 = initial energy; E = reduced energy.)

The differential cross section $\sigma(\theta)$ for Compton scattering is defined as the cross section per electron for scattering through a given angle θ per unit solid angle. Expressed in Thomson units, this cross section is given by the Klein-Nishina formula[†20]

$$\sigma(\theta) = \frac{d\sigma}{d\bar{\Omega}} = \frac{3}{16\pi}\frac{E^2}{E_0^2}\left(\frac{E_0}{E} + \frac{E}{E_0} - \sin^2\theta\right), \quad (2.118)$$

†This form of the equation does not include polarization effects that are due to scattering. However, this effect is of no consequence to practical problems in radiation transport.

where 1 Thomson unit = $(8\pi/3)\ (e^2/mc^2)^2 = 0.665$ barn. The dependence of the differential cross section on the scattering angle θ for various initial energies is illustrated in Fig. 2.15. It is noted that $\sigma(\theta)$ is symmetric only for the nonrelativistic limit $E \to 0$. As the initial energy increases, the cross section becomes more and more sharply peaked in the forward direction. Consider an initial energy E = 2.5 MeV: the cross section decreases to one-half its initial value at a scattering angle of about 20° and then drops to about 3% of its initial value for θ = 180°. This characteristically forward scattering of the high-energy gamma rays strongly influences the nature of the deep-penetration problem.

The total cross section for Compton scattering per electron is obtained by integrating the differential cross section over 4π solid angle:

$$\sigma_C(E) = \int_{4\pi} \sigma(\theta)\, d\bar{\Omega}\,, \tag{2.119}$$

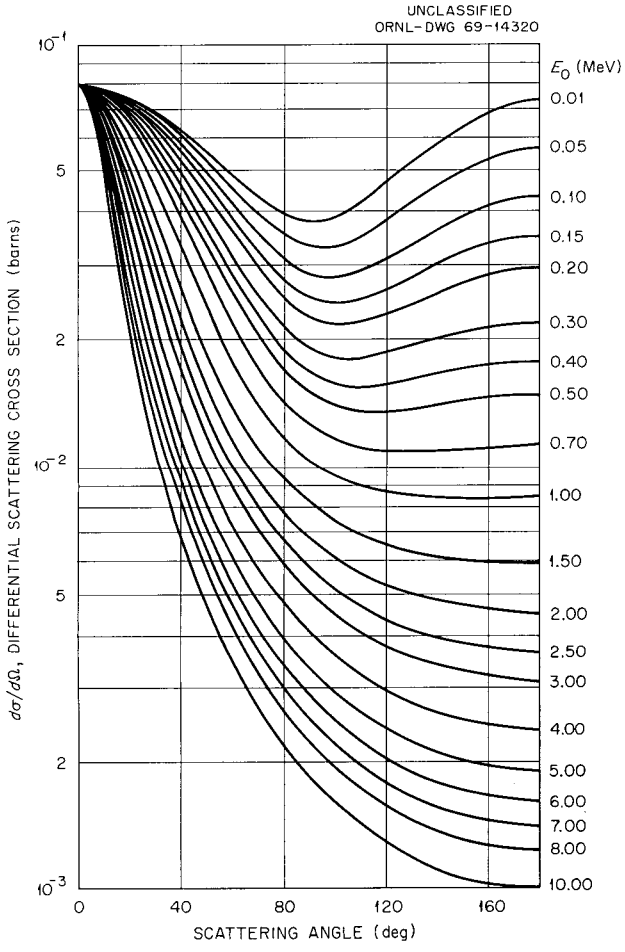

Fig. 2.15. Differential Klein-Nishina Cross Sections.

where $d\bar{\Omega} = 2\pi \sin\theta\, d\theta$. Substituting Eq. 2.118 into Eq. 2.119 and integrating provides the following expression for the total cross section:

$$\sigma_C(E) = \frac{3}{4}\left\{\frac{1+E}{E^3}\left[\frac{2E(1+E)}{1+2E} - \ln(1+2E)\right] + \frac{1}{2E}\ln(1+2E) - \frac{1+3E}{(1+2E)^2}\right\}, \tag{2.120}$$

where the units of the gamma-ray energy E are given in terms of the electron rest-mass energy (m_0c^2 = 0.5110 MeV). For small gamma-ray energies ($E \ll 1\ m_0c^2$) the value of $\sigma_C(E)$ approaches one Thomson unit and for large gamma-ray energies it approaches $(3/8E)(\ln 2E + 1/2)$.

The cross section related to the average fractional energy carried off by the scattered gamma ray is defined as

$$\sigma_{C_s}(E) \equiv \int^{4\pi} \frac{E}{E_0}\, \sigma(\theta)\, d\bar{\Omega}\,, \tag{2.121}$$

which on integration yields

$$\sigma_{C_s}(E) = \frac{3}{8}\left[\frac{\ln(1+2E)}{E^3} + \frac{2(1+E)(2E^2-2E-1)}{E^2(1+2E)^2} + \frac{8E^2}{3(1+2E)^3}\right]. \tag{2.122}$$

The other cross section of importance relates to the average fractional energy lost by a gamma ray suffering a Compton collision; the fraction increases monotonically as the gamma-ray energy increases. This cross section represents the energy absorption or energy deposition* cross section and is defined by

$$\sigma_{C_a}(E) \equiv \int^{4\pi} \frac{E-E'}{E}\, \sigma(\theta)\, d\bar{\Omega}\,, \tag{2.123}$$

*The term energy deposition was suggested by A. B. Chilton of the University of Illinois as a replacement for the term energy absorption since the ICRU has designated the energy absorption coefficient to mean an essentially similar quantity but with correction terms to account for subsequent transport of the energy after having made an absorption collision. A discussion of these considerations is given in ORNL-RSIC-16 (ref. 21). One must be careful in the use of such correction terms, which should be consistent with the transport model assumed or energy may not be conserved.

which is also simply expressed as

$$\sigma_{C_a}(E) = \sigma_C(E) - \sigma_{C_s}(E) . \quad (2.124)$$

It is noted that the various Compton cross sections are usually given on a per electron basis since the scattering occurs with free electrons. The cross sections are simply multiplied by the atomic number Z to obtain the atomic cross section. More detailed descriptions of the Compton cross sections are presented elsewhere.[18,19]

2.7.4. NEGLECTED PROCESSES

As pointed out above, the three processes described in the preceding paragraphs are usually the only gamma-ray interactions considered in shielding attenuation calculations since all other processes make only negligible contributions. Some of the interactions that are ignored are described below.

Rayleigh Scattering

Of the neglected processes Rayleigh scattering is the most important and of some slight significance at low gamma-ray energies, but it is still less probable than Compton scattering by 1 or 2 orders of magnitude for energies greater than 0.1 MeV. Rayleigh scattering is elastic coherent scattering by tightly bound electrons, and the process is more probable with heavy elements. In the energy range of interest to shielding, Rayleigh scattering results in small changes in direction and in essentially no energy loss. The net result of coherent scattering is to make the angular distribution of low-energy scattered gamma rays more nearly isotropic. Tabulations of total attenuation coefficients for practical design calculations generally do not include the Rayleigh scattering cross section, which neglect tends to produce a slight overestimate of the gamma-ray flux at field points removed from the source.

Thomson Scattering

Thomson scattering is quite similar to Rayleigh scattering, with the interaction involving the nucleus rather than atomic electrons. The effect is very small and is truly negligible.

Nuclear Resonance Scattering

Nuclear resonance scattering involves the excitation of a nuclear level by the complete absorption of an incident gamma ray followed by the re-emission of the excitation energy. The probability for nuclear resonance scattering is extremely small and its effect would be to increase the isotropy of the gamma-ray flux.

Photodisintegration

Photodisintegration of nuclei is possible if the gamma-ray energy exceeds the separation energy of a nucleon. Except for the $^9Be(\gamma,n)$ and $^2H(\gamma,n)$ reactions, this effect is confined to gamma rays with energies in excess of 8 MeV. The cross sections for photodisintegration are usually negligible when compared with those for Compton scattering and pair production.

2.7.5. GAMMA-RAY CROSS SECTIONS

The total gamma-ray interaction cross section for the usual shielding calculation is given by

$$\sigma_t = \sigma_{PE} + \sigma_{PP} + Z\sigma_C , \quad (2.125)$$

where

σ_t = total gamma-ray interaction cross section per atom,

σ_{PE} = photoelectric microscopic cross section per atom,

σ_{PP} = pair-production microscopic cross section per atom,

σ_C = total Compton cross section per electron,

Z = atomic number.

More useful macroscopic variations of the total gamma-ray cross section are the linear attenuation coefficient μ, given in units of cm^{-1} and defined as

$$\mu = \sigma_t \frac{\rho N_0}{A} , \quad (2.126)$$

where ρ is the density (g/cm^3), N_0 is Avogadro's number = 6.023×10^{23} nuclei/g-atom, and the mass attenuation coefficient is designated by μ/ρ in units of cm^2/g.

The gamma-ray energy deposition coefficient is usually taken as

$$\mu_a = \frac{\rho N_0}{A}(\sigma_{PE} + \sigma_{PP} + Z\sigma_{C_a}) , \quad (2.127)$$

where σ_{C_a} is the Compton energy-deposition cross section per electron. This relation presumes that the photoelectric and pair-production reactions are pure absorptions; other variations are sometimes used (see Section 2.9.3). These cross sections are often reported as mass energy absorption coefficients, μ_a/ρ. Extensive tables for the cross sections of these gamma-ray interactions, as well as others, have been prepared by Plechaty and Terrall[22] for elements 1 through 100 and gamma-ray energies ranging from 0.001 to 100 MeV, and later data for the energies 1 keV to 1 MeV have been published by McMaster *et al.*[23]

2.8. Gamma-Ray Production Processes

It was pointed out in Section 2.4.2 that the electromagnetic radiations of primary concern in shielding are the nuclear transition gamma rays. Gamma rays produced by a weapons burst are due to a number of sources, with only one, the fission reaction, a direct result of the detonation. All other sources are produced either by the interaction of fission or fusion neutrons with various materials or by the radioactive decay of the fission products. The important sources are listed below.

2.8.1. FISSION REACTION

The fission reaction utilized in weapons detonations is always accompanied by the emission of prompt gamma rays, whose energies total about 8 MeV per fission. These prompt gamma rays, like prompt neutrons, are released whenever the compound nucleus formed by an incident neutron and a target nucleus splits into two (or more) fission fragments (see Section 2.6.1). The energy spectrum of such gamma rays is known reasonably well only for ^{235}U, measurements having been made for this isotope by Motz[24] and by Maienschein *et al.*[25]

2.8.2. NEUTRON INELASTIC SCATTERING

In the neutron inelastic-scattering process described in Section 2.5.2 the energy of the target nucleus is elevated to an excited state, from which it returns to the ground state by the emission of gamma rays. In weapons detonations the target nuclei can be weapons materials or environmental materials, such as those comprising the atmosphere and the ground. Investigations of the production of such gamma rays have been carried out by Dickens and Perey[26] and by Orphan and Hoot.[27] (See also Chapter 6 of this Handbook.)

2.8.3. NEUTRON CAPTURE

The neutron radiative-capture process, also described in Section 2.5.2, results in the de-excitation of the compound nucleus via the emission of gamma rays. And again, the target nuclei can be weapons materials or environmental materials such as those comprising the atmosphere and the ground. The gamma rays emitted following radiative capture can be given off immediately, in which case they are called capture gamma rays, or they can be emitted at later times, in which case they are called activation gamma rays. Activated materials can contribute to fallout or can prevent access to regions in the vicinity of a detonation.

The radiative capture process is most important for low-energy neutrons. Early data on capture gamma rays produced by neutron captures in various nuclei were published by Bartholomew and Campion,[28] Keller *et al.*,[29] and Troubetzkoy and Goldstein,[30] and later information has been presented by Maerker and Muckenthaler,[31] Bartholomew *et al.*,[32] and Groshev *et al.*[33,34] Data on long-term emitters of activation gamma rays have been published by Crocker and Conners[35] and by Crocker and Wong.[36]

2.8.4. FISSION-PRODUCT DECAY

The fission fragments produced in the fission process undergo radioactive decay through the emission of gamma (and beta) radiations. These gamma rays constitute an important source from the moment of detonation to long periods following the detonation. Studies of the early-time ($<$ 1 min) fission-product gamma rays have been made by Engle and Fisher.[37] Data on the total radiative decay of fission products for times up to 70 years have been reported by Crocker and Turner.[38] The total gamma-ray energy released through fission-product decay is about 7 MeV per fission.

2.8.5. BREMSSTRAHLUNG

Electromagnetic radiation, called bremsstrahlung, is emitted when a free charged particle experiences an acceleration or deceleration by the electrostatic field of a nucleus. The total bremsstrahlung produced varies as the square of the atomic number of the recoil nucleus and inversely with the square of the mass of the incident particle. Bremsstrahlung is characterized by a continuous spectrum, with the energy emitted by a particular particle ranging from zero up to its total

kinetic energy. Because of the strong dependence on the incident particle's mass, charged particles other than electrons can be completely neglected insofar as the production of bremsstrahlung is concerned.

Large numbers of electrons are produced as secondaries during the attenuation of gamma rays; for example, photoelectrons, Compton recoils, and the electron-positron pairs. All these electrons will produce numerous bremsstrahlung radiations; however, their energies will be relatively low and for all present shielding calculations they are assumed to be absorbed at the point of formation.

2.9. Quantities Used to Describe Responses to Radiation

Although calculations of the interactions of radiation with matter deal with the fluxes and currents described in Section 2.1, such quantities are not easily measured in the laboratory, especially as a function of energy and direction. However, the property of a radiation field called *dose,* which is related to the energy deposited in a medium by the radiation interacting within it, is determinable, and this is the quantity that is used to relate a radiation field to the biological damage it causes in a human body.

In an ideal situation a given dose would always produce the same biological effect irrespective of the nature and energy of the radiation or of the body organ being irradiated. But studies by radiobiologists in which doses and biological damage to specific organs are correlated for known radiation fields have established that nature is not that simple. In addition to being a function of absorbed energy, biological responses are functions of the irradiated organ and of the type, rate, and energy of the radiation. From this discovery has evolved the concept of a *relative biological effect (RBE),* which is a weighting factor that can be used to compare the biological effects produced by the same *physical dose* (same amount of energy deposited) due to radiation of a different type and/or energy. When the physical dose is multiplied by the RBE it becomes a *biological dose.*

The foregoing gives some indication of the problems associated with establishing doses for shield design that are related to biological hazards. The shield designer's task is further complicated by the perturbation of the radiation field by the human body, an effect not usually included in a typical shielding calculation. Obviously the dose received at a particular location within the body is not the same as the dose in a small detector at the same location in space with the body absent. It is apparent that shielding studies should include anthropomorphic phantoms as part of the shield configuration, a theoretically possible but usually impractical consideration.

As an alternative, slab or cylindrical phantoms with compositions resembling that of the human body have been used, and the doses have been calculated or measured as a function of depth in the phantom for a given incident radiation field. The results are then used as response functions to relate an unperturbed radiation field (usually called a free field) to the dose in a human body if it had been present.

It will be apparent in the following discussion on the various quantities used to define physical and biological doses that confusion has developed in the terminology and in the definition of units, both because of the burgeoning nuclear science and technology and because radiobiologists and shield designers basically differ in their viewpoints. The International Commission on Radiation Units and Measurements* recognized this confusion and in an effort to mitigate it recommended[1,21] a consistent set of definitions and units. While shield designers have accepted most of their recommendations, they have continued to use terms not included in the ICRU recommendations because these terms are so ingrained in the shielding field and because the ICRU did not include all the concepts needed in shield design. In the descriptions given below the ICRU recommendations and the traditional viewpoints are contrasted.

In addition to descriptions of the quantities themselves, this section includes data for some of the quantities considered most pertinent for shield design.

2.9.1. ABSORBED DOSE

Absorbed dose is the energy imparted by radiation to a unit mass of matter and as such is a *physical* quantity as opposed to a *biological* effect. A formal definition for the energy imparted, E_D, is: *The energy imparted*

*The International Commission on Radiation Units and Measurements has as its principal objective the development of internationally acceptable recommendations regarding quantities and units of radiation and radioactivity, procedures suitable for the measurement and application of these quantities, and physical data needed in the application of these procedures.

by ionizing radiation to the matter in a volume is the difference between the sum of the energies of all the directly and indirectly ionizing particles which have entered the volume and the sum of the energies of all those which have left it, plus the energy equivalent (Q) of any decrease in rest mass that took place in nuclear or elementary particle reactions within the volume.* For all practical purposes the energy imparted is usually equal to the heating effect, but in some cases part of the energy deposited may result in changes in interatomic bond energies.

As proposed by the ICRU,[1] the energy imparted can be expressed as

$$E_D = \sum E_{\text{in}} - \sum E_{\text{ex}} + \sum Q , \tag{2.128}$$

where

$\sum E_{\text{in}}$ = the sum of the energies (excluding rest energies) of all those directly and indirectly ionizing particles which have entered the volume,

$\sum E_{\text{ex}}$ = the sum of the energies (excluding rest energies) of all those directly and indirectly ionizing particles which have left the volume,

$\sum Q$ = the sum of all the energies released, minus the sum of all the energies expended, in any nuclear reactions, transformations and elementary particle processes which have occurred within the volume.

The absorbed dose (D) is the quotient of ΔE_D by ΔM, where ΔE_D[†] is the energy imparted by ionizing radiation to the matter in a volume element and ΔM is the mass of the matter in that volume element:

$$D = \frac{\Delta E_D}{\Delta M} . \tag{2.129}$$

*Ionizing radiation is a radiation consisting of directly or indirectly ionizing particles or a mixture of both. Directly ionizing particles are charged particles (electrons, protons, alpha particles, etc.) having sufficient kinetic energy to produce ionization by collision. Indirectly ionizing particles are uncharged particles (neutrons, gamma rays, etc.) which can liberate directly ionizing particles or can initiate a nuclear transformation.

[†]The notation ΔE_D implies that the volume element ΔV associated with the element of mass ΔM be of an appropriate size such that the limiting process $D = \Delta E_D/\Delta M$ yield a meaningful estimate of the absorbed dose. The difficulties arise because the interactions between radiations and atoms are macroscopic and the limiting process cannot proceed to the usual mathematical limit $\Delta M \to 0$.

The special unit of absorbed dose is the rad, which is

$$1 \text{ rad} = \frac{1}{100} \text{ J/kg} = 100 \text{ ergs/g} . \tag{2.130}$$

The absorbed dose rate is the quotient of ΔD divided by Δt, where ΔD is the increment in absorbed dose in time Δt; i.e.,

$$\text{Absorbed dose rate} = \frac{\Delta D}{\Delta t} . \tag{2.131}$$

A special unit of absorbed dose rate is any quotient of the rad or its multiple or submultiple by a suitable unit of time (rads/sec, mrads/hr, etc.).

Energy can be imparted to a volume of matter by many different particle reactions, and particles having the same initial energy do not necessarily deposit the same amount of energy. This, of course, is because the energy deposition depends not only on the initial energy but also on the type of radiation and the kinds of interactions that occur. Schematic representations of energy imparted to the matter contained within a volume element ΔV for two particles having initial energies E_0^1 and E_0^2 are shown in Fig. 2.16 (superscripts 1 and 2 identify the reactions produced by particles 1 and 2 respectively). The corresponding equations for the energy imparted are

$$\Delta E_D^1 = E_0^1 - E_\beta^1 - E_\gamma^1 - Q^1 , \tag{2.132a}$$

$$\Delta E_D^2 = E_0^2 - E_\gamma^2 + Q^2 , \tag{2.132b}$$

where ΔE_D is the energy imparted to the matter within the volume element ΔV, Q is the energy equivalent of any change in the rest mass due to nuclear or elementary particle reactions within the volume, and subscripts β and γ refer to the type of particle leaving the volume. In reaction 1, an incident gamma ray undergoes a Compton scattering within the volume element ΔV. Q^1 is the binding energy of the Compton electron which is usually of negligible magnitude. The Compton electron loses some of its energy through ionization within the volume and then departs with the energy E_β^1. The scattered (degraded) gamma ray also leaves the volume. In the second reaction, a neutron undergoes radiative capture and a gamma ray is produced which leaves the volume. Q^2 is the binding energy associated with the neutron capture which appears as excitation energy. Note that no secondary collisions within the volume element were included in this schematic representation. This was purposely done

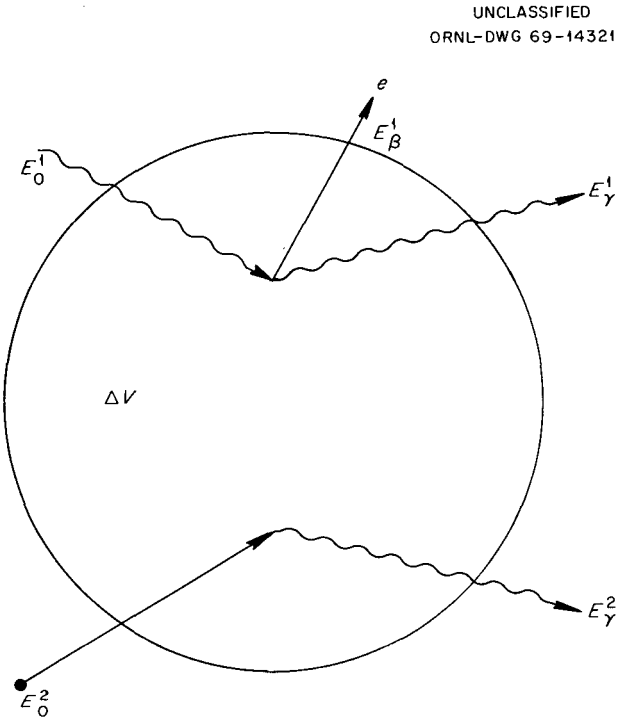

Fig. 2.16. Schematic Representation of Relationship Between Absorbed Dose (Energy Deposition) and Kerma.

to illustrate that the volume element ΔV should be large enough for many primary interactions to occur but sufficiently small so that a primary particle and/or secondary neutrons or gamma rays usually do not suffer collisions subsequent to the initial collision by the incident particle within the volume element ΔV.

The average energy imparted to the matter within the volume element ΔV by all reactions of particles of a particular type and energy can be written as

$$\bar{E}_D(E) = \frac{\sum_i R_i(E)\, E_i(E)}{\sum_i R_i(E)}, \qquad (2.133)$$

where

$\bar{E}_D(E)$ = the average energy imparted in ergs or MeV,

$R_i(E)$ = rate of the ith type of reaction for particles of energy E within the volume element ΔV,

$E_i(E)$ = energy imparted, in ergs or MeV, associated with a particle of energy E undergoing reaction i within the volume element ΔV.

2.9.2. FIRST-COLLISION DOSE AND KERMA

The quantity absorbed dose discussed in the previous section is a physical variable that is closely related to the potential hazard of a radiation field but for a real situation is sometimes very difficult to calculate accurately or to relate to the response in a human being. Consequently, other concepts have often been used.

One of the concepts used is the *first-collision dose* (also called the single-collision dose). This quantity has been subject to several interpretations that differ from one another in subtle ways. One of the most comprehensive reviews of the meanings of first-collision dose has been written by Attix,[39] who says that the first-collision dose due to a radiation field (neutrons and/or gamma rays) can be interpreted in each of the following three ways:

1. The first-collision dose is the absorbed dose contributed by *all* particles incident on an isolated small mass (unless the term is explicitly modified to include only one component, e.g., neutrons) in which charged-particle equilibrium* exists.

2. The first-collision dose is the absorbed dose contributed by primary radiation only in a small mass that can be located anywhere and in which charged particle equilibrium exists.

3. The first-collision dose is the energy transferred from *uncharged* incident radiation, regardless of origin, to the charged particles formed in a limitingly small probe that may be located anywhere. Charged-particle equilibrium in the probe is not a requirement.

The small mass specified in interpretations 1 and 2 means that the probe is small enough to leave the radiation field unperturbed and the probability is negligible that the incident particles will interact with the probe more than once or that secondary gamma rays† produced within the mass will be absorbed within it. The small probe specified in interpretation 3 has the same requirements but it can be smaller than that required for the other interpretations because charged-particle equilibrium is not necessary.

It can be stated at this point that interpretation 2 is a special and seldom used definition that will not be elaborated on here. Interpretation 1, on the other hand, is a widely used definition – particularly by experimentalists – and is often referred to as the free-field dose, the air dose, the free-air dose, etc. But in an

*Charged-particle equilibrium may be viewed as that condition when on the average as many charged particles such as electrons enter the volume element ΔV as leak out, thereby resulting in an essentially zero net transfer of energy by the flow of electrons.

† As used here, secondary gamma rays refer to those gamma rays produced by the interaction of the incident radiation (e.g., capture gamma rays and inelastic-scattering gamma rays).

attempt to alleviate confusion, the ICRU chose interpretation 3 to use as a basis for an exact definition and called the quantity so defined the kerma (*k*inetic *e*nergy *r*eleased in *ma*terial). In fact, the ICRU encourages the exclusive use of the term kerma[1] with the implication that the term first-collision dose and its other interpretations should be relegated to the archives.

The definition of kerma, K, as recommended by the ICRU[1] is

$$K \equiv \Delta E_K / \Delta M , \tag{2.134}$$

where ΔE_K = sum of the initial kinetic energies (ergs) of all the charged particles liberated by indirectly ionizing particles in a volume element of material ΔV, and ΔM = mass (g) of the material contained in the volume element ΔV.

The *kerma rate* is the quotient of ΔK by Δt, where ΔK is the increment in kerma in time Δt:

$$\text{Kerma rate} = \Delta K / \Delta t. \tag{2.135}$$

Since ΔE_K is the sum of the initial kinetic energies of all charged particles liberated by indirectly ionizing particles, it includes not only the kinetic energy these charged particles expend in collisions but also the bremsstrahlung they radiate and the energy of any charged particles that are produced in secondary processes.

The kerma or kerma rate for a specified material in free space or at a point inside a different material will be that which would be obtained if a small quantity of the specified material were placed at the point of interest.

With the definition of kerma in mind, the reactions shown in Fig. 2.16 are interpreted in terms of the initial kinetic energy imparted to charged particles:

$$\Delta E_K^1 = E_0^1 - E_\gamma^1 - Q^1 , \tag{2.136a}$$

$$\Delta E_K^2 = E_0^2 - E_\gamma^2 + Q^2 . \tag{2.136b}$$

It is noted that the expression for ΔE_K^2 and the expression given in Eq. 2.132*b* for ΔE_D^2 are the same, while the expression for ΔE_K^1 differs from that given in Eq. 2.132*a* for ΔE_D^1. This is because the Compton electron produced by reaction 1 did not deposit all of its energy within the volume element and there was no compensating in-leakage of an electron; i.e., charged-particle equilibrium did not exist.

Auxier[40] strongly criticizes the ICRU for not formally recognizing first-collision dose as given by interpretation 1. His objections are based on the fact that the first-collision doses obtained from measurements with ionization chambers, proportional counters, etc., are absorbed (imparted) energy and not transferred kinetic energy. Therefore, since measured doses cannot be interpreted as kerma, except by deduction, some dosimetrists are insisting on retaining the term first-collision dose. On the other hand, if charged-particle equilibrium exists, which it may or may not, and if bremsstrahlung radiation is ignored, then first-collision dose and kerma are equivalent. It can be seen that, in bulk shields or large tissue masses, first-collision dose and kerma have nearly the same magnitude but that in thin layers, such as clothing or skin, they can be quite different.

The early calculations of first-collision dose per unit fluence were performed by Snyder[41] for monoenergetic neutrons incident on a four-element tissue model. Although the term kerma had not yet been introduced, the doses obtained by Snyder are those described by interpretation 3 above and thus are kerma per unit fluence. His calculations considered only neutron captures and elastic scatterings, with the latter assumed to take place isotropically in the center-of-mass system. Later, Henderson[42] made similar calculations for neutrons for a four-element tissue model and for ethylene. He reported his results as absorbed dose (in rads/hr per unit flux), but they are actually kerma rate per unit flux.

The most recent and most comprehensive calculations of neutron kerma factors (kerma per unit fluence) were made by Ritts *et al.*[43] They included essentially all reactions, considered anisotropic scattering in those reactions for which angular cross-section data were available, and in all cases used the most recent cross-section data. They used several models, one of which was an 11-element "standard man" model in which all tissue organs and bone were homogenized and the other models were for specific body organs. The elemental compositions used in the calculations are shown in Table 2.8, and all the reactions considered are listed in Table 2.9.

The calculations by Ritts *et al.* were made for 816 discrete neutron energies corresponding to the supergroup-subgroup structure of the 05R Monte Carlo code[44] over an energy range 0.023 eV to 19.2 MeV. The kerma factor for a particular irradiated material was found by summing the averages of the kinetic energies imparted to the struck nuclei and the energies associated with charged particles that were emitted.

Table 2.8. Elemental Percentages and Number Densities Used in Neutron Kerma Calculations[a]

Element	Percent Composition						Number Density (10^{24} atoms/g)					
	Standard Man	Lung	Muscle	Bone	Brain	Red Marrow	Standard Man	Lung	Muscle	Bone	Brain	Red Marrow
H	10	10	10	7.1	10	10	5.977(−2)[c]	6.062(−2)	5.977(−2)	4.50(−2)	5.977(−2)	5.977(−2)
O	60	75	75	39.5	71	74[b]	2.259(−2)	2.864(−2)	2.824(−2)	1.49(−2)	2.674(−2)	2.7866(−2)
C	24	10	11	22.4	15	12.5[b]	1.204(−2)	5.09(−3)	5.518(−2)	1.13(−2)	7.52(−3)	6.270(−3)
N	2.9	2.6	2.6	4.7	1.9	3.2	1.25(−3)	1.13(−3)	1.118(−3)	2.05(−3)	8.17(−4)	1.377(−3)
Ca	1.2	0.011	0.0031	12.37	0.0086		1.77(−4)	1.68(−6)	4.66(−7)	1.87(−3)	1.29(−6)	
P	1.1	0.11	0.18	13.16	0.34		2.14(−4)	2.17(−5)	3.50(−5)	2.57(−3)	6.61(−5)	
S	0.24	0.24	.24	0.41	0.17		4.51(−4)	4.57(−5)	4.51(−5)	7.69(−5)	3.19(−5)	
K	0.20	0.20	0.30		0.30		3.08(−5)	3.13(−5)	4.62(−5)		4.62(−5)	
Na	0.20	0.18	0.16	0.08	0.18		524(−5)	4.78(−5)	4.19(−5)	2.08(−5)	4.72(−5)	
Cl	0.20	0.25	0.18		0.23	0.12	3.40(−5)	4.31(−5)	3.06(−5)		3.91(−5)	2.039(−5)
Mg	0.03	0.0096	0.019	0.28	0.015		7.43(−6)	4.78(−6)	4.71(−6)	6.87(−5)	3.72(−6)	

[a]From ref. 43.
[b]The values for oxygen and carbon were increased by 1% and 0.5% respectively.
[c]Read: 5.977×10^{-2}, etc.

Table 2.9. Reactions Considered in Calculations of Neutron Kerma Calculations[a]

Type of Reaction	H	O	C	N	Ca	P	S	K	Na	Cl	Mg
Radiative capture	x			x		x	x	x	x[b]	x	x
Elastic scattering	x	x	x	x	x	x	x	x	x	x	x
Inelastic scattering		x	x	x	x	x	x	x	x		x
(n,p) reaction		x[b]		x		x[b]		x		x	x
(n,α) reaction		x	x	x		x[b]		x		x[b]	x
$(n,n'3\alpha)$ reaction			x								
$(n,2n)$ reaction				x[c]		x[c]		x[c]			
(n,d) reaction				x				x			
(n,t) reaction				x							
$(n,2\alpha)$ reaction				x							
$(n,n'p)$ reaction						x		x			x
$(n,n'\alpha)$ reaction								x			

[a]From ref. 43.

[b]Includes beta decay after reaction.

[c]Includes positron decay.

Therefore the kerma per unit fluence may be expressed as

$$\mu_K = \sum_i \sum_j C N_i(E)\, \sigma_{ij}(E)\, E_{ij}\,, \qquad (2.137)$$

where

N_i = number density of element i (atoms/g),

σ_{ij} = microscopic cross section of reaction j for element i (cm^2/atom),

E_{ij} = average energy deposited by reaction j for element i (MeV),

$C = 1.602 \times 10^{-6}$ (ergs/MeV).

Since the kerma values are given per unit fluence, they are fluence-to-kerma conversion factors (usually referred to simply as kerma factors). Such kerma factors for the standard man model are plotted in Fig. 2.17 and tabulated in Table 2A.1 in Appendix 2A, along with kerma factors for the individual elements making the greatest contributions to the total factor. Kerma factors for specific body components (lung, muscle, bone, brain, and red marrow) are also tabulated in Appendix 2A, as well as *unweighted* kerma factors for the important elements in the standard man. With these values a total kerma factor for any arbitrary composition of these materials can be easily calculated.

Kerma rate factors for monoenergetic gamma rays incident on carbon, air, and a four-element tissue model were calculated by Henderson[42] and are plotted in Fig. 2.18. (Henderson's gamma-ray results, like his neutron results, were actually reported as absorbed dose, the term kerma not having been introduced yet.) Prior to Henderson's work, exposure factors for air published by Rockwell[45] were generally used as the equivalent flux-to-dose rate conversion factors for tissue.

2.9.3 EXPOSURE

Exposure is a term that should be used only for gamma rays. Formerly referred to as *exposure dose,* it came into common usage after the problem of specifying biological dose associated with X rays was first encountered. As recommended by the ICRU, exposure (X) describes the deposition of energy in air by electromagnetic radiation and is defined by

$$X \equiv \Delta Q / \Delta M\,, \qquad (2.138)$$

where ΔQ = sum of the electrical charges of all the ions of one sign produced in air when all electrons liberated by photons in a volume of air ΔV are completely stopped,* and ΔM = mass of the material contained in the volume element ΔV. *Exposure rate* is given by

*The ionization that would be produced by the bremsstrahlung associated with secondary electrons is not included in ΔQ. Except for this small difference, which is insignificant for photon energies less than 15 MeV, exposure is equivalent to kerma.

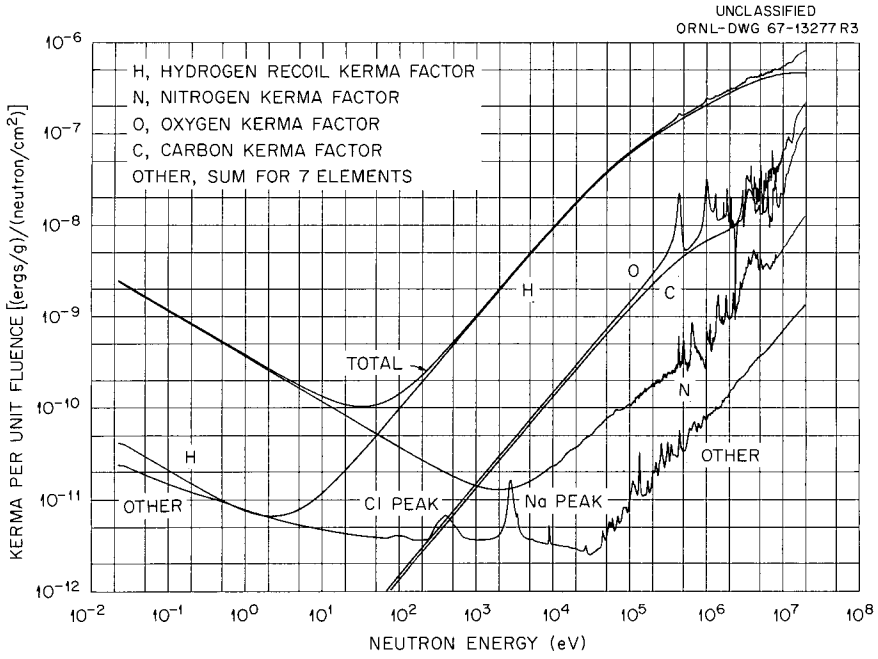

Fig. 2.17. Neutron Fluence-to-Kerma Factors for Standard-Man Model and for Elements Contributing to Standard-Man Model. (From Ritts *et al.*, ref. 43.)

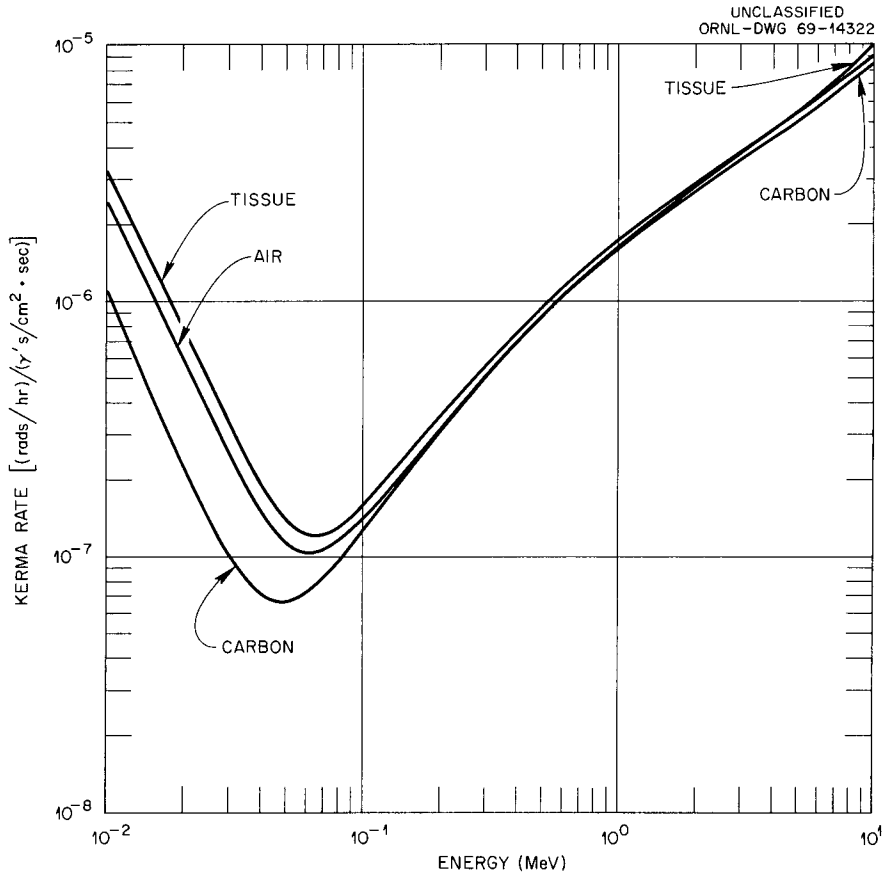

Fig. 2.18. Gamma-Ray Kerma-Rate Factors for Air, Carbon, and Tissue. (From Henderson, ref. 42.)

$\Delta X/\Delta t$, where ΔX is the increment of exposure during the increment of time Δt.

The unit of exposure is the roentgen (r). It is the quantity of X or gamma radiation that produces, in air, ions carrying 1 electrostatic unit of charge per 0.001293 g of dry air (or 2.58×10^{-4} coulombs/kg). In terms of ergs, the roentgen is equal to 87.7 ergs per gram of air or 96 ergs per gram of tissue. For gamma rays above 3 MeV in energy, the range of secondary electrons in low-atomic-number materials becomes comparable with the relaxation length of the gamma rays. Consequently, the ionization produced in a small volume is no longer a sole measure of the intensity of the radiation at that point. The ICRU does not recommend the use of the roentgen above 3 MeV, but in practice, it is still used above 3 MeV with instruments calibrated in terms of energy absorption in air.

Since 1 rad is equal to 100 ergs per gram of irradiated material (see Section 2.9.1), the roentgen and the rad are frequently interchanged when tissue exposure is referred to, the difference of 4% being no real consequence in shielding calculations. Strictly speaking, however, the rad should be reserved for describing an absorbed dose.

Away from boundaries, the distinction between kerma and exposure loses relevance if only the three principal processes (Compton scattering, photoelectric effect, and pair production) are considered and if the photoelectric effect and pair production are assumed to be absorptions. For this simple and widely used model* the fluence-to-exposure conversion factor is proportional to the product of the photon energy and the energy-deposition coefficient, in which case exposure, absorbed dose, first-collision dose, and kerma in air are all equal in magnitude.

In some calculations, however, a slightly more complex model is used in which only the photoelectric process is treated as an absorption. As in the above model, the total kinetic energy of the electron pair created in the pair-production process is assumed to be absorbed at the point of their emission. However, the two 0.51-MeV gamma rays produced by the annihilation of the positron are treated as scattered gamma rays, and pair production is viewed as a scattering process. This is described in terms of a modified pair-production cross section which is given by

$$\mu_{\mathrm{PP}_m} = \mu_{\mathrm{PP}} \left(1 - \frac{1.022}{E}\right), \quad E > 1.022 \text{ MeV}, \quad (2.139)$$

where E is the energy of the incident photon (MeV).

*For this and the subsequent model it is assumed that the bremsstrahlung radiation that would be produced by the secondary electrons (and positrons) is immediately absorbed.

2.9.4 RBE DOSE; DOSE EQUIVALENT

Whenever the biological response of a human organ to radiation exposure is of concern, merely knowing the absorbed dose (energy deposited) is not enough. Biological responses vary both with the nature and energy of the radiation and with the composition and function of the irradiated organs. Thus when an organ is exposed to a mixed radiation field or to a field of radiation comprised of one type of particle with various energies, the energy deposited by each type of particle of a given energy must be weighted by some factor before the total biological dose received by the organ can be determined by a summing of the individual contributions.

For a specific biological effect in a particular mass the weighting factor is mainly a function of the *l*inear rate of *e*nergy *t*ransfer (*LET*) to the system by charged particles set in motion by the interactions of incident radiation. The LET of a material is related to the linear stopping power but the concepts are different. The linear stopping power is the average energy loss per unit path length by a charged particle in traversing a medium regardless of where the energy is absorbed. The LET, however, refers to energy imparted within a limited volume. These two quantities are equal only in the special case when the LET includes the absorption of all secondary particles, in which case it is called LET_∞. These quantities are described more completely in ref. 21 (p. 51).

The LET-dependent weighting factor is called the *relative biological effectiveness* (*RBE*) and is defined as

$$\mathrm{RBE} = \frac{\text{rads of standard radiation producing a given biological effect}}{\text{rads of another type of radiation producing the same effect}}. \quad (2.140)$$

The standard radiation referred to is X rays of 250-keV energy, and thus by definition the RBE for 250-keV X rays is 1.

When a dose given in rads is weighted by an RBE value, the resulting dose, sometimes referred to as the RBE dose, is given in rems, a unit derived from the term *r*oentgen *e*quivalent *m*an:

$$\text{RBE dose in rems} \equiv \text{dose in rads} \times \text{RBE}. \quad (2.1.41)$$

It follows that for 250-keV X rays the rad dose and the rem dose are numerically equal.

The rem is quantitatively defined as: *the absorbed dose due to any ionizing radiation that has the same biological effectiveness as 1 rad of X rays with an average specific ionization of 100 ion pairs per micron of water in terms of its air equivalent.* It turns out that X rays and gamma rays generally do not exceed this specific ionization (LET < 3.5 keV/μ), which is considered to be the boundary between low-LET and high-LET radiation and thus to be the limiting condition for RBE = 1.

In the past RBE has been used in the fields of both radiobiology and radiation protection, but this generated concern because of the differences in application and, to some extent, in concept. Consequently ICRU recommends that RBE be used only for correlating radiobiological experiments and that a new term, the *quality factor* (*QF*), be used in the field of radiation protection. Quality factors are actually those values of RBE that are intended to embrace all effects that are hazardous to human beings. In other words, QF values are not related to specific organs of the body as are some of the RBE values. When a QF value is used to weight absorbed dose, the resulting dose in rems is identified as the *dose equivalent* (*DE*). It is assumed that dose equivalents, like RBE doses, are additive.

Although QF is defined in purely physical terms (that is, as a function of LET only, which in turn is a function of the number of ion pairs produced per centimeter of travel by charged particles), the basis of the legislated value is biological. Table 2.10 shows the recommendations[46,47] of the International Committee on Radiological Protection (ICRP) for the relation between QF and both LET and ion pair formation.

The ICRP recommends a QF of 1 for X rays, gamma rays, electrons, and positrons of any specific ionization;[46] QF's for neutrons, protons, and heavy recoil nuclei vary with energy. The ICRP recommendations for QF for neutrons between 0.01 and 1000 MeV are plotted in Fig. 2.19. Tabulated values for lower energy neutrons are also shown. These values are based on the calculated results of Snyder and Neufeld[48] and of Neary and Mulvey.[49] As a rough and conservative approximation, a QF of 10 is applicable to protons and a QF of 20 can be used for heavy-recoil nuclei.

The preceding QF's are assumed to be applicable for whole-body irradiation. When specific organs are being considered, additional modifying factors may be needed. For example, ICRP specifies that when the lens of the eye is being irradiated a modifying factor of 3 should be used if the QF is equal to or greater than 10 and a modifying factor of 1 should be used when QF = 1. Strangely enough no recommendations are given for $1 < \text{QF} < 10$. Presumably, linear interpolation is to be used between these limits.

When the dose in an organ is nonuniform, a dose distribution factor (DF) should also be applied. These factors cannot be established with certainty and only one is in current use. It is the relative damage factor applied in calculating the dose equivalent in bone from internal radiation.

In general the shielding community has accepted the use of QF and DE, as is reflected by the latest shielding literature. From a practical viewpoint the change merely amounts to replacing RBE by QF and calling the product of the quality factor and absorbed dose the *dose equivalent* (*DE*) instead of the RBE dose. Consequently no confusion should exist when the older

Table 2.10. QF as a Function of LET and Ion Pair Formation[a]

QF	Average Specific Ionization (ion pairs/μ^b)	Average LET (keV/μ^b)
1	<100	<3.5
2	200	7.0
5	650	23
10	1500	53
20	2000	175

[a]From refs. 46 and 47.
[b]Of water.

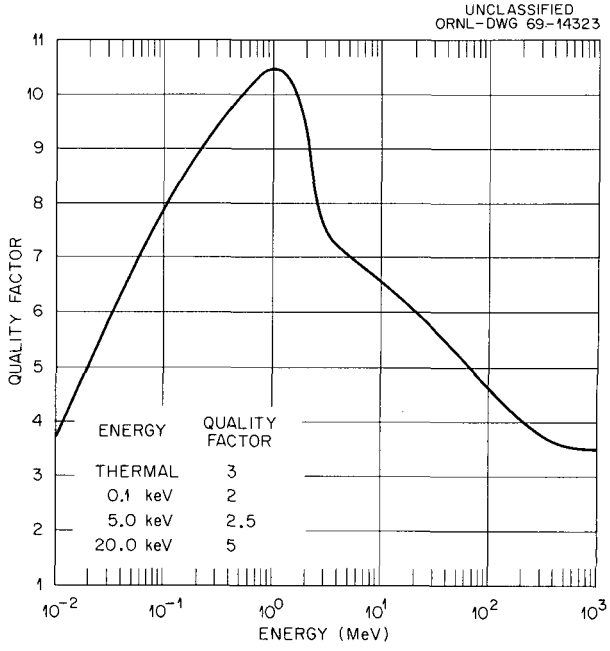

Fig. 2.19. Quality Factors for Neutrons. (From ref. 46.)

literature is consulted. It should be kept in mind, however, that QF values are chosen by such groups as the ICRP and thus are more subject to change than would be an RBE value based on experimental data.

It should also be pointed out that all QF's and other modifying factors are intended solely for chronic exposure to low-level radiation fields, with genetic damage being the hazard considered. High accidental exposures must be assessed on the basis of particular circumstances. The ICRP has no recommendations for such exposures, but in many cases the absorbed dose will give a better indication of the biological risks than will the dose equivalent. In other words, for acute effects due to massive exposures, the QF should be taken as unity, which partially results because energy may be wasted from the standpoint of the production of biological effects. Consequently for military applications during war, when early death or incapacitation is the effect to be considered, the dose in rems may be taken as numerically equal to the absorbed or physical dose until better information becomes available.

2.9.5 MAXIMUM ABSORBED DOSE; MAXIMUM DOSE EQUIVALENT

As is pointed out in the introduction to this section, the usual shielding calculation provides a detailed description of the unperturbed radiation field (free field). That is, perturbations of the field by a human body are not considered. This greatly simplifies the analysis without seriously compromising the overall accuracy. But the results must somehow be related to the hazards to a human being if he were exposed to such a radiation field.

A correlation between the unperturbed radiation field and the dose in a human body has been accomplished through the use of slab and cylindrical phantoms, which have dimensions and compositions resembling those of the human body. Calculations (or measurements) of the absorbed dose or the biological dose were made as a function of depth in the phantom for given monoenergetic neutrons or gamma rays incident on the phantom. The incident angular distribution was a monodirectional beam or an isotropic flux. (Calculations for neutrons include the contribution to the dose by secondary gamma rays.) The maximum values in the depth-dose distributions were identified as the *maximum absorbed dose* and *maximum dose equivalent* for the absorbed (physical) and biological doses respectively. Since these values were obtained and reported on the basis of a unit particle entering the phantom, they can be used as response functions to relate an unperturbed field of mixed radiation to the maximum dose that would be received by some part of the body. Use of these maximum values is dictated by a conservative design philosophy that does not allow the permissible dose to be exceeded at any point in the body.

Neutron Doses in Phantoms

The first dose calculations in a phantom were performed by Snyder and Neufeld[48] for a beam of monoenergetic neutrons normally incident on a phantom represented by a slab of tissue. The slab, infinite in the transverse directions, was assumed to be 30 cm thick. Snyder and Neufeld determined the distribution of the absorbed dose through the slab, finding that the maximum dose occurred at nearly the surface or within a few centimeters of the surface. In these calculations, only neutron captures and elastic scatterings were considered, which limited the contribution by secondary gamma rays to capture gamma rays. The resulting maximum absorbed doses and biological doses as a function of the incident neutron energy are shown in Table 2.11. These values have been widely used in reactor shield design to convert neutron fluences to doses and have become a virtual standard since these dose equivalents have been stipulated for use by the Federal Register.[50]

Table 2.11. Maximum Absorbed Dose and Maximum Dose Equivalent for Monoenergetic Neutrons Incident on a Slab Tissue Phantom[a]

Neutron Energy (MeV)	Maximum Absorbed Dose[b] (mrad neutron^{-1} cm^{-2})	Maximum Dose Equivalent[b] (mrem neutron^{-1} cm^{-2})	Effective QF
Thermal	3.2(−7)[c]	1.04(−6)	3.25
0.0001	6.9(−7)	1.39(−6)	2.01
0.005	5.7(−7)	1.22(−6)	2.14
0.02	5.7(−7)	2.35(−6)	4.12
0.1	1.10(−6)	8.3(−6)	7.55
0.5	2.4(−6)	2.30(−5)	9.61
1.0	3.8(−6)	3.80(−5)	10.0
2.5	4.3(−6)	3.41(−5)	7.93
5.0	5.8(−6)	3.80(−5)	6.55
7.5	7.1(−6)	4.16(−5)	5.85
10	7.0(−6)	4.16(−5)	5.94

[a] From ref. 48.

[b] Multiply by 3600 to convert to (mrad/hr)/(neutron/cm^2·sec) or to (mrem/hr)/(neutron/cm^2·sec).

[c] Read: 3.2×10^{-7}, etc.

In similar calculations, performed later by Auxier *et al.*,[51] the infinite slab was replaced by a finite cylindrical phantom that more nearly mocked up a human body. A schematic of the phantom, 60 cm high and 30 cm in diameter, is given in Fig. 2.20. The maximum doses (averaged for a volume element) occurred in the outermost volume element at the midplane on the side facing the beam. These maximum doses are given in Table 2.12, and the doses for each volume element are presented in Appendix 2B.

The *effective* quality factors shown in Tables 2.11 and 2.12 are the ratios of the maximum dose equivalent to the maximum absorbed dose for a given incident neutron energy and phantom configuration. The magnitude of the effective quality factor is very close to but usually slightly less than the QF's recommended by the ICRP (see Fig. 2.19). The differences in the values would be expected since the QF's recommended by the ICRP consider only the initial collision of the neutron whereas the effective QF's represent an average of all collisions experienced by the neutron within the phantom.

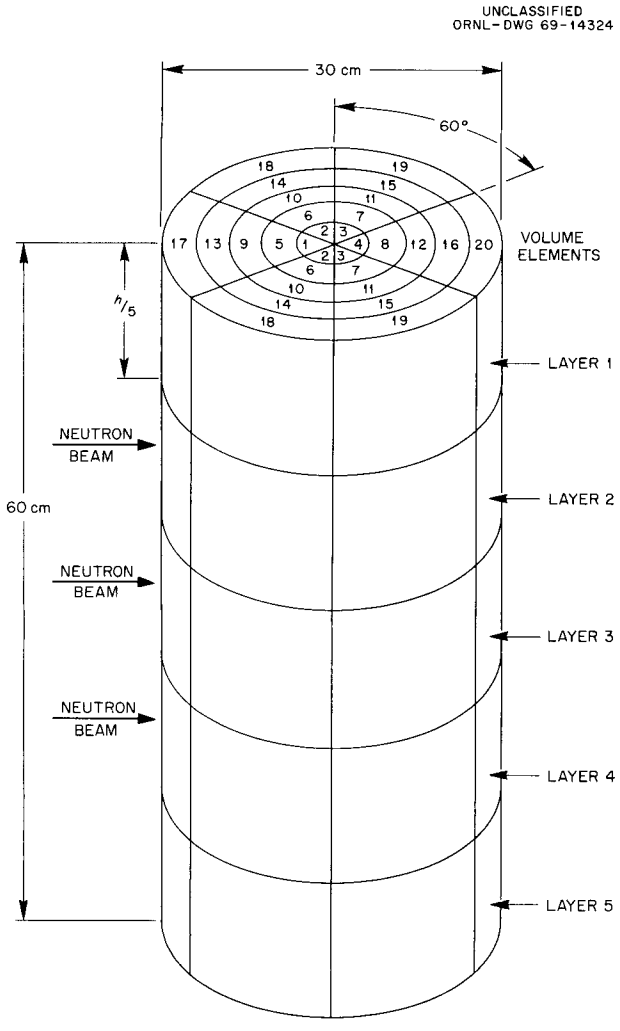

Fig. 2.20. Cylindrical Phantom Used in Neutron Dose Calculations. (From Auxier *et al.*, ref. 51.)

Table 2.12. Maximum Absorbed Dose and Maximum Dose Equivalent for Monoenergetic Neutrons Incident on a Cylindrical Tissue Phantom[a]

Neutron Energy (MeV)	Maximum Absorbed Dose[b] (mrad neutron^{-1} cm^{-2})	Maximum Dose Equivalent[b] (mrem neutron^{-1} cm^{-2})	Effective QF
Thermal	4.68(−7)[c]	1.15(−6)	2.46
0.000001	5.89(−7)	1.34(−6)	2.27
0.00001	5.18(−7)	1.21(−6)	2.34
0.0001	4.45(−7)	1.01(−6)	2.27
0.001	4.32(−7)	8.85(−6)	2.04
0.01	4.34(−7)	9.92(−6)	2.29
0.1	8.02(−7)	4.86(−6)	6.06
0.5	1.81(−6)	1.89(−5)	10.4
1	3.01(−6)	3.26(−5)	10.8
2.5	3.99(−6)	3.50(−5)	8.77
5	5.72(−6)	4.41(−5)	7.70
7	5.70(−6)	4.03(−5)	7.07
10	7.25(−6)	4.31(−5)	5.94
14	8.31(−6)	6.15(−5)	7.40

[a]From ref. 51.

[b]Multiply by 3600 to convert to (mrad/hr)/(neutron/cm^2·sec) or to (mrem/hr)/(neutron/cm^2·sec).

[c]Read: 4.68×10^{-7}, etc.

The Snyder-Neufeld calculations of maximum absorbed dose have recently been improved upon by Ritts *et al.*[43] They increased the number of elements in the infinite-slab phantom from 4 to 11, considered a much larger number of neutron source energies, allowed for neutron inelastic scattering (and the associated inelastic-scattering gamma rays) and for a number of other nonelastic events, corrected the elastic scattering to linear anisotropy, used more accurate secondary-gamma-ray spectra, used the latest cross sections available, and handled the neutrons with energies below 1 eV more accurately. The percentages of the 11 elements in the slab were the same as those used for the standard man kerma calculations (see Table 2.8), and the reactions considered were also the same as for the kerma calculations (see Table 2.9). The resulting maximum absorbed doses are presented in Fig. 2.21 (solid line) and in the second column of Table 2.13. A comparison with the Snyder-Neufeld results of Table

Table 2.13. Neutron Maximum Absorbed Doses Within Standard-Man Slab Phantoms[a]

Source Energy (eV)	Dose [(rads/g)/(neutron/cm^2)] [b]			
	Beam Source		Isotropic Flux	
	Infinite Slab	Finite Slab[c]	Infinite Slab	Finite Slab[c]
1.4208(+7)[d]	7.9598(−9)	7.4605(−9)	1.4616(−8)	1.3638(−8)
1.2856(+7)	7.3683(−9)	6.8683(−9)	1.3436(−8)	1.2553(−8)
1.1633(+7)	7.2273(−9)	6.7712(−9)	1.3077(−8)	1.2274(−8)
1.0526(+7)	6.8462(−9)	6.4060(−9)	1.2342(−8)	1.1592(−8)
1.0000(+7)	6.7111(−9)	6.2789(−9)	1.2070(−8)	1.1341(−8)
9.5242(+6)	6.5745(−9)	6.1445(−9)	1.1798(−8)	1.1091(−8)
8.6178(+6)	6.3415(−9)	5.9153(−9)	1.1308(−8)	1.0641(−8)
7.7977(+6)	6.3362(−9)	5.9281(−9)	1.1207(−8)	1.0574(−8)
7.0557(+6)	6.0811(−9)	5.6837(−9)	1.0736(−8)	1.0136(−8)
6.3843(+6)	5.8372(−9)	5.4736(−9)	1.0319(−8)	9.7712(−9)
5.7767(+6)	5.7003(−9)	5.3445(−9)	1.0002(−8)	9.2060(−9)
5.2270(+6)	5.4689(−9)	5.1380(−9)	9.6108(−9)	8.8640(−9)
5.0000(+6)	5.4174(−9)		9.4514(−9)	
4.7296(+6)	5.3667(−9)	5.0331(−9)	9.0074(−9)	8.5870(−9)
4.2795(+6)	5.2731(−9)	4.9584(−9)	8.8140(−9)	8.4324(−9)
3.5038(+6)	5.2205(−9)	4.9916(−9)	8.5412(−9)	8.2110(−9)
3.1703(+6)	4.7108(−9)	4.4959(−9)	7.7798(−9)	7.4682(−9)
2.5956(+6)	4.1653(−9)	3.9630(−9)	6.8302(−9)	6.5576(−9)
2.0000(+6)	3.8389(−9)		6.1462(−9)	
1.9229(+6)	3.7840(−9)	3.6060(−9)	6.0154(−9)	5.7972(−9)
1.5743(+6)	3.4752(−9)	3.3079(−9)	5.4326(−9)	5.2392(−9)
1.0553(+6)	3.1381(−9)	2.9991(−9)	4.6764(−9)	4.5326(−9)
5.2405(+5)	2.1666(−9)	2.0390(−9)	2.9434(−9)	2.8266(−9)
5.0000(+5)	2.1724(−9)	2.0494(−9)	2.9096(−9)	2.7980(−9)
4.7418(+5)	2.1766(−9)	2.0577(−9)	2.8652(−9)	2.7590(−9)
4.2906(+5)	2.1845(−9)		2.6712(−9)	
1.9279(+5)	1.3014(−9)	1.1931(−9)	1.5449(−9)	1.4506(−9)
9.8803(+4)	9.2925(−10)	8.2811(−10)	1.0393(−9)	9.5232(−10)
4.6671(+4)	6.5317(−10)	5.5685(−10)	6.6372(−10)	5.7892(−10)
2.8308(+4)	5.3582(−10)	4.4115(−10)	5.1846(−10)	4.3284(−10)
1.0414(+4)	4.5827(−10)	3.5333(−10)	4.2532(−10)	3.2792(−10)
4.9191(+3)	4.6004(−10)	3.5522(−10)	4.2712(−10)	3.2960(−10)
1.0976(+3)	5.2192(−10)	4.0294(−10)	4.3888(−10)	3.4036(−10)
3.1447(+2)	5.3477(−10)	4.1505(−10)	4.4894(−10)	3.4994(−10)
9.0097(+1)	5.4829(−10)	4.2781(−10)	4.5880(−10)	3.5930(−10)
3.3145(+1)	5.5774(−10)	4.3691(−10)	4.6500(−10)	3.6674(−10)
9.4962(0)	5.6353(−10)	4.4345(−10)	4.7006(−10)	3.7620(−10)
4.4857(0)	5.6082(−10)	4.4543(−10)	4.7066(−10)	3.7836(−10)
2.1189(0)	5.5112(−10)	4.4173(−10)	4.6484(−10)	3.7528(−10)
1.0009(0)	5.2998(−10)	4.2684(−10)	4.4830(−10)	3.6328(−10)
6.0707(−1)	5.0478(−10)	4.0796(−10)	4.2706(−10)	3.4692(−10)
4.7279(−1)	4.8934(−10)	3.9628(−10)	4.1224(−10)	
2.1800(−1)	3.5443(−10)	2.9505(−10)	1.9709(−10)	1.6567(−10)

[a]From ref. 43.

[b]These values correspond to one neutron per cm^2 entering the slab.

[c]The calculations for the finite slab include a buckling term to compensate for transverse leakage; the transverse dimensions for the finite slab phantom were taken as 40 by 61 cm.

[d]Read: 1.4208×10^7, etc.

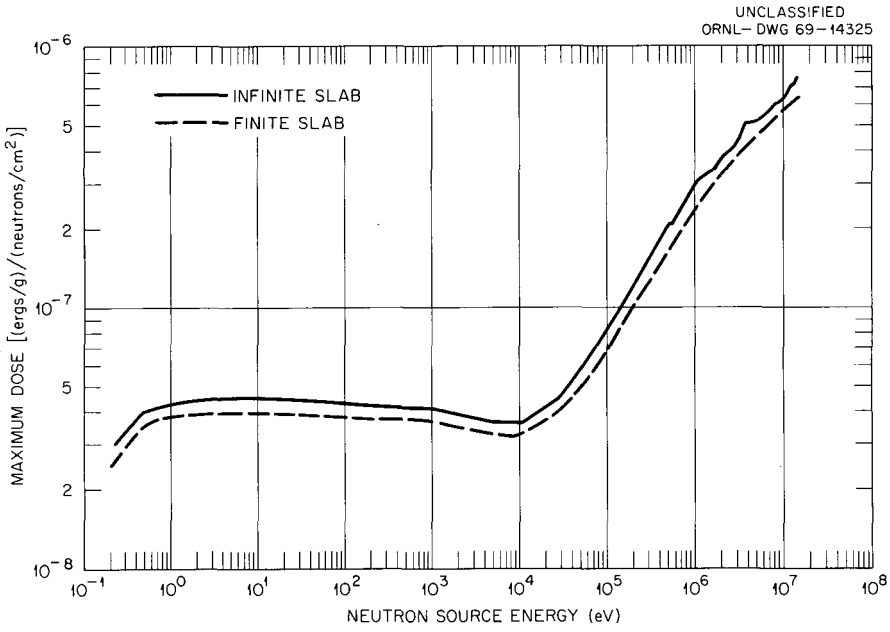

Fig. 2.21. Neutron Maximum Absorbed Doses in Standard-Man Slab Phantom Due to a Beam Source. (From Ritts *et al.*, ref. 43.)

2.11 reveals that the new values are consistently lower, as would be expected since the Snyder-Neufeld calculations were purposely conservative.

In order to determine the effect that transverse leakage would have on the calculated doses, Ritts *et al.* also performed one-dimensional calculations for a 30-cm-thick slab with a geometric buckling* value that was equivalent to a length of 61 cm and a width of 40 cm. In general they found that a 5 to 10% reduction in the dose could be attributed to transverse leakage. The results for the finite slab are included in Fig. 2.21 (dashed line) and in the third column of Table 2.13. These values for the finite slab are 10 to 20% lower than the doses calculated by Snyder and Neufeld for the slab with no transverse leakage.

Ritts *et al.* also made calculations with and without a buckling value for an isotropic neutron flux incident on a slab. The results are presented in Fig. 2.22 and in the last two columns of Table 2.13.

*The geometric buckling, B_g^2, is the lowest eigenvalue that results from solving the wave equation for a system of particular size and shape subject to the condition that the flux vanish at the extrapolated boundary. In one-dimensional calculations, leakage in the infinite directions can be approximated by using DB^2 (D = diffusion coefficient) as a fictitious macroscopic absorption cross section.

Gamma-Ray Doses in Phantoms

The doses delivered to various parts of a man-like phantom by 0.027- to 1.24-MeV gamma rays were measured by Jones,[52] who later reported his results in terms of calibration factors[53] for dosimeters. The calibration factors were recommended for use in the design and calibration of gamma-ray exposure meters to permit a direct reading of the maximum dose (in rads) delivered to the critical organ for the particular environmental condition. The composition of the phantom matched soft tissue with respect to density and effective atomic number and included a full set of bones for the head and trunk.

For each of 11 photon energies used in the experiment (see Table 2.14), measurements were made of the free-field dose† (the dose with the phantom removed) at a distance from the source corresponding to a particular dose position in the phantom. Measurements within the phantom were made at positions corresponding to the location of the brain (front), eye (lens), skin (front and back of chest and forehead), gut mucosa, ovaries, testes, and bone marrow (seven representative sites). For each source energy the measure-

†This is effectively a measurement of the first-collision dose as described in Section 2.9.2.

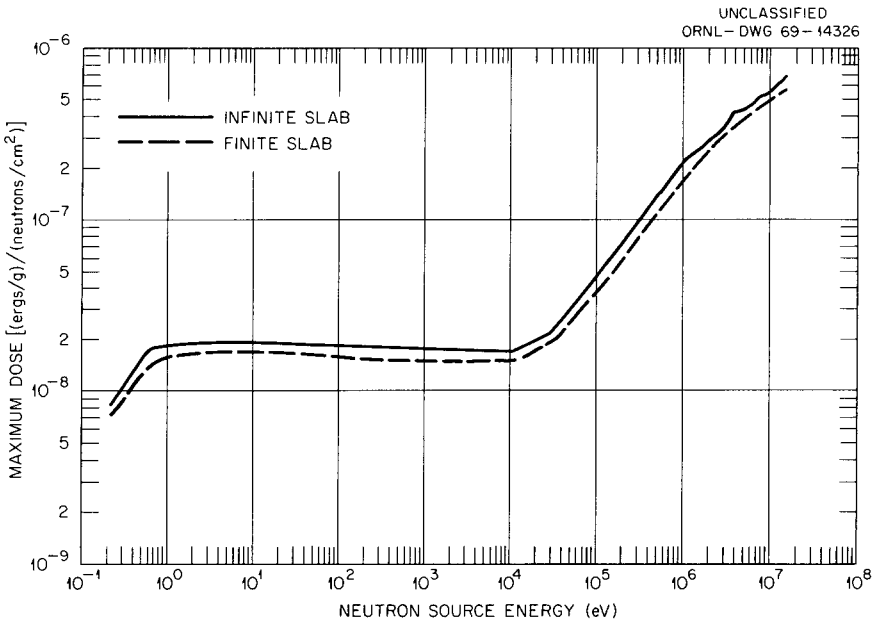

Fig. 2.22. Neutron Maximum Absorbed Doses in Standard-Man Slab Phantom Due to an Isotropic Source. (From Ritts *et al.*, ref. 43.)

ments were made with the phantom being irradiated from in front, from behind, and while being rotated about the vertical axis. Table 2.14 shows the location at which the maximum dose was received within the phantom for each exposure to gamma rays of different energies. The results are given in terms of the ratio of the absorbed dose to the free-field exposure (rads/r).

Recent Monte Carlo calculations by Sidwell *et al.*[54] for monoenergetic gamma rays incident on a phantom assumed to have the characteristics of water and to be shaped like an elliptic cylinder yielded dose results that are reported to be in good agreement with Jones' measurements.

Other recent calculations of the dose delivered to a phantom by monoenergetic gamma rays were performed by Claiborne and Trubey.[55] Using the discrete ordinates method, with some checks by the Monte Carlo method, they calculated the dose distributed in a 30-cm-thick infinite-slab phantom having the standard man composition shown in Table 2.8. Their maximum dose rates, which occurred at nearly the surface or within the first 2 cm of the surface, are compared in Fig. 2.23 with Jones' experimental results (converted to the same units). First-collision dose rates for the standard-man composition based on the use of flux-to-kerma-rate conversion factors are also plotted in Fig. 2.23. These values show that the customary practice of using kerma-rate factors underestimates the maximum

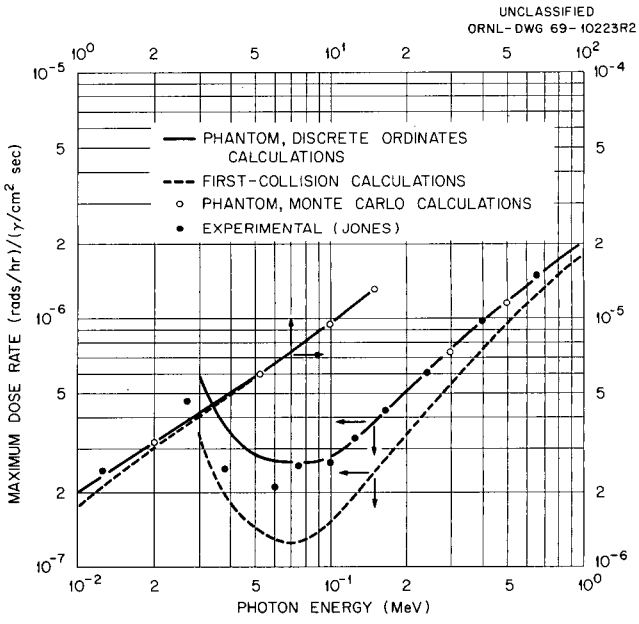

Fig. 2.23. Maximum Gamma-Ray Dose Rate in Slab Phantom of Standard-Man Composition. Comparison with kerma calculations and with phantom measurements. (From Claiborne and Trubey, ref. 55.)

Table 2.14. Gamma-Ray Maximum Absorbed Doses at Various Locations in a Man-Like Phantom[a]

Source	Gamma-Ray Energy (MeV)	Location in Phantom	Ratio of Maximum Dose to Exposure (rads/r)
^{60}Co	1.24	Skin on back[b]	1.06
^{137}Cs	0.660	Skin on chest	1.11
^{192}In	0.400	Skin on forehead and testes	1.19
Bremsstrahlung			
Narrow band	0.240	Skin on forehead	1.30
	0.165	Gut mucosa	1.47
	0.125	Testes	1.57
Filtered by U	0.100	Skin on forehead	1.65
Filtered by Pb	0.075	Gut mucosa	2.03
Filtered by Ta	0.060	Skin on chest	1.75
Filtered by Nd	0.038	Skin on chest	1.34
Filtered by Sn	0.027	Skin on chest	1.28

[a]From ref. 52.

[b]Maximum occurred when phantom was irradiated from behind; all other maxima occurred when phantom was irradiated from in front.

dose delivered to a position within a body, especially for the lower gamma-ray energies. This is because the energy deposition due to collisions subsequent to the first collisions is not accounted for in the kerma-rate factors.*

The excellent agreement between the Claiborne-Trubey calculations and the Jones experiment for energies greater than 0.07 MeV seems surprising in view of the large differences in the configurations. However, since most of the energy deposition apparently comes from the first collision, the effect due to the geometry difference will be small.

2.9.6. MULTICOLLISION DOSE

The term *multicollision dose,* which until recently has been used solely for neutron exposure, is not recognized by the ICRU. The multicollision dose concept was developed by health physicists in an effort to relate the neutron flux or fluence incident upon a configuration of tissue representing the human body to the absorbed dose or to the dose equivalent. The multicollision dose could, in turn, be related to a maximum permissible dose (MPD) established by shield design criteria. The term has tacitly been defined by common usage in shield design as the sum of the maximum dose equivalents (or maximum absorbed doses) delivered by each neutron energy group to a slab of tissue of a particular composition.* This includes the dose due to secondary gamma rays produced by the neutrons in the slab. This dose is calculated by

$$\text{Multicollision dose} = \sum_g \psi_g D_{\max}(E_g) , \qquad (2.142)$$

where ψ_g is the group fluence as defined in Section 2.1 and $D_{\max}(E_g)$ is the maximum dose equivalent (or maximum absorbed dose) in the slab for an incident neutron of the energy corresponding to the gth neutron group.

Gamma-ray multicollision doses are similarly calculated with Eq. 2.142, with, of course, ψ_g and $D_{\max}(E_g)$ being the appropriate values for gamma rays. Because the gamma-ray maximum absorbed doses reported in Section 2.9.5 have only recently become available, most multicollision doses for gamma rays have in the past been determined by using the product of the gamma-ray energy, the mass energy deposition coefficient for tissue or air, and a factor to convert to rads for the $D_{\max}(E_g)$ term.

*The dose rate in a slab-tissue phantom due to high-energy photons has been calculated by Alsmiller and Moran,[56] but except for the values for 10-MeV gamma rays their results are for photon energies not encountered in weapons radiation or reactor shielding.

*See slab tissue phantom described in Section 2.9.5 for Snyder-Neufeld calculations.[48]

The total dose for a mixed radiation field incident on a tissue slab is determined by adding the neutron and gamma-ray multicollision doses obtained separately for the slab.

Although the concept of multicollision dose, or dose rate, is not recognized by the ICRU, it seems clear that, to fully implement the trend to preciseness in the fields of radiobiology and radiation protection, the dose calculated in shield design should be given recognition by some official body. Perhaps the term *multicollision dose* can be retained for the neutron-induced contribution and the term *total multicollision dose* can be used when the incident gamma-ray contribution is also included. Or perhaps an entirely new term could be introduced, such as the term *m*an *e*quivalent *d*ose (*MED*) proposed by Claiborne and Trubey.[55]

2.10. Radiation Exposure Limits*

Any material will undergo some alteration on exposure to directly or indirectly ionizing radiation, but organic materials are most susceptible to damage, particularly living organisms. The earth and its inhabitants are continuously exposed to radiation from cosmic-ray bombardment and naturally occurring radioisotopes. In addition to these natural sources, the human body may be exposed to X rays used for medical diagnostics and treatments, luminous wrist watch dials, television, etc. To date the effects of these exposures, if any, are essentially unknown.

The International Commission on Radiological Protection (ICRP) has taken the position that radiation in any amount absorbed by the gonads can cause genetic damage and increase the natural mutation rate. Mostly as a result of the fear that small chronic dosages will significantly increase the mutation rate in humans or induce unknown deleterious long-range effects (such as leukemia), the ICRP has recommended that workers in the nuclear industry be limited to a maximum dose of 5 rems/year, which amounts to 2.5 mrems/hr based on a 40-hr work week for 50 weeks/year. This so-called maximum permissible dose (MPD) is about 25 times the dose that the average American will receive each year from environmental radiation. The recommended MPD appears to represent an acceptable risk since conservative estimates indicate that 5 rems/year may increase the natural gene mutation rate by only 10 to 20%, which when related to the probable increase in the number of potentially defective children becomes a statistical exercise. It is interesting to note that no measurable defects attributable to radiation were found in studies of the children conceived after the parents were exposed to intense radiation fields from the atomic weapons exploded over Hiroshima and Nagasaki and to the Marshall Island natives exposed to fallout from the Bikini test shot.

Much higher doses are required to produce significant somatic damage or direct deleterious effects in the body. And since the body can repair itself, dose rate is a factor, a larger total radiation dose being required to produce a given degree of injury if the dose is spread over a long period of time. But the rate, or fractionation, effect is of no consequence for acute doses that could be received in a nuclear war or from an accident in the nuclear industry. Military considerations during war require emphasis on minimizing acute exposure and the attendant probability of an incapacitation that would prevent a necessary mission. Consequently the dose delivered to mucosal layers of the gut becomes the most important consideration.

Although data on the biological effects that might be expected for human beings subjected to acute doses of varying amounts are rather limited, a sufficient amount of knowledge is available for drawing useful conclusions for planning purposes. Such data have been derived from the study of Japanese casualties, a few nuclear accidents, and large animal experiments. The following paragraphs give a general description of the effects that might be expected as the result of whole-body exposure to an acute dose received by healthy adults over a period of up to two to four days. For a more complete and detailed discussion see ref. 58.

Doses up to 100 rems. – Exposures resulting in doses up to 100 rems would give no apparent immediate effects. In some cases nausea or vomiting may occur, but no other symptom of radiation sickness would be apparent. No clinical surveillance or therapy other than reassurance would be required.

Doses from 100 to 200 rems. – Doses between 100 and 200 rems would cause nausea and vomiting within about 3 hr in from 5 to 50% of those exposed. A moderate decrease in the number of white blood cells would result, making clinical and hematologic surveillance desirable. Therapy would consist mainly of reassurance. Prognosis would be excellent with a convalescent period of several weeks. There should be no deaths.

Doses from 200 to 600 rems. – Doses in the range 200 to 600 rems would result in a 100% incidence of vomiting, which would begin within about 2 hr for doses greater than 300 rems. Severe loss of white blood

*This section is largely quoted from Sections 2-8.4 and 2-8.5 of Volume I of the Office of Civil Defense's manual for shelter design and analysis (see ref. 57).

cells (leukopenia) would occur. Purple or livid spots (purpura) would appear on the skin. There would be some hemorrhaging and an incidence of infection. Loss of hair (epilation) would result for exposures above 300 rems. Therapy would include blood transfusions and the administration of antibiotics. A convalescent period of from 1 to 12 months would be required. Deaths from hemorrhage or infection within two months would probably begin at about 250 rems and, for the dose range of 200 to 600 rems, would range up to about 80%. A value of around 300 rems delivered to the mid-line of the body is usually taken as $LD_{50/30}$ (lethal dose for 50% within 30 days) for man.

Doses from 600 to 1000 rems. – Doses approaching 1000 rems would result in all the symptoms of radiation sickness described in the preceding paragraph but at a more severe intensity. Therapy would be only promising and would involve not only blood transfusion and antibiotics but also the consideration of bone marrow transplants. The incidence of deaths would range between 80 and 100%.

Doses Greater Than 1000 rems. – Doses greater than 1000 rems would almost certainly be lethal. Symptoms of radiation sickness would be very severe and would begin within 30 min. Those symptoms described in the preceding paragraphs would be augmented by diarrhea, fever, and disturbance of electrolyte balance as the result of changes in the gastrointestinal tract. Doses over 5000 rems would affect the central nervous system with attendant symptoms of convulsion, tremors, loss of muscular coordination, and lethargy. Prognosis would be hopeless and therapy would consist mainly of the administration of sedatives. For doses of 1000 to 5000 rems, death in almost 100% of the cases would result within 2 weeks from circulatory collapse. For doses above 5000 rems death in 100% of the cases would occur within 48 hr as a respiratory failure or edema of the brain, or both. Doses of 10,000 rems and up directly affect the nerve cells to the point that incapacitation could occur almost immediately.

To summarize, if a person is exposed to a dose of less than about 200 rems, he should not become incapacitated nor should his ability to work be seriously affected. Persons exposed to doses exceeding about 200 rems will suffer increasing radiation sickness with increasing dosage, and the probability of death is extremely high if the dose exceeds 600 rems. For doses greater than 10,000 rems immediate incapacitation can be expected.

The MPD for military purposes during war will depend on the assigned mission and the acceptable casualty rate. Obviously the low MPD set for peacetime occupational work cannot be used as the criterion in military situations. Based on the available information, an MPD = 100 rems (absorbed over a few days) seems reasonable since the effect of such a dose would be hardly noticeable and would not interfere with military operations. Since radiation shelter design will require an estimate of the free-field dose, the maximum probable exposure in a specified time (which includes multiple strikes) should be used as the design criterion for each shelter in a given area.

Appendix 2A. Neutron Fluence-to-Kerma Conversion Factors for Standard Man and Some Specific Body Components

This appendix presents neutron fluence-to-kerma conversion factors calculated by Ritts *et al.*[43] for a standard-man model and for specific body components (see Section 2.9.2). The neutron energies range from approximately 0.022 eV to approximately 15 MeV, and the compositions for the models are those shown in Table 2.8. Table 2A.1 gives the conversion factors for the standard man, together with those for the elements making the greatest contributions in the model. Conversion factors for specific body components are presented in Table 2A.2.

Table 2A.3 gives the conversion factors on an atom density basis for the most common elements contained in man. These values can be used to obtain the kerma factors for any arbitrary combination of these elements by multiplying the individual value of each component by the number of atoms of each element per gram of mixture. For example, the kerma factor for H_2O (11.9 wt % H and 88.81 wt % O) in a field of 15-MeV neutrons is

$$\left\{\left[\frac{0.119}{1.008}\times(0.6023\times10^{24})(7.75\times10^{-6})\right]+\left[\frac{0.881}{16.00}\times(0.6023\times10^{24})(6.67\times10^{-6})\right]\right\}\times10^{-24}$$
$$=7.41\times10^{-7}\ (\text{ergs/g of } H_2O)/(\text{neutron/cm}^2)\,, \quad (A1)$$

where the numbers 1.008 and 16 are the atomic weights of hydrogen and oxygen respectively and 0.6023×10^{24} is Avogadro's number.

Table 2A.1. Neutron Fluence-to-Kerma Factors for Standard Man[a,b]

Energy (MeV)	Fluence-to-Kerma Factor (ergs/g)/(neutron/cm^2)							
	Total	Hydrogen	Oxygen	Carbon	Nitrogen	Phosphorus	Sodium	Chlorine
15.14	7.079(−7)[c]	4.633(−7)	1.53(−7)	8.08(−8)	9.35(−9)			
14.84	6.948(−7)	4.629(−7)	1.46(−7)	7.53(−8)	9.13(−9)			
14.54	6.811(−7)	4.623(−7)	1.40(−7)	6.89(−8)	8.87(−9)			
14.24	6.652(−7)	4.617(−7)	1.29(−7)	6.47(−8)	8.67(−9)			
13.93	6.501(−7)	4.611(−7)	1.18(−7)	6.16(−8)	8.41(−9)			
13.63	6.276(−7)	4.604(−7)	9.90(−8)	5.93(−8)	7.99(−9)			
13.33	6.119(−7)	4.598(−7)	8.63(−8)	5.72(−8)	7.74(−9)			
13.03	6.007(−7)	4.591(−7)	7.87(−8)	5.44(−8)	7.63(−9)			
12.73	5.966(−7)	4.584(−7)	8.03(−8)	4.96(−8)	7.44(−9)			
12.43	5.949(−7)	4.577(−7)	8.30(−8)	4.61(−8)	7.29(−9)			
12.13	5.936(−7)	4.568(−7)	8.45(−8)	4.45(−8)	7.04(−9)			
11.83	5.964(−7)	4.559(−7)	9.28(−8)	4.01(−8)	6.77(−9)			
11.52	5.877(−7)	4.550(−7)	8.90(−8)	3.64(−8)	6.47(−9)			
11.22	5.818(−7)	4.540(−7)	8.48(−8)	3.59(−8)	6.23(−9)			
10.92	5.691(−7)	4.531(−7)	7.49(−8)	3.43(−8)	5.95(−9)			
10.62	5.554(−7)	4.522(−7)	6.75(−8)	2.91(−8)	5.85(−9)			
10.32	5.483(−7)	4.512(−7)	6.81(−8)	2.26(−8)	5.73(−9)			
10.02	5.421(−7)	4.501(−7)	6.46(−8)	2.12(−8)	5.52(−9)			
9.72	5.353(−7)	4.478(−7)	5.98(−8)	2.18(−8)	5.28(−9)			
9.60	5.313(−7)	4.468(−7)	5.70(−8)	2.16(−8)	5.21(−9)			
9.45	5.271(−7)	4.456(−7)	5.40(−8)	2.19(−8)	4.97(−9)			
9.30	5.222(−7)	4.443(−7)	5.00(−8)	2.23(−8)	4.91(−9)			
9.15	5.173(−7)	4.430(−7)	4.74(−8)	2.14(−8)	4.85(−9)			
9.00	5.123(−7)	4.417(−7)	4.78(−8)	1.75(−8)	4.70(−9)			
8.85	5.078(−7)	4.410(−7)	4.54(−8)	1.61(−8)	4.64(−9)			
8.70	5.048(−7)	4.402(−7)	4.37(−8)	1.56(−8)	4.60(−9)			
8.62	5.007(−7)	4.399(−7)	4.01(−8)	1.56(−8)	4.53(−9)			
8.47	4.988(−7)	4.391(−7)	3.90(−8)	1.57(−8)	4.40(−9)			
8.32	5.036(−7)	4.383(−7)	4.38(−8)	1.66(−8)	4.28(−9)			
8.17	5.062(−7)	4.376(−7)	4.24(−8)	2.15(−8)	4.30(−9)			

Table 2A.1. (continued)

Energy (MeV)	Fluence-to-Kerma Factor (ergs/g)/(neutron/cm^2)							
	Total	Hydrogen	Oxygen	Carbon	Nitrogen	Phosphorus	Sodium	Chlorine
8.02	4.977(−7)	4.368(−7)	2.94(−8)	2.63(−8)	4.74(−9)			
7.87	5.038(−7)	4.345(−7)	3.81(−8)	2.62(−8)	4.38(−9)			
7.72	5.060(−7)	4.319(−7)	3.89(−8)	3.09(−8)	3.88(−9)			
7.57	4.935(−7)	4.292(−7)	3.65(−8)	2.34(−8)	3.84(−9)			
7.42	4.970(−7)	4.266(−7)	4.11(−8)	2.49(−8)	3.98(−9)			
7.27	4.995(−7)	4.239(−7)	5.32(−8)	1.80(−8)	3.87(−9)			
7.12	4.773(−7)	4.211(−7)	4.13(−8)	1.08(−8)	3.52(−9)			
6.97	4.650(−7)	4.187(−7)	3.13(−8)	1.10(−8)	3.49(−9)			
6.82	4.745(−7)	4.173(−7)	4.14(−8)	1.21(−8)	3.27(−9)			
6.67	4.707(−7)	4.159(−7)	3.94(−8)	1.17(−8)	3.27(−9)			
6.52	4.605(−7)	4.145(−7)	2.97(−8)	1.25(−8)	3.38(−9)			
6.37	4.731(−7)	4.130(−7)	3.89(−8)	1.71(−8)	3.57(−9)			
6.21	4.611(−7)	4.115(−7)	2.46(−8)	2.09(−8)	3.65(−9)			
6.06	4.572(−7)	4.100(−7)	2.77(−8)	1.53(−8)	3.77(−9)			
5.91	4.633(−7)	4.077(−7)	3.73(−8)	1.42(−8)	3.67(−9)			
5.76	4.457(−7)	4.048(−7)	2.32(−8)	1.38(−8)	3.51(−9)			
5.61	4.502(−7)	4.018(−7)	3.08(−8)	1.37(−8)	3.55(−9)			
5.46	4.312(−7)	3.987(−7)	1.47(−8)	1.42(−8)	3.25(−9)			
5.31	4.294(−7)	3.956(−7)	1.70(−8)	1.30(−8)	3.39(−9)			
5.16	4.449(−7)	3.925(−7)	3.46(−8)	1.33(−8)	4.17(−9)			
5.01	4.344(−7)	3.892(−7)	2.76(−8)	1.32(−8)	4.01(−9)			
4.69	4.180(−7)	3.810(−7)	1.79(−8)	1.50(−8)	3.73(−9)			
4.50	4.116(−7)	3.760(−7)	1.66(−8)	1.42(−8)	4.34(−9)			
4.31	4.181(−7)	3.709(−7)	2.91(−8)	1.33(−8)	4.48(−9)			
4.16	4.245(−7)	3.666(−7)	3.37(−8)	1.89(−8)	4.98(−9)			
4.01	4.102(−7)	3.623(−7)	2.24(−8)	2.05(−8)	4.78(−9)			
3.82	4.121(−7)	3.562(−7)	2.91(−8)	2.26(−8)	3.88(−9)			
3.67	4.099(−7)	3.511(−7)	3.05(−8)	2.42(−8)	3.67(−9)			
3.52	4.060(−7)	3.459(−7)	3.09(−8)	2.45(−8)	4.48(−9)			
3.33	3.981(−7)	3.392(−7)	3.46(−8)	2.07(−8)	3.32(−9)			
3.18	3.727(−7)	3.337(−7)	2.06(−8)	1.54(−8)	2.83(−9)			
3.03	3.555(−7)	3.280(−7)	1.53(−8)	9.44(−9)	2.47(−9)			
2.84	3.499(−7)	3.203(−7)	1.14(−8)	1.60(−8)	2.01(−9)			
2.69	3.396(−7)	3.138(−7)	1.10(−8)	1.26(−8)	1.89(−9)			
2.50	3.279(−7)	3.054(−7)	1.01(−8)	1.09(−8)	1.34(−9)			
2.40	3.150(−7)	3.000(−7)	3.40(−9)	1.03(−8)	1.07(−9)			
2.31	3.136(−7)	2.950(−7)	7.36(−9)	9.85(−9)	1.21(−9)			
2.21	3.119(−7)	2.898(−7)	1.08(−8)	9.51(−9)	1.61(−9)			
2.10	3.057(−7)	2.835(−7)	1.14(−8)	9.68(−9)	9.62(−10)			
2.00	2.995(−7)	2.780(−7)	1.13(−8)	9.16(−9)	9.20(−10)			
1.91	2.952(−7)	2.721(−7)	1.31(−8)	8.82(−9)	9.82(−10)			
1.80	2.883(−7)	2.648(−7)	1.31(−8)	8.56(−9)	1.72(−9)			
1.70	2.800(−7)	2.585(−7)	1.21(−8)	8.36(−9)	8.76(−10)			
1.59	2.717(−7)	2.507(−7)	1.18(−8)	8.12(−9)	9.84(−10)			
1.50	2.644(−7)	2.440(−7)	1.15(−8)	7.93(−9)	9.06(−10)			
1.40	2.577(−7)	2.370(−7)	1.13(−8)	7.73(−9)	1.66(−9)			
1.31	2.602(−7)	2.297(−7)	2.23(−8)	7.52(−9)	6.44(−10)			
1.20	2.426(−7)	2.209(−7)	1.39(−8)	7.25(−9)	5.11(−10)			
1.10	2.371(−7)	2.121(−7)	1.63(−8)	7.00(−9)	7.45(−10)			
1.00	2.432(−7)	2.037(−7)	3.21(−8)	6.70(−9)	6.33(−10)			
9.0(−1)	2.122(−7)	1.939(−7)	1.15(−8)	6.35(−9)	3.39(−10)			
8.0(−1)	1.980(−7)	1.834(−7)	7.95(−9)	5.97(−9)	3.90(−10)			
7.0(−1)	1.857(−7)	1.730(−7)	6.61(−9)	5.56(−9)	4.97(−10)			
6.0(−1)	1.719(−7)	1.609(−7)	5.61(−9)	5.07(−9)	2.80(−10)			
5.0(−1)	1.592(−7)	1.483(−7)	5.74(−9)	4.52(−9)	5.32(−10)			
4.5(−1)	1.639(−7)	1.403(−7)	1.90(−8)	4.20(−9)	2.90(−10)			

Table 2A.1. (continued)

Energy (MeV)	Fluence-to-Kerma Factor (ergs/g)/(neutron/cm^2)							
	Total	Hydrogen	Oxygen	Carbon	Nitrogen	Phosphorus	Sodium	Chlorine
4.0(−1)	1.486(−7)	1.318(−7)	1.18(−8)	3.89(−9)	2.96(−10)			
3.5(−1)	1.339(−7)	1.236(−7)	6.52(−9)	3.51(−9)	2.46(−10)			
3.0(−1)	1.223(−7)	1.142(−7)	4.73(−9)	3.12(−9)	2.13(−10)			
2.5(−1)	1.104(−7)	1.037(−7)	3.74(−9)	2.70(−9)	1.93(−10)			
2.0(−1)	9.649(−8)	9.116(−8)	2.89(−9)	2.23(−9)	1.82(−10)			
1.5(−1)	8.165(−8)	7.758(−8)	2.16(−9)	1.75(−9)	1.47(−10)			
1.0(−1)	6.335(−8)	6.056(−8)	1.45(−9)	1.22(−9)	1.08(−10)			
7.0(−2)	4.973(−8)	4.774(−8)	1.02(−9)	8.76(−10)	9.36(−11)			
5.0(−2)	3.830(−8)	3.705(−8)	7.30(−9)	6.37(−10)	7.62(−11)			
3.0(−2)	2.560(−8)	2.472(−8)	4.43(−9)	3.92(−10)	4.97(−11)			
2.0(−2)	1.807(−8)	1.747(−8)	2.98(−9)	2.66(−10)	3.73(−11)			
1.5(−2)	1.361(−8)	1.316(−8)	2.18(−9)	1.95(−10)	3.14(−11)			
1.0(−2)	9.550(−9)	9.287(−9)	1.47(−9)	1.34(−10)	2.29(−11)			
7.0(−3)	6.776(−9)	6.558(−9)	1.03(−9)	9.24(−11)	1.87(−11)			
5.0(−3)	4.880(−9)	4.832(−9)	7.53(−9)	6.74(−11)	1.56(−11)			
4.03(−3)	3.951(−9)	3.820(−9)	5.94(−11)	5.32(−11)	1.44(−11)	2.88(−12)		
3.00(−3)	2.964(−9)	2.855(−9)	4.43(−11)	3.96(−11)	1.32(−11)	3.02(−12)		
2.01(−3)	2.002(−9)	1.928(−9)	2.98(−11)	2.67(−11)	1.27(−11)	3.12(−12)		
1.50(−3)	1.495(−9)	1.436(−9)	2.22(−11)	1.99(−11)	1.30(−11)	3.20(−12)		
1.03(−3)	1.030(−9)	9.832(−10)	1.52(−11)	1.36(−11)	1.40(−11)	3.25(−12)		
7.68(−4)	7.774(−10)	7.368(−10)	1.14(−11)	1.02(−11)	1.52(−11)	3.27(−12)		2.72(−13)
5.13(−4)	5.299(−10)	4.925(−10)	7.60(−12)	6.80(−12)	1.77(−11)	3.30(−12)		1.84(−12)
4.02(−4)	4.244(−10)	3.867(−10)	5.96(−12)	5.34(−12)	1.95(−11)	3.31(−12)		3.28(−12)
3.10(−4)	3.347(−10)	2.986(−10)	4.60(−12)	4.12(−12)	2.19(−11)	3.32(−12)		1.97(−12)
2.01(−4)	2.299(−10)	1.939(−10)	2.98(−12)	2.67(−12)	2.67(−11)	3.33(−12)		5.91(−14)
1.42(−4)	1.764(−10)	1.372(−10)	2.11(−12)	1.88(−12)	3.15(−11)	3.33(−12)		1.12(−13)
1.006(−4)	1.417(−10)	9.753(−11)	1.49(−12)	1.33(−12)	3.73(−11)	3.34(−12)		3.87(−13)
7.1(−5)	1.192(−10)	6.920(−11)	1.05(−12)	9.42(−13)	4.42(−11)	3.34(−12)	3.50(−13)	9.84(−14)
5.03(−5)	1.071(−10)	4.94(−11)	7.46(−13)	6.67(−13)	5.237(−11)	3.34(−12)	4.11(−13)	1.10(−13)
4.11(−5)	1.036(−10)	4.07(−11)	6.09(−13)	5.45(−13)	5.786(−11)	3.34(−12)	4.54(−13)	1.31(−13)
3.43(−5)	1.025(−10)	3.43(−11)	5.09(−13)	4.56(−13)	6.323(−11)	3.34(−12)	4.99(−13)	1.57(−13)
2.74(−5)	1.033(−10)	2.78(−11)	4.07(−13)	3.64(−13)	7.065(−11)	3.35(−12)	5.58(−13)	1.95(−13)
2.05(−5)	1.077(−10)	2.13(−11)	3.05(−13)	2.73(−13)	8.155(−11)	3.35(−12)	6.44(−13)	2.59(−13)
1.60(−5)	1.143(−10)	1.71(−11)	2.38(−13)	2.13(−13)	9.226(−11)	3.35(−12)	7.34(−13)	3.14(−13)
1.26(−5)	1.230(−10)	1.40(−11)	1.86(−13)	1.67(−13)	1.041(−10)	3.35(−12)	8.34(−13)	3.79(−13)
8.0(−6)	1.454(−10)	1.01(−11)	1.19(−13)	1.06(−13)	1.302(−10)	3.35(−12)	1.04(−12)	5.08(−13)
4.0(−6)	1.965(−10)	7.20(−12)	5.94(−14)	5.32(−14)	1.836(−10)	3.35(−12)	1.46(−12)	7.24(−13)
2.0(−6)	2.723(−10)	6.63(−12)	2.97(−14)	2.66(−14)	2.591(−10)	3.35(−12)	2.09(−12)	1.03(−12)
1.0(−6)	3.811(−10)	7.59(−12)	1.49(−14)	1.33(−14)	3.656(−10)	3.35(−12)	2.97(−12)	1.45(−12)
5.0(−7)	5.354(−10)	9.87(−12)			5.159(−10)	3.35(−12)	4.15(−12)	2.07(−12)
2.5(−7)	7.529(−10)	1.35(−11)			7.280(−10)	3.35(−12)	5.89(−12)	2.12(−12)
1.7(−7)	1.144(−9)	2.03(−11)			1.109(−9)	3.35(−12)	9.00(−12)	2.12(−12)
7.2(−8)	1.398(−9)	2.48(−11)			1.356(−9)	3.35(−12)	1.10(−11)	2.12(−12)
4.5(−8)	1.766(−9)	3.14(−11)			1.715(−9)	3.35(−12)	1.39(−11)	2.12(−12)
2.23(−8)	2.489(−9)	4.18(−11)			2.424(−9)	3.35(−12)	1.83(−11)	2.12(−12)

[a]From ref. 43.

[b]The standard-man model also includes the elements calcium, sulfur, potassium, and magnesium but their contributions to the kerma are negligible.

[c]Read: 7.079×10^{-7}, etc.

Table 2A.2. Neutron Fluence-to-Kerma Factors for Specific Body Components[a]

Energy (MeV)	Fluence-to-Kerma Factors (ergs/g)/(neutron/cm^2)				
	Lung	Muscle	Bone	Brain	Red Marrow
15.00	7.04(−7)[b]	6.97(−7)	5.60(−7)	6.98(−7)	7.01(−7)
14.54	6.85(−7)	6.78(−7)	5.41(−7)	6.78(−7)	6.81(−7)
13.94	6.52(−7)	6.46(−7)	5.17(−7)	6.46(−7)	6.48(−7)
13.48	6.14(−7)	6.08(−7)	4.94(−7)	6.10(−7)	6.11(−7)
13.03	5.96(−7)	5.90(−7)	4.81(−7)	5.92(−7)	5.93(−7)
12.43	5.96(−7)	5.90(−7)	4.73(−7)	5.91(−7)	5.92(−7)
11.98	6.00(−7)	5.94(−7)	4.72(−7)	5.94(−7)	5.96(−7)
11.52	5.96(−7)	5.90(−7)	4.63(−7)	5.88(−7)	5.91(−7)
11.07	5.85(−7)	5.79(−7)	4.55(−7)	5.78(−7)	5.80(−7)
10.47	5.61(−7)	5.54(−7)	4.34(−7)	5.53(−7)	5.55(−7)
10.00	5.53(−7)	5.46(−7)	4.25(−7)	5.44(−7)	5.47(−7)
9.53	5.38(−7)	5.31(−7)	4.15(−7)	5.30(−7)	5.32(−7)
9.00	5.21(−7)	5.14(−7)	4.01(−7)	5.13(−7)	5.15(−7)
8.55	5.05(−7)	4.99(−7)	3.90(−7)	4.98(−7)	5.00(−7)
8.02	4.96(−7)	4.90(−7)	3.91(−7)	4.92(−7)	4.92(−7)
7.49	4.94(−7)	4.88(−7)	3.85(−7)	4.89(−7)	4.98(−7)
6.97	4.73(−7)	4.67(−7)	3.60(−7)	4.66(−7)	4.67(−7)
6.52	4.67(−7)	4.61(−7)	3.57(−7)	4.60(−7)	4.61(−7)
6.00	4.58(−7)	4.53(−7)	3.52(−7)	4.52(−7)	4.53(−7)
5.54	4.41(−7)	4.36(−7)	3.40(−7)	4.36(−7)	4.37(−7)
5.00	4.39(−7)	4.34(−7)	3.36(−7)	4.33(−7)	4.35(−7)
4.50	4.13(−7)	4.08(−7)	3.20(−7)	4.08(−7)	4.09(−7)
4.00	4.09(−7)	4.04(−7)	3.19(−7)	4.05(−7)	4.06(−7)
3.52	4.05(−7)	4.00(−7)	3.15(−7)	4.01(−7)	4.02(−7)
3.00	3.59(−7)	3.54(−7)	2.77(−7)	3.55(−7)	3.55(−7)
2.50	3.28(−7)	3.24(−7)	2.51(−7)	3.25(−7)	3.25(−7)
2.00	3.01(−7)	2.97(−7)	2.29(−7)	2.98(−7)	2.98(−7)
1.80	2.90(−7)	2.87(−7)	2.20(−7)	2.87(−7)	2.87(−7)
1.60	2.74(−7)	2.71(−7)	2.08(−7)	2.71(−7)	2.71(−7)
1.40	2.59(−7)	2.56(−7)	1.97(−7)	2.56(−7)	2.57(−7)
1.20	2.45(−7)	2.42(−7)	1.84(−7)	2.42(−7)	2.42(−7)
1.00	2.51(−7)	2.47(−7)	1.83(−7)	2.46(−7)	2.47(−7)
8.05(−1)	2.00(−7)	1.97(−7)	1.51(−7)	1.98(−7)	1.98(−7)
6.0(−1)	1.73(−7)	1.71(−7)	1.31(−7)	1.71(−7)	1.71(−7)
5.0(−1)	1.60(−7)	1.58(−7)	1.21(−7)	1.58(−7)	1.58(−7)
4.0(−1)	1.51(−7)	1.48(−7)	1.11(−7)	1.48(−7)	1.50(−7)
3.0(−1)	1.23(−7)	1.22(−7)	9.27(−8)	1.22(−7)	1.22(−7)
2.0(−1)	9.73(−8)	9.67(−8)	7.33(−8)	9.61(−8)	9.63(−8)
1.0(−1)	6.39(−8)	6.30(−8)	4.80(−8)	6.31(−8)	6.31(−8)
5.03(−2)	3.88(−8)	3.83(−8)	2.92(−8)	3.84(−8)	3.84(−8)
2.04(−2)	1.82(−8)	1.80(−8)	1.38(−8)	1.80(−8)	1.80(−8)
1.02(−2)	9.69(−9)	9.57(−9)	7.54(−9)	9.57(−9)	9.57(−9)
4.97(−3)	4.90(−9)	4.84(−9)	4.02(−9)	4.84(−9)	4.84(−9)
3.00(−3)	2.99(−9)	2.95(−9)	2.61(−9)	2.96(−9)	2.94(−9)
2.014(−3)	2.02(−9)	2.00(−9)	1.90(−9)	2.00(−9)	1.99(−9)
1.025(−3)	1.04(−9)	1.03(−9)	1.18(−9)	1.03(−9)	1.025(−9)
4.94(−4)	5.16(−10)	5.11(−10)	7.94(−10)	5.12(−10)	5.08(−10)
2.01(−4)	2.30(−10)	2.29(−10)	5.94(−10)	2.27(−10)	2.29(−10)
1.00(−4)	1.39(−10)	1.39(−10)	5.38(−10)	1.36(−10)	1.41(−10)
5.03(−5)	1.03(−10)	1.04(−10)	5.26(−10)	9.59(−11)	1.09(−10)
3.43(−5)	9.72(−11)	9.78(−11)	5.32(−10)	8.76(−11)	1.05(−10)
2.05(−5)	1.01(−10)	1.01(−10)	5.52(−10)	8.65(−11)	1.12(−10)
1.03(−5)	1.22(−10)	1.22(−10)	6.00(−10)	9.93(−11)	1.40(−10)
5.14(−6)	1.61(−10)	1.61(−10)	6.75(−10)	1.27(−10)	1.88(−10)
2.00(−6)	2.49(−10)	2.47(−10)	8.33(−10)	1.90(−10)	2.93(−10)
1.00(−6)	3.48(−10)	3.45(−10)	1.01(−9)	2.62(−10)	4.12(−10)
5.0(−7)	4.89(−10)	4.83(−10)	1.26(−9)	3.65(−10)	5.81(−10)
2.5(−7)	6.87(−10)	6.79(−10)	1.61(−9)	5.09(−10)	8.18(−10)
1.07(−7)	1.04(−9)	1.03(−9)	2.24(−9)	7.68(−10)	1.25(−9)
4.5(−8)	1.61(−9)	1.59(−9)	3.24(−9)	1.18(−9)	1.93(−9)
2.23(−8)	2.27(−9)	2.24(−9)	4.42(−9)	1.66(−9)	2.72(−9)

[a]From ref. 43.
[b]Read: 7.04 × 10^{-7}, etc.

Table 2A.3. Unweighted Neutron Fluence-to-Kerma Factors for the Most Common Elements in Man[a]

Energy (MeV)	Unweighted Fluence-to-Kerma Factor [(ergs/g)/(neutron/cm^2)]/[atoms/g] × 10^{24}										
	Hydrogen	Oxygen	Carbon	Nitrogen	Calcium	Phosphorus	Sulfur	Potassium	Sodium	Chlorine	Magnesium
15.00	7.75(−6)[b]	6.67(−6)	6.56(−6)	7.41(−6)	5.02(−7)	7.92(−6)	9.67(−7)	1.35(−5)	1.38(−6)	4.75(−6)	1.11(−5)
14.84	7.74(−6)	6.48(−6)	6.25(−6)	7.32(−6)	5.02(−7)	7.84(−6)	9.51(−7)	1.34(−5)	1.37(−6)	4.70(−6)	1.11(−5)
14.54	7.73(−6)	6.20(−6)	5.73(−6)	7.11(−6)	4.99(−7)	7.69(−6)	9.17(−7)	1.30(−5)	1.35(−6)	4.61(−6)	1.11(−5)
14.24	7.72(−6)	5.72(−6)	5.37(−6)	6.95(−6)	4.94(−7)	7.55(−6)	8.83(−7)	1.28(−5)	1.33(−6)	4.52(−6)	1.11(−5)
13.94	7.71(−6)	5.23(−6)	5.11(−6)	6.75(−6)	4.91(−7)	7.41(−6)	8.46(−7)	1.25(−5)	1.31(−6)	4.36(−6)	1.10(−5)
13.63	7.70(−6)	4.38(−6)	4.93(−6)	6.41(−6)	4.95(−7)	7.26(−6)	8.01(−7)	1.23(−5)	1.29(−6)	4.19(−6)	1.08(−5)
13.33	7.69(−6)	3.82(−6)	4.75(−6)	6.21(−6)	4.99(−7)	7.10(−6)	7.57(−7)	1.20(−5)	1.28(−6)	4.03(−6)	1.07(−5)
13.03	7.68(−6)	3.48(−6)	4.52(−6)	6.12(−6)	4.97(−7)	6.94(−6)	7.20(−7)	1.18(−5)	1.25(−6)	3.87(−6)	1.04(−5)
12.73	7.67(−6)	3.55(−6)	4.12(−6)	5.97(−6)	4.93(−7)	6.79(−6)	6.84(−7)	1.15(−5)	1.21(−6)	3.73(−6)	1.01(−5)
12.43	7.66(−6)	3.67(−6)	3.83(−6)	5.84(−6)	4.96(−7)	6.64(−6)	6.53(−7)	1.13(−5)	1.18(−6)	3.61(−6)	9.74(−6)
12.13	7.64(−6)	3.74(−6)	3.69(−6)	5.65(−6)	5.00(−7)	6.49(−6)	6.23(−7)	1.10(−5)	1.15(−6)	3.50(−6)	9.34(−6)
11.83	7.63(−6)	4.11(−6)	3.33(−6)	5.43(−6)	4.93(−7)	6.30(−6)	5.96(−7)	1.08(−5)	1.13(−6)	3.40(−6)	8.89(−6)
11.52	7.61(−6)	3.94(−6)	3.02(−6)	5.19(−6)	4.85(−7)	6.08(−6)	5.71(−7)	1.06(−5)	1.11(−6)	3.30(−6)	8.44(−6)
11.22	7.60(−6)	3.75(−6)	2.98(−6)	4.99(−6)	4.74(−7)	5.87(−6)	5.50(−7)	1.04(−5)	1.09(−6)	3.21(−6)	7.90(−6)
10.92	7.58(−6)	3.32(−6)	2.85(−6)	4.77(−6)	4.63(−7)	5.66(−6)	5.30(−7)	1.01(−5)	1.07(−6)	3.13(−6)	7.38(−6)
10.62	7.56(−6)	2.99(−6)	2.41(−6)	4.69(−6)	4.63(−7)	5.46(−6)	5.12(−7)	9.86(−6)	1.05(−6)	3.04(−6)	6.85(−6)
10.32	7.55(−6)	3.01(−6)	1.88(−6)	4.59(−6)	4.62(−7)	5.26(−6)	4.95(−7)	9.61(−6)	1.02(−6)	2.97(−6)	6.32(−6)
10.02	7.53(−6)	2.86(−6)	1.76(−6)	4.42(−6)	4.54(−7)	5.06(−6)	4.81(−7)	9.37(−6)	9.91(−7)	2.91(−6)	5.76(−6)
9.72	7.49(−6)	2.65(−6)	1.81(−6)	4.24(−6)	4.44(−7)	4.88(−6)	4.69(−7)	9.13(−6)	9.58(−7)	2.84(−6)	5.22(−6)
9.60	7.48(−6)	2.52(−6)	1.80(−6)	4.17(−6)	4.41(−7)	4.81(−6)	4.64(−7)	9.03(−6)	9.44(−7)	2.81(−6)	5.02(−6)
9.45	7.45(−6)	2.39(−6)	1.82(−6)	3.99(−6)	4.36(−7)	4.72(−6)	4.59(−7)	8.91(−6)	9.23(−7)	2.78(−6)	4.76(−6)
9.30	7.43(−6)	2.21(−6)	1.85(−6)	3.94(−6)	4.31(−7)	4.62(−6)	4.57(−7)	8.78(−6)	9.00(−7)	2.75(−6)	4.51(−6)
9.15	7.41(−6)	2.10(−6)	1.78(−6)	3.89(−6)	4.26(−7)	4.53(−6)	4.57(−7)	8.66(−6)	8.77(−7)	2.72(−6)	4.28(−6)
9.00	7.39(−6)	2.12(−6)	1.45(−6)	3.77(−6)	4.21(−7)	4.44(−6)	4.57(−7)	8.53(−6)	8.57(−7)	2.69(−6)	4.06(−6)
8.85	7.38(−6)	2.01(−6)	1.34(−6)	3.72(−6)	4.17(−7)	4.27(−6)	4.56(−7)	8.39(−6)	8.43(−7)	2.66(−6)	3.81(−6)
8.70	7.37(−6)	1.93(−6)	1.30(−6)	3.69(−6)	4.14(−7)	4.37(−6)	4.57(−7)	8.26(−6)	8.32(−7)	2.63(−6)	3.56(−6)
8.62	7.36(−6)	1.78(−6)	1.29(−6)	3.63(−6)	4.12(−7)	4.34(−6)	4.57(−7)	8.20(−6)	8.28(−7)	2.62(−6)	3.45(−6)
8.47	7.35(−6)	1.73(−6)	1.30(−6)	3.53(−6)	4.09(−7)	4.05(−6)	4.56(−7)	8.07(−6)	8.30(−6)	2.58(−6)	3.23(−6)
8.32	7.33(−6)	1.94(−6)	1.38(−6)	3.44(−6)	4.03(−7)	4.07(−6)	4.54(−7)	7.94(−6)	8.27(−7)	2.54(−6)	3.05(−6)
8.17	7.32(−6)	1.87(−6)	1.78(−6)	3.45(−6)	3.97(−7)	3.58(−6)	4.53(−7)	7.80(−6)	8.23(−7)	2.50(−6)	2.89(−6)
8.02	7.31(−6)	1.30(−6)	2.18(−6)	3.80(−6)	3.92(−7)	3.74(−6)	4.51(−7)	7.67(−6)	8.16(−7)	2.46(−6)	2.63(−6)
7.87	7.27(−6)	1.69(−6)	2.18(−6)	3.51(−6)	3.88(−7)	3.65(−6)	4.49(−7)	7.52(−6)	8.06(−7)	2.42(−6)	2.41(−6)
7.72	7.22(−6)	1.72(−6)	2.56(−6)	3.11(−6)	3.84(−7)	3.45(−6)	4.48(−7)	7.37(−6)	7.95(−7)	2.37(−6)	2.24(−6)
7.57	7.18(−6)	1.61(−6)	1.95(−6)	3.08(−6)	3.83(−7)	3.45(−6)	4.47(−7)	7.21(−6)	7.87(−7)	2.33(−6)	2.04(−6)
7.42	7.14(−6)	1.82(−6)	2.07(−6)	3.19(−6)	3.82(−7)	3.28(−6)	4.47(−7)	7.05(−6)	7.79(−7)	2.29(−6)	1.85(−6)
7.27	7.09(−6)	2.36(−6)	1.50(−6)	3.10(−6)	3.82(−7)	3.15(−6)	4.46(−7)	6.88(−6)	7.72(−7)	2.24(−6)	1.65(−6)
7.12	7.05(−6)	1.83(−6)	8.98(−7)	2.83(−6)	3.82(−7)	2.90(−6)	4.46(−7)	6.71(−6)	7.64(−7)	2.20(−6)	1.46(−6)
6.97	7.00(−6)	1.39(−6)	9.13(−7)	2.80(−6)	3.82(−7)	2.93(−6)	4.46(−7)	6.54(−6)	7.57(−7)	2.16(−6)	1.31(−6)
6.82	6.98(−6)	1.83(−6)	1.00(−6)	2.62(−6)	3.78(−7)	2.91(−6)	4.43(−7)	6.37(−6)	7.61(−7)	2.11(−6)	1.24(−6)
6.67	6.96(−6)	1.74(−6)	9.76(−7)	2.62(−6)	3.74(−7)	2.77(−6)	4.39(−7)	6.21(−6)	7.69(−6)	2.07(−6)	1.07(−6)
6.52	6.93(−6)	1.31(−6)	1.04(−6)	2.71(−6)	3.70(−7)	2.65(−2)	4.37(−7)	6.06(−6)	7.81(−6)	2.02(−6)	9.97(−7)
6.37	6.91(−6)	1.72(−6)	1.42(−6)	2.86(−6)	3.66(−7)	2.58(−6)	4.34(−7)	5.90(−6)	8.06(−6)	1.98(−6)	8.69(−7)

Table 2A.3. (continued)

Energy (MeV)	Unweighted Fluence-to-Kerma Factor [(ergs/g)/(neutron/cm^2)]/[atoms/g] $\times 10^{24}$										
	Hydrogen	Oxygen	Carbon	Nitrogen	Calcium	Phosphorus	Sulfur	Potassium	Sodium	Chlorine	Magnesium
6.21	6.89(−6)	1.09(−6)	1.74(−6)	2.93(−6)	3.63(−7)	2.50(−6)	4.35(−7)	5.74(−6)	8.19(−6)	1.92(−6)	7.65(−7)
6.06	6.86(−6)	1.22(−6)	1.27(−6)	3.03(−6)	3.62(−7)	2.39(−6)	4.38(−7)	5.57(−6)	7.72(−6)	1.87(−6)	6.84(−7)
5.91	6.82(−6)	1.65(−6)	1.18(−6)	2.95(−6)	3.65(−7)	2.34(−6)	4.29(−7)	5.40(−6)	7.42(−6)	1.82(−6)	7.93(−7)
5.76	6.77(−6)	1.03(−6)	1.14(−6)	2.82(−6)	3.71(−7)	2.26(−6)	4.12(−7)	5.23(−6)	7.45(−6)	1.77(−6)	8.22(−7)
5.61	6.72(−6)	1.36(−6)	1.14(−6)	2.85(−6)	3.77(−7)	2.19(−6)	4.07(−7)	5.05(−6)	7.58(−6)	1.71(−6)	8.18(−7)
5.46	6.67(−6)	6.49(−6)	1.18(−6)	2.61(−6)	3.83(−7)	2.11(−6)	4.12(−7)	4.91(−6)	7.72(−6)	1.65(−6)	7.85(−7)
5.31	6.62(−6)	7.52(−6)	1.08(−6)	2.72(−6)	3.94(−7)	2.04(−6)	4.14(−7)	4.76(−6)	7.84(−6)	1.59(−6)	7.44(−7)
5.16	6.57(−6)	1.53(−6)	1.10(−6)	3.34(−6)	4.06(−7)	1.98(−6)	4.15(−7)	4.60(−6)	7.74(−6)	1.53(−6)	7.87(−7)
5.01	6.51(−6)	1.22(−6)	1.10(−6)	3.22(−6)	4.23(−7)	1.92(−6)	4.18(−7)	4.43(−6)	6.98(−6)	1.47(−6)	7.68(−7)
4.69	6.37(−6)	7.91(−7)	1.25(−6)	2.99(−6)	4.34(−7)	1.87(−6)	4.29(−7)	4.04(−6)	7.22(−6)	1.34(−6)	7.91(−7)
4.50	6.29(−6)	7.36(−7)	1.18(−6)	3.48(−6)	4.39(−7)	1.64(−6)	4.25(−7)	3.84(−6)	6.35(−6)	1.26(−6)	7.20(−7)
4.31	6.20(−6)	1.29(−6)	1.11(−6)	3.60(−6)	4.47(−7)	1.61(−6)	4.21(−7)	3.57(−6)	7.53(−6)	1.17(−6)	7.10(−7)
4.16	6.13(−6)	1.49(−6)	1.57(−6)	4.00(−6)	4.56(−7)	1.40(−6)	4.21(−7)	3.35(−6)	6.55(−6)	1.10(−6)	7.29(−7)
4.01	6.06(−6)	9.91(−7)	1.70(−6)	3.83(−6)	4.64(−7)	1.40(−6)	4.22(−7)	3.15(−6)	6.88(−6)	1.03(−6)	5.85(−7)
3.82	5.96(−6)	1.29(−6)	1.88(−6)	3.12(−6)	4.65(−7)	1.38(−6)	4.20(−7)	2.78(−6)	6.21(−6)	9.42(−7)	5.26(−7)
3.67	5.87(−6)	1.35(−6)	2.01(−6)	2.94(−6)	4.69(−7)	1.37(−6)	3.95(−7)	2.49(−6)	7.04(−6)	8.67(−7)	5.83(−7)
3.52	5.79(−6)	1.37(−6)	2.03(−6)	3.59(−6)	4.74(−7)	1.06(−6)	3.71(−7)	2.16(−6)	6.81(−6)	7.95(−7)	6.59(−7)
3.33	5.68(−6)	1.53(−6)	1.72(−6)	2.67(−6)	5.00(−7)	9.83(−7)	3.77(−7)	1.80(−6)	6.19(−6)	7.26(−7)	5.58(−7)
3.18	5.58(−6)	9.11(−7)	1.27(−6)	2.27(−6)	5.03(−7)	1.09(−6)	4.10(−7)	1.50(−6)	5.62(−6)	6.74(−7)	4.19(−7)
3.03	5.49(−6)	6.77(−7)	7.84(−7)	1.98(−6)	4.91(−7)	9.22(−7)	4.35(−7)	1.29(−6)	5.13(−6)	6.40(−7)	6.20(−7)
2.84	5.36(−6)	5.04(−7)	1.33(−6)	1.61(−6)	4.76(−7)	8.27(−7)	4.43(−7)	1.13(−6)	6.13(−6)	6.01(−7)	5.72(−7)
2.69	5.25(−6)	4.88(−7)	1.05(−6)	1.52(−6)	4.64(−7)	8.06(−7)	4.30(−7)	1.01(−6)	5.95(−6)	5.79(−7)	6.12(−7)
2.50	5.11(−6)	4.45(−7)	9.01(−7)	1.07(−6)	4.35(−7)	6.26(−7)	3.70(−7)	8.51(−7)	6.67(−6)	5.51(−7)	4.67(−7)
2.40	5.02(−6)	1.50(−7)	8.52(−7)	8.57(−7)	4.12(−7)	5.57(−7)	3.47(−7)	7.67(−7)	6.70(−6)	5.36(−7)	4.42(−7)
2.31	4.93(−6)	3.26(−7)	8.18(−7)	9.74(−7)	3.92(−7)	5.33(−7)	3.23(−7)	7.03(−7)	6.00(−6)	5.21(−7)	5.05(−7)
2.21	4.85(−6)	4.78(−7)	7.90(−7)	1.29(−6)	3.60(−7)	5.05(−7)	3.12(−7)	6.42(−7)	5.89(−6)	5.04(−7)	5.65(−7)
2.10	4.74(−6)	5.05(−7)	8.04(−7)	7.72(−7)	3.44(−7)	4.57(−7)	2.96(−7)	5.77(−7)	6.45(−6)	4.84(−7)	5.57(−7)
2.00	4.64(−6)	5.00(−7)	7.60(−7)	7.38(−7)	3.30(−7)	4.23(−7)	2.83(−7)	5.52(−7)	5.41(−6)	4.66(−7)	5.19(−7)
1.89	4.53(−6)	7.33(−7)	7.29(−7)	7.90(−7)	3.10(−7)	3.79(−7)	2.59(−7)	4.98(−7)	3.88(−6)	4.43(−7)	4.47(−7)
1.80	4.43(−6)	5.78(−7)	7.11(−7)	1.38(−6)	2.98(−7)	3.77(−7)	2.45(−7)	4.32(−7)	5.33(−6)	4.23(−7)	4.13(−7)
1.70	4.32(−6)	5.37(−7)	6.94(−7)	7.03(−7)	2.69(−7)	3.58(−7)	2.44(−7)	3.99(−7)	4.59(−6)	4.02(−7)	4.90(−7)
1.59	4.19(−6)	5.20(−7)	6.75(−7)	7.89(−7)	2.42(−7)	3.43(−7)	2.30(−7)	3.43(−7)	4.42(−6)	3.75(−7)	3.15(−7)
1.50	4.08(−6)	5.07(−7)	6.58(−7)	7.26(−7)	2.23(−7)	3.05(−7)	2.09(−7)	3.24(−7)	4.01(−6)	3.51(−7)	3.10(−7)
1.40	3.96(−6)	4.98(−7)	6.42(−7)	1.33(−6)	2.10(−7)	2.85(−7)	2.02(−7)	2.64(−7)	4.73(−6)	3.25(−7)	3.66(−7)
1.31	3.84(−6)	9.87(−7)	6.24(−7)	5.17(−7)	2.02(−7)	2.66(−7)	2.41(−7)	2.43(−7)	4.40(−6)	2.99(−7)	4.69(−7)
1.20	3.70(−6)	6.13(−7)	6.02(−7)	4.10(−7)	1.96(−7)	2.49(−7)	1.80(−7)	2.07(−7)	3.85(−7)	2.70(−7)	3.02(−7)
1.10	3.55(−6)	7.55(−7)	5.79(−7)	5.10(−7)	1.87(−7)	2.16(−7)	1.46(−7)	1.80(−7)	4.62(−7)	2.42(−7)	1.72(−7)
1.00	3.41(−6)	1.42(−7)	5.56(−7)	5.08(−7)	1.85(−7)	1.76(−7)	1.58(−7)	1.54(−7)	3.13(−7)	2.16(−7)	1.99(−7)
9.0(−1)	3.24(−6)	5.10(−7)	5.28(−7)	2.72(−7)	1.86(−7)	1.55(−7)	1.30(−7)	1.20(−7)	3.98(−7)	1.88(−7)	2.37(−7)
8.0(−1)	3.07(−6)	3.45(−7)	4.95(−7)	3.08(−7)	1.30(−7)	1.16(−7)	1.34(−7)	1.01(−7)	4.58(−7)	1.62(−7)	2.48(−7)
7.0(−1)	2.89(−6)	2.93(−7)	4.62(−7)	3.99(−7)	1.19(−7)	1.07(−7)	1.27(−7)	8.99(−8)	6.13(−7)	1.34(−7)	2.54(−7)
6.0(−1)	2.69(−6)	2.48(−7)	4.21(−7)	2.24(−7)	1.52(−7)	1.51(−7)	7.73(−8)	7.85(−8)	3.54(−7)	1.16(−7)	1.97(−7)
5.0(−1)	2.48(−6)	2.54(−7)	3.76(−7)	4.26(−7)	7.55(−7)	1.05(−7)	7.24(−8)	7.30(−8)	1.36(−7)	9.81(−8)	1.89(−7)

Table 2A.3. (continued)

Energy (MeV)	Unweighted Fluence-to-Kerma Factor [(ergs/g)/(neutron/cm^2)]/[atoms/g] × 10^{24}										
	Hydrogen	Oxygen	Carbon	Nitrogen	Calcium	Phosphorus	Sulfur	Potassium	Sodium	Chlorine	Magnesium
4.5(−1)	2.35(−6)	8.41(−7)	3.49(−7)	2.32(−7)	1.51(−7)	1.12(−7)	7.19(−8)	7.05(−8)	2.18(−7)	9.06(−8)	3.71(−7)
3.98(−1)	2.20(−6)	4.80(−7)	3.20(−7)	2.21(−7)	4.27(−7)	8.09(−8)	6.63(−8)	6.00(−8)	2.11(−7)	9.05(−8)	2.13(−7)
3.51(−1)	2.07(−6)	2.88(−7)	2.92(−7)	1.97(−7)	1.14(−7)	9.92(−8)	5.64(−8)	5.88(−8)	1.45(−7)	8.28(−7)	2.19(−7)
3.00(−1)	1.91(−6)	2.09(−7)	2.59(−7)	1.71(−7)	5.84(−7)	6.22(−8)	4.84(−8)	7.89(−8)	1.66(−7)	5.31(−8)	3.34(−7)
2.51(−1)	1.73(−6)	1.65(−7)	2.25(−7)	1.55(−7)	7.38(−7)	5.80(−8)	4.10(−8)	3.62(−8)	1.51(−7)	3.86(−8)	2.90(−7)
2.00(−1)	1.53(−6)	1.28(−7)	1.89(−7)	1.46(−7)	1.50(−7)	5.62(−8)	9.06(−8)	2.16(−8)	1.76(−7)	3.99(−8)	1.33(−7)
1.50(−1)	1.30(−6)	9.55(−8)	1.45(−7)	1.18(−7)	6.74(−9)	5.06(−8)	5.18(−8)	4.31(−8)	6.38(−8)	2.82(−8)	7.57(−8)
1.01(−1)	1.01(−6)	6.41(−8)	1.01(−7)	8.64(−8)	1.02(−8)	3.40(−8)	7.10(−8)	3.27(−8)	4.31(−8)	1.84(−8)	9.51(−8)
7.03(−2)	7.99(−7)	4.50(−8)	7.27(−8)	7.51(−8)	7.04(−9)	2.38(−8)	2.80(−9)	5.91(−8)	3.70(−8)	1.69(−8)	5.44(−8)
5.03(−2)	6.20(−7)	3.23(−8)	5.29(−8)	6.12(−8)	5.05(−9)	1.93(−8)	2.39(−9)	2.56(−9)	3.51(−8)	1.35(−8)	2.25(−8)
3.05(−2)	4.13(−7)	1.96(−8)	3.26(−8)	3.99(−8)	3.07(−9)	1.61(−8)	1.98(−9)	4.09(−9)	1.78(−8)	9.12(−9)	1.40(−8)
2.04(−2)	2.92(−7)	1.32(−8)	2.21(−8)	2.99(−8)	2.06(−9)	6.21(−8)	1.71(−9)	2.72(−9)	1.22(−8)	6.93(−9)	1.92(−8)
1.50(−2)	2.20(−7)	9.64(−9)	1.62(−8)	2.52(−8)	1.51(−9)	8.75(−8)	1.48(−9)	2.06(−9)	9.65(−9)	5.83(−9)	6.95(−9)
1.02(−2)	1.55(−7)	6.62(−9)	1.11(−8)	1.84(−8)	1.03(−9)	1.09(−7)	1.15(−9)	2.27(−9)	8.45(−9)	2.94(−9)	4.48(−9)
7.03(−3)	1.10(−7)	4.57(−9)	7.67(−9)	1.50(−8)	7.10(−10)	1.24(−7)	8.04(−10)	7.21(−10)	7.83(−9)	2.96(−9)	3.06(−9)
5.11(−3)	8.08(−8)	3.33(−9)	5.60(−9)	1.26(−8)	5.17(−10)	1.33(−7)	5.89(−10)	5.69(−10)	9.44(−9)	3.89(−9)	2.22(−9)
4.03(−3)	6.39(−8)	2.63(−9)	4.42(−9)	1.15(−6)	4.07(−10)	1.38(−7)	4.67(−10)	5.54(−10)	1.76(−8)	3.35(−9)	1.74(−9)
3.00(−3)	4.78(−8)	1.96(−9)	3.29(−9)	1.06(−8)	3.03(−10)	1.43(−7)	3.51(−10)	2.46(−10)	1.71(−7)	1.92(−9)	1.29(−9)
2.01(−3)	3.23(−8)	1.32(−9)	2.21(−9)	1.02(−8)	2.04(−10)	1.47(−7)	2.40(−10)	2.09(−10)	1.62(−8)	1.65(−9)	8.66(−10)
1.50(−3)	2.40(−8)	9.82(−10)	1.65(−9)	1.04(−8)	1.52(−10)	1.50(−7)	1.81(−10)	1.68(−10)	6.77(−9)	1.97(−9)	6.43(−10)
1.03(−3)	1.64(−8)	6.72(−10)	1.13(−9)	1.12(−8)	1.04(−10)	1.52(−7)	1.28(−10)	1.23(−10)	4.29(−9)	3.54(−9)	4.40(−10)
7.68(−4)	1.23(−8)	5.04(−10)	8.46(−10)	1.22(−8)	7.77(−11)	1.53(−7)	9.83(−11)	9.78(−11)	3.67(−9)	8.01(−9)	3.30(−10)
5.13(−4)	8.24(−9)	3.36(−10)	5.65(−10)	1.42(−8)	5.19(−11)	1.54(−7)	6.98(−11)	7.30(−11)	3.43(−9)	5.42(−8)	2.21(−10)
3.10(−4)	5.00(−9)	2.04(−10)	3.42(−10)	1.76(−8)	3.14(−11)	1.55(−7)	4.80(−11)	5.48(−11)	3.64(−9)	5.80(−8)	1.34(−10)
1.42(−4)	2.30(−9)	9.32(−11)	1.56(−10)	2.53(−8)	1.44(−11)	1.56(−7)	3.21(−11)	4.74(−11)	4.70(−9)	3.30(−9)	6.22(−11)
1.01(−4)	1.63(−9)	6.60(−11)	1.11(−10)	2.99(−8)	1.02(−11)	1.56(−7)	3.00(−11)	4.90(−11)	5.63(−9)	1.14(−8)	4.49(−11)
7.10(−5)	1.16(−9)	4.66(−11)	7.82(−11)	3.54(−8)	7.27(−12)	1.56(−7)	2.93(−11)	5.38(−11)	6.68(−9)	2.89(−9)	3.27(−11)
5.03(−5)	8.27(−10)	3.30(−11)	5.54(−11)	4.20(−8)	8.43(−12)	1.56(−7)	2.98(−11)	6.09(−11)	7.85(−9)	3.23(−9)	2.44(−11)
3.88(−5)	6.44(−10)	2.55(−11)	4.28(−11)	4.77(−8)	6.87(−12)	1.56(−7)	3.16(−11)	6.82(−11)	8.93(−9)	4.11(−9)	1.99(−11)
3.43(−5)	5.73(−10)	2.25(−11)	3.79(−11)	5.07(−8)	5.61(−12)	1.56(−7)	3.28(−11)	7.23(−11)	9.52(−9)	4.61(−9)	1.82(−11)
2.74(−5)	4.65(−10)	1.80(−11)	3.03(−11)	5.67(−8)	3.76(−12)	1.56(−7)	3.45(−11)	8.05(−11)	1.07(−8)	5.72(−9)	1.57(−11)
2.05(−5)	3.57(−10)	1.35(−11)	2.27(−11)	6.54(−8)	2.23(−12)	1.56(−7)	3.80(−11)	9.29(−11)	1.23(−8)	7.62(−9)	1.34(−11)
1.60(−5)	2.87(−10)	1.05(−11)	1.77(−11)	7.40(−8)	1.62(−12)	1.56(−7)	4.14(−11)	1.05(−10)	1.40(−8)	9.23(−9)	1.20(−11)
1.26(−5)	2.35(−10)	8.25(−12)	1.39(−11)	8.34(−8)	1.27(−12)	1.56(−7)	4.54(−11)	1.19(−10)	1.59(−8)	1.11(−8)	1.12(−11)
8.01(−6)	1.69(−10)	5.26(−12)	8.83(−12)	1.04(−7)	8.11(−13)	1.56(−7)	5.58(−11)	1.51(−10)	1.99(−8)	1.49(−8)	1.08(−11)
4.00(−6)	1.20(−10)	2.63(−12)	4.42(−12)	1.47(−7)	4.05(−13)	1.56(−7)	7.82(−11)	2.13(−10)	2.79(−8)	2.13(−8)	1.21(−11)
2.00(−6)	1.11(−10)	1.31(−12)	2.21(−12)	2.08(−7)	2.03(−13)	1.56(−7)	1.11(−10)	3.04(−10)	3.99(−8)	3.03(−8)	1.56(−11)
1.00(−6)	1.27(−10)	6.57(−13)	1.10(−12)	2.93(−7)	1.01(−13)	1.56(−7)	1.58(−10)	9.99(−10)	5.67(−8)	4.27(−8)	2.13(−11)
5.01(−7)	1.65(−10)	3.30(−13)	5.52(−13)	4.14(−7)	5.07(−14)	1.56(−7)	2.21(−10)	1.39(−9)	7.91(−8)	6.08(−8)	2.97(−11)
2.50(−7)	2.26(−10)	1.67(−13)	2.76(−13)	5.84(−7)	2.53(−14)	1.56(−7)	3.14(−10)	1.39(−9)	1.12(−7)	6.23(−8)	4.18(−11)
1.07(−7)	3.40(−10)	7.26(−14)	1.18(−13)	8.90(−7)	1.08(−14)	1.56(−7)	4.88(−10)	1.40(−9)	1.72(−7)	6.23(−8)	6.38(−11)
7.16(−8)	4.15(−10)	4.93(−14)	7.89(−14)	1.09(−6)	7.24(−15)	1.56(−7)	5.84(−10)	1.60(−9)	2.10(−7)	6.23(−8)	7.81(−11)
4.46(−8)	5.25(−10)	3.18(−14)	4.92(−14)	1.38(−6)	4.52(−15)	1.56(−7)	7.37(−10)	2.01(−9)	2.65(−7)	6.23(−8)	9.89(−11)
2.23(−8)	7.00(−10)	1.67(−14)	2.47(−14)	1.94(−6)	2.26(−15)	1.56(−7)	7.99(−10)	2.65(−9)	3.49(−7)	6.23(−8)	1.40(−10)

Appendix 2B. Spatial Distributions of Absorbed Dose and Dose Equivalent in Cylindrical Phantom Due to Incident Monoenergetic Neutrons

This appendix presents calculated absorbed doses and dose equivalents in a four-element cylindrical tissue phantom due to a broad beam of 0.025-eV to 14-MeV monoenergetic neutrons incident on the phantom. The calculations, performed by Auxier *et al.*[51] for the phantom schematic shown in Fig. 2.20, considered dose contributions by both the incident neutrons and the capture gamma rays they produced. The neutron beam was assumed to be incident normal to the axis of the cylinder, and the absorbed doses and dose equivalents given in Table 2B.1 each represent the average value over a radial volume element in layer 3, which is located at the midplane of the cylinder. These values are multicollision doses per unit fluence and thus are fluence-to-dose conversion factors for cylindrical phantoms.

Table 2B.2 gives the absorbed doses due to the secondary (capture) gamma rays only.

Table 2B.1. Absorbed Dose and Dose Equivalent Due to Monoenergetic Neutrons Incident on a Cylindrical Phantom[a]

Layer 3 Volume Element[c]	Absorbed Dose [10^{-10} rads/(n/cm^2)] for E_n of[b]							Dose Equivalent [10^{-10} rems/(n/cm^2)] for E_n of[b]						
	0.025 eV	1 eV	10 eV	100 eV	1 keV	10 keV	100 keV	0.025 eV	1 eV	10 eV	100 eV	1 keV	10 keV	100 keV
1	0.608	1.114	1.533	1.600	1.427	1.616	1.794	0.789	1.472	1.752	2.059	1.912	2.085	2.981
2	0.474	1.006	1.324	1.378	1.036	1.378	1.783	0.618	1.179	1.550	1.725	1.422	1.799	2.559
3	0.415	0.562	0.870	1.020	0.759	0.834	1.107	0.466	0.651	0.973	1.174	0.978	1.128	1.530
4	0.336	0.574	0.789	0.655	0.647	0.737	1.016	0.401	0.630	0.846	0.746	0.824	0.872	1.322
5	1.175	1.816	2.502	2.360	2.404	2.358	2.796	1.427	2.653	3.489	3.653	3.447	3.790	4.775
6	0.801	1.361	1.587	1.700	1.660	1.743	2.385	0.962	1.695	2.130	2.451	2.405	2.677	3.785
7	0.358	0.727	0.689	0.766	0.622	1.041	0.784	0.403	0.788	0.780	0.911	0.821	1.368	1.140
8	0.164	0.377	0.333	0.414	0.394	0.474	0.553	0.199	0.408	0.351	0.452	0.451	0.536	0.652
9	1.762	3.467	3.964	3.800	3.928	3.926	4.592	2.386	5.580	6.876	6.896	7.237	7.827	9.324
10	1.161	1.952	2.178	2.364	2.336	2.314	2.961	1.583	2.892	3.560	3.943	3.858	4.103	5.911
11	0.269	0.549	0.500	0.591	0.636	0.655	0.917	0.310	0.645	0.569	0.742	0.820	0.981	1.347
12	0.084	0.192	0.251	0.263	0.255	0.342	0.436	0.090	0.206	0.252	0.301	0.267	0.368	0.493
13	3.141	5.306	5.816	5.482	5.185	4.844	6.333	5.560	10.566	12.416	11.758	11.148	10.766	17.638
14	1.603	2.876	3.014	3.022	3.025	2.651	3.280	2.640	5.380	5.816	5.849	6.058	5.441	8.515
15	0.239	0.378	0.420	0.560	0.462	0.262	0.687	0.272	0.536	0.570	0.741	0.598	0.521	1.044
16	0.081	0.144	0.167	0.184	0.178	0.145	0.212	0.089	0.148	0.167	0.196	0.183	0.167	0.242
17	4.680	5.890	5.179	4.449	4.322	4.338	8.018	11.530	13.416	12.096	10.053	8.852	9.916	48.559
18	2.379	3.130	2.989	2.761	2.548	2.538	5.018	5.500	6.871	6.462	5.586	5.191	5.559	29.011
19	0.205	0.252	0.347	0.387	0.295	0.299	0.412	0.245	0.376	0.459	0.502	0.376	0.422	0.840
20	0.052	0.090	0.086	0.141	0.092	0.117	0.112	0.056	0.091	0.086	0.145	0.094	0.119	0.118

Table 2B.1 (continued)

Layer 3 Volume Element[c]	Absorbed Dose [10^{-10} rads/(n/cm^2)] for E_n of[b]							Dose Equivalent [10^{-10} rems/(n/cm^2)] for E_n of[b]						
	500 keV	1 MeV	2.5 MeV	5 MeV	7 MeV	10 MeV	14 MeV	500 keV	1 MeV	2.5 MeV	5 MeV	7 MeV	10 MeV	14 MeV
1	2.870	4.79	13.1	39.5	52.8	43.4	62.1	6.192	25.71	106.6	274.2	353.9	293.7	379.7
2	2.608	2.73	12.6	21.0	39.5	43.5	47.4	5.601	9.16	93.2	163.3	277.3	279.3	324.6
3	2.286	2.11	12.4	21.9	35.5	42.3	50.7	3.627	5.49	94.9	174.9	242.3	280.6	336.0
4	1.882	1.94	11.7	18.2	27.5	44.2	42.3	2.635	6.73	96.0	139.2	229.0	279.9	322.8
5	4.712	5.92	16.9	37.5	39.8	56.5	50.0	14.444	32.30	129.8	272.3	295.6	364.0	369.5
6	3.372	3.71	16.0	31.0	36.5	45.5	49.6	9.020	15.34	128.9	231.5	272.1	284.3	354.9
7	1.744	1.80	9.5	22.2	25.2	32.8	36.1	4.401	5.64	69.0	165.6	182.9	212.9	238.0
8	1.274	1.15	6.6	12.0	21.0	21.7	38.6	1.877	3.52	42.5	102.3	151.5	149.1	245.9
9	6.903	9.37	24.5	42.3	49.7	54.5	68.1	33.346	63.02	208.1	333.1	362.1	360.8	491.4
10	4.332	5.31	19.5	36.8	46.2	51.5	56.7	18.130	32.40	161.3	285.4	324.8	336.7	427.6
11	1.300	1.51	7.6	17.9	24.8	35.9	43.0	2.561	5.72	57.5	132.4	182.2	239.9	317.5
12	0.685	0.52	3.0	11.4	11.7	28.5	27.0	0.894	1.35	19.3	85.8	89.7	183.9	185.8
13	11.631	17.30	34.9	48.9	54.6	58.0	75.6	87.508	161.78	303.9	378.4	394.2	362.3	554.2
14	6.627	9.67	25.1	38.6	49.5	56.6	66.1	43.063	84.08	217.4	298.4	358.7	357.7	482.9
15	1.034	1.39	7.1	14.7	22.7	32.4	39.7	2.814	7.82	58.4	110.4	162.7	209.7	286.5
16	0.312	0.37	2.6	6.0	11.3	20.6	22.4	0.370	0.75	18.5	43.2	85.4	146.2	144.4
17	18.110	30.14	39.9	57.2	57.0	72.5	83.1	188.500	326.28	349.6	440.7	402.9	431.3	614.9
18	13.619	21.33	34.8	46.7	55.3	64.7	77.4	140.369	226.59	301.6	361.7	391.3	403.1	592.5
19	0.991	1.55	8.4	15.2	24.7	30.1	38.4	5.766	12.76	70.4	117.5	169.2	193.2	278.2
20	0.225	0.22	1.5	6.7	8.4	17.4	18.4	0.225	0.30	11.8	52.3	58.9	116.1	131.0

[a]From ref. 51; values include contributions from capture gamma rays.
[b]E_n is energy of incident neutrons.
[c]See Fig. 2.20.

Table 2B.2. Absorbed Dose Due to Capture Gamma Rays Produced by Monoenergetic Neutrons Incident on a Cylindrical Phantom[a]

Layer 3 Volume Element[c]	Absorbed Dose [10^{-10} rad/(n/cm^2)] for E_n of[b]													
	0.025 eV	1 eV	10 eV	100 eV	1 keV	10 keV	100 keV	500 keV	1 MeV	2.5 MeV	5 MeV	7 MeV	10 MeV	14 MeV
1	0.590	1.079	1.511	1.554	1.379	1.569	1.676	2.561	2.600	4.810	4.24	3.19	3.46	10.1
2	0.460	0.989	1.302	1.344	0.998	1.336	1.702	2.307	2.133	2.851	3.55	3.53	4.59	6.08
3	0.410	0.553	0.860	1.005	0.737	0.805	1.065	2.147	1.781	3.040	2.76	3.17	4.21	5.78
4	0.330	0.569	0.783	0.646	0.630	0.724	0.986	1.807	1.518	2.238	3.42	2.93	4.43	6.42
5	1.150	1.733	2.404	2.232	2.300	2.216	2.599	3.744	3.391	3.637	4.13	3.27	4.60	8.16
6	0.785	1.328	1.533	1.625	1.586	1.650	2.244	2.813	2.607	2.940	3.26	3.18	4.52	6.31
7	0.354	0.721	0.680	0.752	0.602	1.009	0.749	1.495	1.457	2.899	2.76	2.55	3.71	5.81
8	0.160	0.374	0.331	0.410	0.388	0.468	0.543	1.209	0.914	2.563	2.28	2.38	3.22	6.16
9	1.700	3.257	3.675	3.493	3.599	3.538	4.093	4.426	4.396	3.478	3.34	2.80	5.02	8.36
10	1.120	1.859	2.041	2.207	2.185	2.136	2.653	3.020	2.707	3.012	2.84	2.68	4.36	6.63
11	0.265	0.540	0.493	0.576	0.618	0.623	0.873	1.170	1.099	2.010	2.34	2.19	3.40	4.77
12	0.083	0.191	0.251	0.259	0.254	0.339	0.430	0.663	0.443	1.430	1.74	1.91	3.14	3.72
13	2.900	4.784	5.161	4.859	4.590	4.233	4.988	4.668	3.675	3.194	2.48	2.39	4.98	7.21
14	1.500	2.628	2.756	2.741	2.723	2.365	2.670	3.253	2.629	2.786	2.51	2.27	4.23	6.09
15	0.236	0.362	0.405	0.542	0.449	0.236	0.650	0.861	0.777	1.405	1.60	1.72	2.77	4.41
16	0.080	0.144	0.167	0.183	0.178	0.143	0.209	0.306	0.334	0.762	1.08	1.31	1.71	3.14
17	4.000	5.143	4.492	3.888	3.827	3.420	3.309	2.800	2.230	1.840	1.48	1.68	3.79	7.21
18	2.070	2.759	2.644	2.478	2.260	2.039	2.221	2.269	1.985	1.744	1.65	1.79	3.52	5.69
19	0.201	0.240	0.336	0.375	0.287	0.286	0.358	0.558	0.538	1.049	1.15	1.26	2.07	3.78
20	0.051	0.090	0.086	0.141	0.092	0.117	0.111	0.224	0.186	0.695	0.459	0.76	1.20	1.74

[a]From ref. 51; capture-gamma-ray dose largely due to $^1H(n,\gamma)^2H$ reaction.
[b]E_n is energy of incident neutrons.
[c]See Fig. 2.20.

References

[1] *Radiation Quantities and Units,* International Commission on Radiation Units and Measurements, ICRU Report 11 (Sept. 1, 1968).

[2] J. Chadwick, "The Existence of a Neutron," *Proc. Roy. Soc. (London)* **A136**, 692–708 (1932).

[3] R. D. Evans, *The Atomic Nucleus,* McGraw-Hill Book Company, New York (1955).

[4] R. R. Coveyou, R. R. Bate, and R. K. Osborn, *J. Nuc. Energy* 2, 153 (1956).

[5] M. D. Goldberg, S. F. Mughabghab, B. A. Magurno, and V. M. May, *Neutron Cross Sections,* Brookhaven National Laboratory Report BNL-325 (1966).

[6] M. D. Goldberg, V. M. May, and J. R. Stehn, *Angular Distributions in Neutron-Induced Reactions,* Brookhaven National Laboratory Report BNL-400 (1962).

[7] H. C. Honeck, *ENDF/B Specifications for an Evaluated Nuclear Data File for Reactor Applications,* Brookhaven National Laboratory Report BNL-50066 Rev. (T-467) (or ENDF-102), revised by S. Pearlstein (July 1967).

[8] R. J. Howerton, D. Braff, W. J. Cahill, and N. Chazan, *Thresholds of Nuclear Reactions,* University of California Radiation Laboratory Report UCRL-1400 (1964).

[9] J. J. Schmidt, *Neutron Cross Sections for Fast Reactor Materials. Part I: Evaluation,* Institut fur Neutronenphysik und Reaktortechnik, Karlsruhe, KFK-120, Pt. I (ENADC-E-35 U) (1966).

[10] *An Index to the Literature on Microscopic Neutron Data. Parts I and II,* CINDA-67, Parts I and II (Oct. 1, 1967).

[11] K. J. Yost and M. Solomito, "Sensitivity of Gamma-Ray Dose Calculations to the Energy Dependence of Gamma-Ray Production Cross Sections," p. 53 in *Neutron Cross Sections and Technology,* Proceedings of a Conference, Washington, D.C., March 4–7, 1968, National Bureau of Standards Special Publication 299, Volume 1.

[12] K. J. Yost, "A Method for the Calculation of Neutron-Capture Gamma-Ray Spectra," *Nuc. Sci. Eng.* 32, 62 (1968).

[13] S. Glasstone and M. C. Edlund, *The Elements of Nuclear Reactor Theory,* D. Van Nostrand Company, New York, 1952.

[14] A. M. Weinberg and E. P. Wigner, *The Physical Theory of Nuclear Chain Reactors,* University of Chicago Press, 1958.

[15] *Reactor Handbook, Vol. III, Part A, Physics,* H. Soodak, editor, pp. 10–11, Interscience Publishers, New York, 1962.

[16] B. E. Watt, "Energy Spectrum of Neutrons from Thermal Fission of U^{235}," *Phys. Rev.* **87**, 1037 (1952).

[17] L. Cranberg, N. Nereson, and L. Rosen, "Fission Spectrum of U^{235}," *Phys. Rev.* **103**, 662 (1956).

[18] H. Goldstein, *Fundamental Aspects of Reactor Shielding,* Addison-Wesley Publishing Company, Reading, Mass., 1959.

[19] A. L. Hughes and L. A. DuBridge, *Photoelectric Phenomena,* p. 193, McGraw-Hill, New York, 1932.

[20] O. Klein and Y. Nishina, *Z. Physik* **52**, 853 (1929).

[21] D. K. Trubey, *Use of ICRU-Defined Units in Shielding,* Oak Ridge National Laboratory Report ORNL-RSIC-16 (1968).

[22] E. F. Plechaty and J. R. Terrall, *An Integrated System for Production of Neutronics and Photonics Calculational Constants. Vol. VI. Photon Cross Sections 1 keV to 100 MeV,* Lawrence Radiation Laboratory Report UCRL-50,400, Vol. 6 (Oct. 22, 1968).

[23] W. H. McMaster, N. K. Del Grande, J. H. Mallett, and J. H. Hubbell, *Compilation of X-Ray Cross Sections,* Lawrence Radiation Laboratory Report UCRL-50174, Sec. II, Rev. 1 (May 1969).

[24] J. W. Motz, "Gamma-Ray Spectra of the Los Alamos Reactors," *Phys. Rev.* **86**, 753 (1952).

[25] F. C. Maienschein, R. W. Peelle, W. Zobel, and T. A. Love, "Gamma Rays Associated with Fission," *Proc. U N Intern. Conf. Peaceful Uses At. Energy, 2nd,* **15** (1958) 366; see also *Neutron Physics Division Annual Progress Report for Period Ending September 1, 1958,* Oak Ridge National Laboratory Report ORNL-2609; later data published in *Trans. Am. Nucl. Soc.* **12**, No. 1 (1969) and in ORNL-4457.

[26] J. K. Dickens and F. G. Perey, "The $^{14}N(n,x\gamma)$ Reaction for $5.8 \leqslant E_n \leqslant 8.6$ MeV," *Nucl. Sci. Eng.* **36**, 280 (1969).

[27] V. J. Orphan and C. G. Hoot, *Neutron Cross Section Data for Radiation Transport Calculations,* Gulf General Atomic Report GA-8006 (Jan. 31, 1969).

[28] G. A. Bartholomew and P. J. Campion, "Neutron Capture Gamma Rays from Lithium, Boron, and Nitrogen," *Can. J. Phys.* **35**, 1347 (1957).

[29] F. L. Keller, C. D. Zerby, and W. W. Dunn, *Gamma-Ray Dose Rates from Neutron Captures in Air,* Oak Ridge National Laboratory Report ORNL-2642 (Dec. 31, 1958).

[30] E. S. Troubetzkoy and H. Goldstein, *A Compilation of Information on Gamma-Ray Spectra Resulting from Thermal-Neutron Capture,* Oak Ridge National Laboratory Report ORNL-2904 (May 17, 1960).

[31] R. E. Maerker and F. J. Muckenthaler, *Gamma-Ray Spectra Arising from Thermal-Neutron Capture in*

Elements Found in Soils, Concretes, and Structural Materials, Oak Ridge National Laboratory Report ORNL-4382 (1969).

[32] G. A. Bartholomew *et al., Compendium of Thermal-Neutron Capture γ-Ray Measurements. Part I. Z ⩽ 46,* Nuclear Data, A3, p. 367, Academic Press, New York and London (December 1967).

[33] L. V. Groshev *et al., Compendium of Thermal-Neutron-Capture γ-Ray Measurements. Part II. Z-47 to Z-67 (Ag to Ho),* Nuclear Data, A5, p. 1, Academic Press, New York and London (November 1968).

[34] L. V. Groshev *et al., Compendium of Thermal-Neutron-Capture γ-Ray Measurements, Part III. Z = 68 to Z = 94 (Er to Pu),* Nuclear Data, A5, p. 243, Academic Press, New York and London (February 1969).

[35] G. R. Crocker and M. A. Conners, *Gamma-Emission Data for the Calculation of Exposure Rates from Nuclear Debris. Volume I. Fission Products,* U.S. Naval Radiological Defense Laboratory Report USNRDL-TR-876 (June 10, 1965).

[36] G. R. Crocker and D. T. Wong, *Gamma-Emission Data for the Calculation of Exposure Rates from Nuclear Debris. Volume II. Induced Activities,* U.S. Naval Radiological Defense Laboratory Report USNRDL-TR-888 (Aug. 13, 1965).

[37] L. B. Engle and P. C. Fisher, *Energy and Time Dependence of Delayed Gammas from Fission,* Los Alamos Scientific Laboratory Report LAMS-2642 (July 6, 1962).

[38] G. R. Crocker and T. Turner, *Calculated Activities, Exposure Rates, and Gamma Spectra for Unfractionated Fission Products,* U.S. Naval Radiological Defense Laboratory Report USNRDL-TR-1009 (Dec. 28, 1965).

[39] F. H. Attix, "The Meanings of 'First Collision Dose,' " *Health Phys.* **12**, 793 (1966).

[40] J. A. Auxier, "Kerma Versus First Collision Dose: The Other Side of the Controversy," *Health Phys.* **17**, 342 (1969).

[41] W. S. Snyder, in *Protection Against Neutron Radiation up to 30 MeV,* Report of the National Committee on Radiation Protection and Measurements, National Bureau of Standards Handbook 63, p. 6, 1957.

[42] B. J. Henderson, *Conversion of Neutron or Gamma Ray Flux to Absorbed Dose Rate,* General Electric Co. Report XDC-59-8-179 (Aug. 14, 1959).

[43] J. J. Ritts, E. Solomito, and P. N. Stevens, *Calculation of Neutron Fluence-to-Kerma Factors for the Human Body,* Oak Ridge National Laboratory Report ORNL-TM-2079 (1968).

[44] D. C. Irving, R. M. Freestone, Jr. and F. B. K. Kam, *05R, A General Purpose Monte Carlo Neutron Transport Code,* Oak Ridge National Laboratory Report ORNL-3622 (1965).

[45] T. Rockwell III, Ed., *Reactor Shielding Design Manual,* D. Van Nostrand Co., New York, 1956.

[46] *Recommendations of the International Commission on Radiological Protection,* ICRP Publication 4, Report of Committee IV (1953–1959) on "Protection Against Electromagnetic Radiation above 3 MeV and Electrons, Neutrons and Protons," The MacMillan Company, New York, 1964.

[47] "Report of the RBE Committee on the International Commissions on Radiological Protection and on Radiological Units and Measurements," *Health Phys.* **9**, 357–386 (1963).

[48] W. S. Snyder and C. Neufeld, "On the Passage of Heavy Particles Through Tissue," *Radiation Res.* **6**, 67 (1957); also reprinted in NBS Handbook 63.

[49] G. J. Neary and J. Mulvey, "Maximum Permissible Fluxes of High Energy Neutrons and Protons in the Range 40–1000 MeV," unpublished (revised by Neary, 1958).

[50] Federal Register, Title 10, Part 20, *Standards for Protection Against Radiation,* 1966.

[51] G. A. Auxier, W. S. Snyder and T. D. Jones, "Neutron Interactions and Penetration in Tissue," Chapter 6 of *Radiation Dosimetry,* Vol. I, F. H. Attix and W. C. Roesch, Editors, Academic Press, New York, 1968.

[52] A. R. Jones, *Measurement of the Dose Absorbed in Various Organs as a Function of the External Gamma Ray Exposure,* Atomic Energy of Canada Limited Report AECL-2240 (October 1964).

[53] A. R. Jones, "Proposed Calibration Factors for Various Dosimeters at Different Energies," *Health Phys.* **12**, 663–671 (1966).

[54] J. M. Sidwell, T. E. Burlin, and B. M. Wheatley, "Calculations of the Absorbed Dose in a Phantom from Photon Fluence and Some Applications to Radiological Protection," *British J. Radiol.* **42**, 522 (1969).

[55] H. C. Claiborne and D. K. Trubey, *Dose Rates in a Slab Phantom from Monoenergetic Gamma Rays,* Oak Ridge National Laboratory Report ORNL-TM-2574 (Apr. 28, 1969); accepted for publication in *Nucl. Appl. Technol.* **8(5)**, 450 (1970).

[56] R. G. Alsmiller, Jr. and H. S. Moran, "Dose Rate from High-Energy Electrons and Photons," *Nucl. Instr. Methods* **58**, 343 (1968).

[57] *Shelter Design and Analysis. Vol. I. Fallout Radiation Shielding,* Office of Civilian Defense, Report TR-20 (1967); supersedes TR-20 dated June, 1965.

[58] W. H. Langham, Editor, *Radiobiological Factors in Manned Space Flight,* Report of the Space Radiation Study Panel of the Life Sciences Committee, National Academy of Sciences, National Research Council, Washington, D.C., 1967.

UNCLASSIFIED

Security Classification

DOCUMENT CONTROL DATA - R & D

(Security classification of title, body of abstract and indexing annotation must be entered when the overall report is classified)

1. ORIGINATING ACTIVITY *(Corporate author)* Oak Ridge National Laboratory Oak Ridge, Tennessee	2a. REPORT SECURITY CLASSIFICATION Unclassified 2b. GROUP

3. REPORT TITLE

"Basic Concepts of Radiation Shield Analysis"
Chapter 2 of *Weapons Radiation Shielding Handbook*

4. DESCRIPTIVE NOTES *(Type of report and inclusive dates)*

Handbook

5. AUTHOR(S) *(First name, middle initial, last name)*

Authors: Paul N. Stevens and H. Clyde Claiborne
Editors: Lorraine S. Abbott, H. Clyde Claiborne, Charles E. Clifford

6. REPORT DATE	7a. TOTAL NO. OF PAGES	7b. NO. OF REFS
December 1969	85	58

8a. CONTRACT OR GRANT NO.	9a. ORIGINATOR'S REPORT NUMBER(S)
Interagency Agreement: 40-36-64 b. PROJECT NO. DASA Task A2-11.033 c. IACRO EO 804-64 d. NWER Subtask PEO33	DASA-1892-5 9b. OTHER REPORT NO(S) *(Any other numbers that may be assigned this report)*

10. DISTRIBUTION STATEMENT

This document has been approved for public release and sale; its distribution is unlimited.

11. SUPPLEMENTARY NOTES	12. SPONSORING MILITARY ACTIVITY
	Defense Atomic Support Agency Washington, D.C. 20305

13. ABSTRACT

The basic concepts underlying the methods used for weapons radiation shield analysis are described in this chapter. They include the quantities used to describe particle populations and the quantities used to describe radiation interactions with materials. The characteristics of the particular radiations produced by weapons, neutrons and gamma rays, are discussed in detail, including their physical properties and their important interactions. The production processes whereby neutrons and gamma rays are produced are also described. In addition, the chapter discusses the various response functions that are used to convert a radiation field to a biological effect.

DD FORM 1 NOV 68 1473 REPLACES DD FORM 1473, 1 JAN 64, WHICH IS OBSOLETE FOR ARMY USE.

Security Classification

UNCLASSIFIED

Security Classification

14. KEY WORDS	LINK A		LINK B		LINK C	
	ROLE	WT	ROLE	WT	ROLE	WT
Particle density						
Flux density						
Fluence						
Current density						
Adjoint flux						
Special radiation fields						
Microscopic cross sections						
Macroscopic cross sections						
Reaction probabilities						
Reaction rates						
Neutron characteristics						
Gamma-ray characteristics						
Neutron elastic scattering						
Neutron inelastic scattering						
Neutron radiative capture						
(n,2n) reaction						
Charged-particle reactions						
Neutron fission						
Neutron transport cross section						
Fusion reaction						
Gamma-ray photoelectric effect						
Gamma-ray pair production						
Gamma-ray Compton scattering						
Gamma-ray cross sections						
Fission-product decay						
Bremsstrahlung						
Absorbed dose						
First-collision dose						
Multicollision dose						
Kerma						
Exposure						
Relative biological effectiveness						
RBE dose						
Dose equivalent						
Maximum absorbed dose						
Maximum dose equivalent						
Phantom dose calculations						
Radiation exposure limits						

Security Classification

DISTRIBUTION

Department of Defense

1. Director, Advanced Research Projects Agency, Washington, D.C. 20301, ATTN: Technical Information Officer
2–7. Director, Defense Atomic Support Agency, Washington, D.C. 20305, ATTN: RARP (4 copies); Technical Library (APTL, 2 copies)
8–27. Administrator, Defense Documentation Center, Cameron Station – Bldg. 5, Alexandria, Virginia 22314, ATTN: Document Control
28. Commandant, Industrial College of the Armed Forces, Ft. Lesley J. McNair, Washington, D.C. 20315, ATTN: Document Control
29. Commandant, National War College, Washington, D.C. 20305, ATTN: Class Rec. Library
30. Assistant to the Secretary of Defense (Atomic Energy), Washington, D.C. 20301
31. Director of Defense Research & Engineering, Washington, D.C. 20301, ATTN: Director of Technical Information
32. Director, Weapons Systems Evaluation Group, Washington, D.C. 20305, ATTN: Library
33. Commander, Field Command, Defense Atomic Support Agency, ATTN: FCTG5 Sandia Base, Albuquerque, New Mexico 87115

Department of the Army

34. Director of Civil Defense, Department of the Army, Washington, D.C. 20310, ATTN: RE (Assistant Director for Research)
35. Chief of Engineers, U.S. Army, Washington, D.C. 20315
36. Chief of Research and Development, Department of the Army, Washington, D.C. 20310, ATTN: Nuclear, Chemical-Biological Division
37. Director, Advanced Ballistic Missile Defense Agency, Department of the Army, Washington, D.C. 20310
38. Commandant, Army Command and General Staff College, Fort Leavenworth, Kansas 66027, ATTN: Acquisitions, Library Division
39. Superintendent, U.S. Military Academy, West Point, New York 10996, ATTN: Document Library
40. Commandant, Army War College, Carlisle Barracks, Pennsylvania 17013
41–43. Commanding Officer, Army Combat Developments Command, Institute of Nuclear Studies, Fort Bliss, Texas 79916, ATTN: Technical Library; Charles N. Davidson, LTC Fraser
44. Commanding Officer, Atmospheric Sciences Laboratory, USAECOM, White Sands Missile Range, New Mexico 88002
45. Commanding General, Army Electronics Command, Ft. Monmouth, New Jersey 07703, ATTN: Technical Documents Center, Evans Area
46. Commanding Officer Army Electronic Proving Ground, Fort Huachuca, Arizona 85613, ATTN: Technical Library
47. Commanding Officer, Army Engineer Nuclear Cratering Group, Lawrence Radiation Laboratory, Livermore, California 94550, ATTN: Document Control
48. Director, Army Engineer Waterways Experiment Station, Box 631, Vicksburg, Mississippi 39180, ATTN: Library
49. Commanding General, Army Materiel Command, Washington, D.C. 20315, ATTN: AMCRD-BN-RE, N. Stulman
50–51. Commanding Officer, Harry Diamond Laboratories, Connecticut Avenue & Van Ness St., Washington, D.C. 20433, ATTN: Chief, Nuclear Vulnerability Branch; Technical Reference Branch
52–53. Commanding Officer, Army Nuclear Effects Laboratories, Edgewood Arsenal, Maryland 21010, ATTN: Technical Library; Dr. Eccleshall

54. Commanding Officer, Army SAFEGUARD System Command Field Office, Bell Telephone Laboratories, Whippany Road, Whippany, New Jersey 07981, ATTN: SENSC-DTF-B, J. Turner
55. Commanding Officer, Army Ballistic Research Laboratories, Aberdeen Proving Ground, Maryland 21005, ATTN: Technical Library
56. Chief, Army Research Office (Durham), Box CM, Duke Station, Durham, North Carolina 27706, ATTN: Dr. R. Mace/Herman Robl

Department of the Navy

57. Superintendent, Naval Academy, Annapolis, Maryland 21402
58. Commanding Officer, Naval Applied Science Laboratory, Flushing and Washington Avenues, Brooklyn, New York 11251
59. Commanding Officer, Naval Civil Engineering Laboratory, Port Hueneme, California 93041, ATTN: Code L31
60. Commander, Naval Oceanographic Office, Washington, D.C. 20390, ATTN: Library (Code 1640)
61. Commander, Naval Ordnance Laboratory, Silver Spring, Maryland 20910, ATTN: Technical Library

62–63. Superintendent, Naval Postgraduate School, Monterey, California 93940, ATTN: Technical Library; Code 0384

64. Director, Naval Research Laboratory, Washington, D.C. 20390, ATTN: Technical Library
65. Commanding Officer, Naval Schools Command, Treasure Island, San Francisco, California 94130, ATTN: NBCD Department (Technical Library)
66. Commanding Officer, Naval School, Civil Engineer Corps Officers, Naval Construction Battalion Center, Port Hueneme, California, 93041, ATTN: Librarian
67. Commander, Naval Ship Research and Development Center, Washington, D.C. 20007, ATTN: Library
68. President, Naval War College, Newport, Rhode Island 02840
69. Commanding Officer, Naval Weapons Evaluation Facility, Kirtland Air Force Base, Albuquerque, New Mexico 87117, ATTN: Document Control

Department of the Air Force

70. Headquarters, USAF, Washington, D.C. 20330, ATTN: AFGOA (Chief, Operations Analysis), Dr. Ray

71–74. Headquarters, Air Force Systems Command, Andrews AFB, Washington, D.C. 20331, ATTN: SCPSL, Technical Library; SCTSW (Weapons & Weapons Effects Div.); SCTS (Director, Science & Tech.); Mr. A. J. Chiota

75. Headquarters, Office of Aerospace Research, 1400 Wilson Blvd., Arlington, Virginia 22209
76. AF Office of Scientific Research, OAR, 1400 Wilson Blvd., Arlington, Virginia 22209, ATTN: Documents Branch
77. AF Aero-Propulsion Laboratory, AFSC, Wright-Patterson AFB, Ohio 45433
78. AF Cambridge Research Laboratories, OAR, L. G. Hanscom Field, Bedford, Massachusetts 01730, ATTN: CRMXLR, Research Library, STOP 29
79. AF Director of Nuclear Safety, Kirtland AFB, New Mexico 87117
80. AF Institute of Technology, AU, Wright-Patterson AFB, Ohio 45433, ATTN: Technical Library
81. AF Materials Laboratory, AFSC, Wright-Patterson AFB, Ohio 45433, ATTN: Library

82–89. AF Weapons Laboratory, AFSC, Kirtland AFB, New Mexico 87117, ATTN: WLOL, Technical Library; WLRET (TREE Group Leader); WLTH; Chief, WLBR (Biophysics Br.); WLR; WLC; WLRE, WLRX

90. Air University Library, AU, Maxwell Air Force Base, Alabama 36112
91. Electronic Systems Division, AFSC, L. G. Hanscom Field, Bedford, Massachusetts 01730, ATTN: ESTI, Science and Technical Info. Division
92. Foreign Technology Division, AFSC, Wright-Patterson AFB, Ohio 45433, ATTN: TD-BTA, Library

93–94. Rome Air Development Center, AFSC, Griffiss Air Force Base, New York 13440, ATTN: Documents Library (EMLAL-1); EMTLD (Documents Library)

95. Space and Missile Systems Organization, AFSC, AF Unit Post Office, Los Angeles, California 90045, ATTN: Library
96. Space and Missile Systems Organizations, AFSC, Norton AFB, Calif. 92409, ATTN: Library

Atomic Energy Commission

97–305. U.S. Atomic Energy Commission, Division of Tech. Info. Ext., P. O. Box 62, Oak Ridge, Tennessee 37830, ATTN: Document Control and given distribution as shown in TID-4500 under Reactor Technology category (25 copies – CFSTI)

306. U.S. Atomic Energy Commission, New York Operations Office, 376 Hudson Street, New York, New York 10014, ATTN: Document Control

307. Argonne National Laboratory, 9700 South Cass Avenue, Argonne, Illinois 60440, ATTN: Document Control For – Library Services Dept./Report Sec.

308. Battelle Memorial Institute, Pacific Northwest Laboratory, P. O. Box 999, Richland, Washington 99352, ATTN: Document Control For: K. H. Larson

309–310. Brookhaven National Laboratory, P. O. Box 150, Upton, Long Island, New York 11973, ATTN: Document Control For – Document Section; NCSC

311–313. University of California, Lawrence Radiation Laboratory, Technical Information Division, P. O. Box 808, Livermore, California 94550, ATTN: Document Control For – Technical Library; Dr. R. Howerton, Dr. John Anderson

314–317. Los Alamos Scientific Laboratory, P. O. Box 1663, Los Alamos, New Mexico 87544, ATTN: Document Control For: R. Taschek; Dr. Diven; Dr. Young; Dr. Stewart

318. Sandia Laboratories, P. O. Box 5800, Albuquerque, New Mexico 87115, ATTN: Document Control For: C. R. Mehl

319–1367. Union Carbide Corporation, Nuclear Division, Oak Ridge National Laboratory, P. O. Box X, Oak Ridge, Tennessee 37830, ATTN: Document Control For: Radiation Shielding Info. Ctr. (1000 copies); C. E. Clifford, (2), L. S. Abbott (10), H. C. Claiborne (2), P. N. Stevens (25), J. Auxier (1), Civil Defense Library (1), Central Research Library (3), Document Reference Section (1), Laboratory Records, ORNL R.C. (1), ORNL Patent Office (1), R. B. Parker (1), A. M. Weinberg (1)

Other Government

1368–1369. National Bureau of Standards, Washington, D.C. 20234, ATTN: R. B. Schwartz; Mr. C. M. Eisenhauer

Department of Defense Contractors

1370. National Academy of Sciences, 2101 Constitution Avenue, N.W., Washington, D.C. 20418

1371. The Trustees of Boston College, Chestnut Hill Campus, Chestnut Hill, Massachusetts 02167, ATTN: Dr. I. J. Russell

1372. California Institute of Technology, Jet Propulsion Laboratory, 4800 Oak Grove Drive, Pasadena, California 91103, ATTN: Document Control Office

1373. University of California, San Diego, P. O. Box 109, La Jolla, California 92038, ATTN: Keith A. Brueckner

1374. University of Illinois, Urbana Campus, 112 English Bldg., Urbana, Ill. 61801, ATTN: Classified Information Supervisor For – Dr. Arthur Chilton

1375. University of New Mexico, Albuquerque, New Mexico 87106, ATTN: Library

1376. Eric H. Wang Civil Eng. Research Facility, University of New Mexico, Box 188, University Station, Albuquerque, New Mexico 87106

1377. Pennsylvania State University, University Park, Penn. 16802, ATTN: Dr. A. Forderaro

1378. Aerospace Corporation, P. O. Box 95085, Los Angeles, California 90045, ATTN: Off. of Tech., Surviv. Dir. (V. Josephson)

1379. Aerospace Corporation, P. O. Box 5866, San Bernardino, California 92408, ATTN: Mr. Greenhow

1380–1381. Battelle Memorial Institute, 505 King Avenue, Columbus, Ohio 43201, ATTN: Radiation Effects Information Center; Library

1382–1384. Bell Telephone Laboratories, Inc., Whippany Road, Whippany, New Jersey 07981, ATTN: Tech. Rpt. Ctr., Rm 2A-165B/Dr. Benedict; Tech. Rpt. Ctr., Rm 2A-165B/Dr. McAfee; Tech. Rpt. Ctr., Rm 2A-165B/E. Oberer

1385. The Boeing Company, P. O. Box 3707, Seattle, Washington 98124, ATTN: G. Keister
1386. EG&G, Inc., Santa Barbara Division, P. O. Box 98, 130 Robin Hill Road, Goleta, California 93017, ATTN: Technical Library
1387. Fairchild, Space & Defensive Systems Division, 30 Space Park, Paramus, New Jersey 07652, ATTN: J. D. O'Neill
1388. General Electric Company, TEMPO-Center for Advanced Studies, 816 State Street, Santa Barbara, California 93102, ATTN: DASA Information and Analysis Center
1389. Gulf General Atomic, Inc., P. O. Box 1111, San Diego, California 92112, ATTN: Chief, Tech. Information Services For – Dr. V. A. J. Van Lint
1390. IIT Research Institute, 10 West 35th Street, Chicago, Illinois 60616, ATTN: Library
1391. ION Physics Corporation, South Bedford Street, Burlington, Mass. 01803
1392. Kaman Sciences Corporation, Kaman Nuclear Division, 1700 Garden of the Gods Road, Colorado Springs, Colorado 80907, ATTN: Dr. Frank Shelton
1393. LFE, Inc., Trapelo/West Division, 2030 Wright Avenue, Richmond, California 94804
1394. Lockheed Missiles and Space Company, A Division of Lockheed Aircraft Corporation, P. O. Box 504, Sunnyvale, California 94088, ATTN: Library
1395. Lovelace Foundation for Medical Education and Research, 5200 Gibson Blvd., S.E., Albuquerque, New Mexico 87108, ATTN: Dr. Clayton White
1396. Mathematical Applications Group, Inc., 180 S. Broadway, White Plains, New York 10605
1397. MITRE Corporation, Route 62 and Middlesex Turnpike, Bedford, Massachusetts 01730, ATTN: Technical Library
1398. North American Rockwell Corp., Autonetics Division, 3370 Miraloma Avenue, Anaheim, California 92803, ATTN: Technical Library
1399. Physics International Company, 2700 Merced Street, San Leandro, California 94577, ATTN: Technical Library
1400–1403. Radiation Research Associates, Inc., 3550 Hulen Street, Fort Worth, Texas 76107 (N. M. Schaeffer, M. B. Wells, L. G. Mooney, R. French)
1404–1406. The RAND Corporation, 1700 Main Street, Santa Monica, California 90406, ATTN: Technical Library/Dr. R. LeLevier; Library; Dr. W. Graham
1407. Stanford Research Institute, 333 Ravenswood Avenue, Menlo Park, California 94025, ATTN: Library
1408. System Development Corporation, 2500 Colorado Avenue, Santa Monica, California 90406, ATTN: Technical Library
1409. Systems, Science and Software, Inc., P. O. Box 1620, La Jolla, California 92037, ATTN: Dr. L. Schalit
1410. Technical Operations, Inc., South Avenue, Burlington, Massachusetts 01804, ATTN: Dr. Eric Clarke
1411. Texas Nuclear Corporation, Box 9267, Allendale Station, Austin, Texas 78756
1412. TRW Systems Group, San Bernardino Operations, P. O. Box 1310, San Bernardino, California 92402, ATTN: Library
1413. TRW Systems Group, One Space Park, Redondo Beach, California 90278, ATTN: STL Technical Library
1414. United Nuclear Corporation, Grasslands Road, Route 100C, Elmsford, New York 10523
1415. Westinghouse Electric Corporation, Defense and Space Center, P. O. Box 1693, Baltimore, Maryland 21203, ATTN: Dr. Pan/Eng. Dir. of Sci. and Tech.
1416. Dr. M. H. Kalos, Courant Institute of Mathematical Sciences, 251 Mercer Street, New York, New York 10012
1417. Dr. Reed Johnson, Department of Nuclear Engineering, University of Virginia, Charlottesville, Virginia 22901
1418. Physics International Company, 2700 Merced Street, San Leandro, California 94577, ATTN: Dr. W. E. Kreger
1419. Department of the Army, USAMC Main Battle Tank Engineering Agency, 28150 DeQuindre, Warren, Michigan 48092